POROSITY EVOLUTION ASSOCIATED WITH CLOSELY-SPACED DISCONFORMITIES, MID-CRETACEOUS CARBONATE PLATFORM, MEXICO

By

ABDUL WAHAB

B.S., UNIVERSITY OF PESHAWAR, 2012

Submitted to the graduate degree program in Department of Geology and the Graduate Faculty of the University of Kansas in partial fulfillment of the requirements for the degree of Master of Science.

Advisory Committee

_____

PAUL ENOS (Chairperson)

_____

ROBERT H. GOLDSTEIN (Co-chair)

_____

GEORGE TSOFLIAS

Date Defended: May 19, 2016

The Thesis Committee for ABDUL WAHAB
Certifies that this is the approved version of the following thesis:

POROSITY EVOLUTION ASSOCIATED WITH CLOSELY-SPACED DISCONFORMITIES,

MID-CRETACEOUS CARBONATE PLATFORM, MEXICO

_____

PAUL ENOS (Chair)

_____

ROBERT H. GOLDSTEIN (Co-chair)

Date approved: December 12, 2016

ABSTRACT

El Abra Formation was cyclically deposited on an isolated, steep-sided, high-relief carbonate platform in the Tampico-Misantla basin during the mid-Cretaceous. Sea-level oscillations recorded by shallowing-upward cycles, truncated cycles, and rhythms were of low amplitude (<10 m) and high frequency, possibly modulated by sub-Milankovitch (< 12 ka) cycles. The El Abra platform missed some sea level oscillations above the platform resulting in relatively thick subtidal units. Paleosols, karst surfaces, laminated caliche crusts, voluminous solution porosity, blackened clasts, rhizoliths, desiccation and wetting cracks, and solution-collapse breccia record subaerial disconformities in the inner platform margin. Meteoric diagenesis associated with intraformational disconformities (D-1) produced molds, vugs, and solution-enlarged fenestrae, followed by the deposition of crystalline internal sediment (CIS) and precipitation of early equant cement (EEC). Crosscutting relationships and cement stratigraphy document intraformational origin of EEC, with cyclic cementation beneath most successive disconformities. Fluids varying in salinity from freshwater, hypersaline water, normal seawater and mixed seawaters precipitated EEC in the inner margin. In the outer margin contemporaneous marine-phreatic diagenesis precipitated meniscate micritic cements and isopachous radiaxial fibrous cements (RFC-1). Disconformities are more numerous and better developed within inner-margin skeletal rudstone and tidal deposits than among the outer-margin reefs and sands, indicating that the inner margin had the highest elevation on the platform, probably as rubble islands and tidal flats. A major dissolution event (D-2) in a regional meteoric aquifer, perhaps in the late Cenomanian, created voluminous megaporosity, reduced by a second generation of marine cement (RFC-2) in the inner margin and by pelagic internal sediments (PIS) and RFC-2 in the outer margin. Major pore occlusion in both the inner- and outer-margin rocks was by late

equant cement (LEC) during shallow burial. Four pervasive, distinctive, cathodoluminescence zones in LEC indicate approximate synchronicity of cementation throughout the platform margin. Fluid-inclusion data from LEC indicate precipitation from freshwater at temperature less than 50°C. Freshwater may have infiltrated through clastic wedges developed at the front of the rising Sierra Madre Oriental during the Late Cretaceous and passed through fractured (?) basinal rocks and porous platform limestones, to exit through the elevated rim of the platform. Deeper burial and the Laramide orogeny produced only minor fractures, fracture-filling cement, and stylolites.

An **e**xtensive diagenetic history, most of it near-surface, resulted in 19.6% extant porosity and permeability as much as 553 md in the outer-platform-margin rocks of El Abra Formation. Inner-margin rocks were not so blessed, but retain 9.3% porosity. Microporosity of inner-margin rocks averages 3.3% with permeability of 0.04 md. Outer-margin rocks likewise retain 3.6% microporosity and permeability of 0.03 md. Mesoporosity, visible in thin section, is negligible for both settings. This range of values underscores the need to measure porosity and permeability in vuggy carbonate rocks over the widest range of scales feasible, more than six orders of magnitude in this study. It also clarifies that, although matrix porosity is very low, large vugs are interconnected, at least locally. Various diagenetic stages affected porosity evolution on different scales and different magnitudes. In order of increasing volume in the inner margin: radiaxial fibrous cement-2, early equant cement, crystalline internal sediment, and late equant cement reduced the reservoir quality. Late, near-surface dissolution produced considerably more pore space than intraformational dissolution episodes beneath successive disconformities. Intraformational diagenesis beneath disconformities compartmentalized the inner margin by reducing porosity to half of its surface values in the first 50 cm, followed by a dramatic increase

to a depth of 2 m. In the outer margin, in order of increasing volume: crystalline internal sediment, radiaxial fibrous cement-2, radiaxial fibrous cement-1, and late equant cement reduced reservoir quality. The late dissolution event, which pervaded the entire platform margin, produced virtually all of the extant porosity in the outer margin, much of it large scale and locally interconnected. The outer margin is thus the optimum zone for reservoir quality in a heavily cemented shallow-water peritidal carbonate system.

ACKNOWLEDGEMENTS

I start with name of ALLAH, the most merciful, and the mightiest. I am grateful to a number of institutions, organizations, and individuals whom made this project an educational and exciting experience.

First and foremost, I am deeply thankful to Fulbright program for awarding me with their most prestigious academic award and for bringing me to the United States of America. I am also thankful to United States Educational Foundation in Pakistan (USEFP) for helping throughout the Fulbright selection and U.S. visa processes. I am also grateful to the Institute of International Education (IIE) in Denver, Colorado, especially Sarah McCormick for her help, who showed the utmost support and encouragement throughout my studies. I am grateful to the Kansas Interdisciplinary Carbonates Consortium (KICC) for funding my project and for providing an annual opportunity to present my research to the experts in the oil and gas industry. I am also grateful to Kansas Geological Survey (KGS) for allowing me to use its valuable equipment during my research work.

I sincerely appreciate Instituto Potosino de Investigación Científica y Tecnológica (IPICYT), for allowing me to use their MD-405 drill press. Special thanks to Dr. Pablo Davila Harris of IPICYT for helping me with fieldwork logistics in Mexico, and for providing amazing students, Edgar Rojas Ortega, Salvador and Raul Edgardo to assist me in the field. Their efforts during the blazing summer of Mexico were admirable.

I would like to thank CEMEX for its cooperation and granting me permission to work in its quarries. I am grateful to Rigoberto Sanchez (Director), Efriam Fernandes, Ivan Mayoral and all other employees of CEMEX who helped me during my fieldwork.

I am in debt to my humble and kind advisors Dr. Paul Enos and Dr. Robert H. Goldstein for helping me select this incredible research project, write grant proposals, prepare for fieldwork, understand and analyze my research data, and finish my thesis. More importantly for helping me develop critical scientific thinking. Their supervision and guidance has prepared me for a career in geology. I also thank Dr. George Tsoflias for being on my committee and providing helpful feedback.

Many students and faculty inspired me during my time at the Department of Geology, University of Kansas. The department provided a friendly and welcoming environment that made it easy for me to adjust to the American educational system.

Finally, I would like to thank my family for their inspirations and blessings. My parents have helped me in every aspect of my life and provided valuable advice in stressful times. My sisters who have showered me with unparalleled love, care, and consistent encouragement helped in keeping focus during my research. I would like to thank my brothers who have shown me from time to time that even the impossible is achievable.

.

TABLE OF CONTENTS

LIST OF FIGURES

CHAPTER II

CHAPTER-III

CHAPTER-IV

LIST OF TABLES

CHAPTER-III

CHAPTER-IV

CHAPTER I: INTRODUCTION

Previous studies have generated numerous criteria for identifying subaerial exposure surfaces and subsequent early diagenesis (Bathurst 1974; James and Choquette 1984; Esteban and Klappa 1983; Goldstein 1988; Budd et al. 1995), but quantitative understanding of the effects of disconformity-associated diagenesis on porosity evolution remains limited. Repeated subaerial exposure surfaces punctuated El Abra Formation, making it ideal for collecting quantitative data on porosity and permeability evolution associated with disconformities. El Abra Formation exposures in quarries in the Sierra El Abra in northeast Mexico provide access. El Abra Formation in the Sierra El Abra hosted a giant oil reservoir (estimated 1 bbl.) that was exhumed and drained of hydrocarbons during post-Oligocene uplift following the Laramide orogeny (Yurewicz et al. 1997).

Cyclicity in El Abra Formation, criteria for recognizing subaerial exposure in ancient carbonate rocks, and diagenetic trends associated with closely spaced disconformities are presented in Chapter II. Field observations of subaerial exposure features, cycle types, thickness, etc. and petrographic study of thin sections and polished slabs are used to determine the nature of cyclicity and details of paragenetic sequences. The details of cyclicity elucidate some controls on deposition, and early diagenetic trends record conditions during and following repeated emergence of El Abra Formation.

Disconformity control on calcite cementation is the focus of Chapter III. Cement stratigraphy is integrated with fluid-inclusion data from two generations of calcite cement, to determine their distribution and origin. Cathodoluminescence zones and their relative ages, determined from crosscutting relationships, established the cement stratigraphy. Early equant cements were precipitated during subaerial exposure beneath successive intraformational

disconformities. Pervasive late equant cement precipitated from freshwater, probably sourced in clastic wedges shed from the rising Laramide orogeny, that entered the Valles-San Luis Potosí platform from the west, and exited on the Campanian seafloor.

Chapter IV provides quantitative estimates of porosity in El Abra Formation at four scales ranging over 6 orders of magnitude from micrometer to decimeter. Paragenetic sequences and quantitative estimates of porosity and permeability are integrated to better understand pore-space evolution associated with closely spaced disconformities, the resulting compartmentalization of carbonate reservoirs, and the contrasts with less-emergent outer-margin deposits of shallow-water platform margins.

Through these objectives, this study characterized diagenetic trends and porosity evolution associated with closely spaced disconformities. The results of this study will provide a reservoir analogue useful in understanding porosity and permeability associated with disconformities, and with more persistent submergence, in shallow-water, carbonate-platform margins.

RFERENCES CITED

BATHURST, R.G.C., 1974, Marine diagenesis of shallow water calcium carbonate sediments: Annual Review of Earth and Planetary Sciences, v. 2, p. 257.

BUDD, D.A., SALLER, A.H., AND HARRIS, P.M., 1995, Unconformities and porosity in carbonate strata: American Association of Petroleum Geologists, Memoir, 63, 301 p.

ESTEBAN, M., AND KLAPPA, C.F., 1983, Subaerial exposure, *in* Scholle, P.A., Bebout, D.G., and Moore, C.H., eds., Carbonate Depositional Environments: American Association of Petroleum Geologists, Memoir, 33, p. 1-63.

GOLDSTEIN, R., 1988, Paleosol of Late Pennsylvanian cyclic strata, New Mexico: Sedimentology, v. 35, p. 777-803.

JAMES, N. P. AND CHOQUETTE, P. W., 1984, Limestones - The meteoric diagenetic environment: Geoscience Canada, v. 11, p. 785-799.

YUREWICZ, D. A., CHUCHLA, R. J., RICHARDSON, M., POTTORF, R. J., GRAY, G. G., KOZAR, M. G., AND FITCHEN, W. M., 1997, Hydrocarbon generation and migration in the Tampico-Misantla Basin and Sierra Madre Oriental, East-Central Mexico: Evidence from an Exhumed Oil Field in the Sierra de El Abra: Dallas Geological Society and Society of Economic Paleontologists and Mineralogists, 24 p.

CHAPTER II: DEPOSITIONAL AND SUBAERIAL-EXPOSURE CYCLES IN EL ABRA CARBONATE PLATFORM (MID-CRETACEOUS), MEXICO

ABSTRACT

El Abra Formation was cyclically deposited on an isolated, steep-sided, high-relief carbonate platform in the Tampico-Misantla basin during the mid-Cretaceous. Sea-level oscillations recorded by shallowing-upward cycles, truncated cycles, and rhythms were of low amplitude (<10 m) and high frequency, possibly modulated by sub-Milankovitch (<12 ka) cycles. Paleosols, karst surfaces, laminated caliche crusts, ubiquitous solution porosity, blackened clasts, rhizoliths, desiccation-and-wetting cracks, and solution-collapse breccia record subaerial disconformities in the inner margin. Meteoric diagenesis associated with intraformational disconformities (D-1) produced molds, vugs, and solution-enlarged fenestrae, followed by the deposition of crystalline internal sediment (CIS) and precipitation of early equant cement (EEC). Fluids varying in salinity from freshwater, hypersaline water, normal seawater and mixed seawaters precipitated EEC in the inner margin. Contemporaneous marine-phreatic diagenesis precipitated meniscate micritic cements and isopachous radiaxial fibrous cements (RFC-1) in the outer margin. A major dissolution event (D-2) in a regional meteoric aquifer, probably in the late Cenomanian, created voluminous megaporosity, reduced by a second generation of marine cement (RFC-2) in the inner margin and by pelagic internal sediments (PIS) and RFC-2 in the outer margin. A major pore occlusion in both the inner- and outer-margin rocks was by precipitation of late equant cements during shallow burial. Deeper burial and the Laramide orogeny produced only minor fractures, fracture-filling cement, and stylolites. More numerous and more intense disconformities within inner-margin skeletal rudstone and tidal deposits, than among the outer-margin reefs and sands, indicate that the inner margin had the highest elevations

on the platform, probably as rubble islands and tidal flats. The influence of depositional morphology on early diagenesis left fingerprints recognizable in reconstructing paleomorphology in ancient rocks.

INTRODUCTION

Disconformities represent a gap in the sedimentation record. During these breaks, sedimentary rocks may be exposed to meteoric and mixing-zone diagenesis and undergo considerable chemical and physical modification in their fabric. Early diagenesis associated with disconformities can profoundly influence reservoir quality and heterogeneity. Previous studies have generated numerous data on diagenesis in shallow-water limestone (Bathurst 1974; James and Choquette 1984; Esteban and Klappa 1983; Budd et al. 1995), but the effects of closely spaced disconformities and consequent early diagenesis require more attention. Repeated and closely spaced (mean 2.7 m) subaerial-surfaces punctuate El Abra Formation, making it ideal for study of near-surface diagenetic modifications in shallow-water platform carbonates. This paper examines criteria for recognizing subaerial exposure, depositional cyclicity, and disconformity-controlled diagenesis in El Abra Formation.

GEOLOGICAL SETTING

El Abra Formation formed on an isolated mid-Cretaceous (Albian-Cenomanian) platform in northeast Mexico surrounded by intracratonic basins (Carrillo 1971; Enos 1974, 1977, 1983). It is spectacularly exposed in the Sierra El Abra, a low-relief; asymmetric anticline, 3-10 km wide and 125 km long (Minero et al. 1983, p.16; Yurewicz et al. 1997), that formed a giant oil reservoir, later breached and drained. Extensive quarries provide nearly continuous, dip-parallel exposure over a distance of 3.5 km (Fig. 2-1). Previous work by Minero (1983, 1988) documented three major lithofacies associations among inner-platform margin rocks: 1) peloid-

miliolid, requienid and bioclastic limestone, 2) fenestral, cryptalgal laminate and lime mudstone and 3) laminated grainstone and rudist-skeletal limestone. These facies associations represent subtidal lagoon, tidal flat, and island/beach depositional environments, respectively. Two generalized facies belts can be recognized in El Abra Formation within the Sierra El Abra: tidally influenced, cyclic deposits in the inner platform margin and Taninul or "reef" facies of the outer margin (Aguayo 1975, 1998; Minero 1983, 1988; Enos 1986). The tidally influenced, cyclic rocks comprise Minero's 1 and 2 lithofacies. Taninul facies consists primarily of rudist-reef and rudist-debris rudstones and grainstones. Shoaling-upward cycles, truncated cycles, and rhythms are represented in El Abra Formation of the inner platform margin. Closely spaced (mean 2.7 m) disconformities punctuated inner-margin deposition. Thick soil horizons, microkarst surfaces, solution-collapse breccia and extensive solution porosity are associated with disconformities. In contrast, within outer-margin rocks equivocal subaerial exposure indicators, such as voluminous solution porosity marks possible disconformities.

El Abra deposition on the Valles-San Luis Potosí platform continued into the Cenomanian, as indicated by early Cenomanian ammonites in Taninul Quarry (Aguayo 1993, 1998, p. 4), and corroborated by Foraminifera (Langoria 1975) and rudists (Alencaster 1984; summarized by Scott, 1990). Colonial, spherical hydrozoans, *Parkeria sphaerica* Carter 1877, found in the platform-margin exposures (Minero et al. 1983; this study) are reported from late Albian and early Cenomanian (Dieni and Trunsek 1979; Wilmsen 2003, p. 164). Aguayo (1978, p. 86; 1998, p. 5) described "laterally continuous thin and wavy layers", up to 10 cm thick, containing late Turonian planktonic foraminifers from El Abra quarries VI, VII, and VIII (fig. 2-1B). He interpreted them as stratigraphic layers, indicating a late Turonian age for at least the uppermost 2/3 of the exposed El Abra Formation, although he noted that the basal exposures are

early Cenomanian. Aguayo could not locate the layers on a visit to the quarries with Enos and C. J. Minero in 1983 and concluded, “They must have been quarried away.” Noting that quarrying in a vertical wall would not remove continuous layers, we conclude that the microfossils had filtered into elongate vugs open to seawater during the Turonian transgression and that the host rocks were probably Cenomanian in age, as concluded by other workers. Other examples of ‘palimpsest’ planktonic fossils in the Sierra El Abra were reported by Aguayo (1978, p. 78; Campanian) from CA quarry and Enos (1986, p. 169; Cenomanian) from TQ (Fig. 2-1C, B). Most of the eastern Valles-San Luis Potosí platform drowned abruptly in the Turonian and accumulated pelagic sediments throughout the late Cretaceous, including the Agua Nueva (Turonian), San Felipe (Coniacian-Santonian) and Méndez (Campanian-Maastrichtian) Formations. The Méndez Shale grades westward into clastic wedges of the Difunta Group that record the onset of the Laramide Orogeny in north-central Mexico (McBride et al. 1975, Soegaard et al. 1996; Ye 1997, p. 112). Neither Agua Nueva nor San Felipe appears to have covered El Abra Formation in the Sierra El Abra study area (Minero et al. 1983; Enos 1986; Aguayo 1998). In the CA quarry, Méndez Shale oversteps the San Felipe Formation and onlaps the El Abra slope deposits. San Felipe pelagic limestone and shale overlie El Abra platform carbonates at the village of San Felipe, 5 km to the west. Very thin Aqua Nueva pelagic limestones cover El Abra platform carbonates 25 km south of Ciudad Valles (Minero et al. 1983, p. 136; Basáñez et al. 1993, p. 57) and 70 km north (in outcrop, Passagno 1969, and Perez-1 well, Basáñez et al. 1993, p. 56). It is not clear, however, whether the Méndez once covered El Abra Formation in the Sierra El Abra study area. It seems certain that the Sierra El Abra was submerged during most or all of the Late Cretaceous, as all deposits in the region are pelagic. The presence of Cenomanian, Turonian, and Campanian planktonic fossils in El Abra vugs


500 m
C
CM-1
CM-2
D
200 m
TQ
A
N
GOM
500 km
B
El Abra
VIII
VII
VI
V
IV
CM-1
CM-2
Tampico
Ciudad Valles
TQ
Sierra El Abra
PM-2
PM-1
Las Palmas
2 km
© 2016 Google
Image © 2016 DigitalGlobe
© 2016 INEGI
Google earth
E
PM-2
PM-1
N
CA
BP
PM-1
F

FIG. 2-1: A) Google Earth image of the location of the study area. GOM refers to Gulf of Mexico. Yellow box represents area in B. B) Location of quarries in the Sierra el Abra. Sections measured for this study were located in CM (abbreviated from Cementos Mexicanos, which owns this quarry) and PM (abbreviated after the town of Las Palmas in which this quarry is located). Roman numerals follow the identification scheme of Aguayo (1975) and Minero (1983). Dashed line traces the slope break of El Abra platform. C) Google Earth image of CM quarry is showing location of stratigraphic sections (traced). CM-1 exposes the tidally influenced cyclic rocks while CM-2 exposes the skeletal grainstone nearer the margin. The quarries west of CM (shown in B) expose rocks deposited in tidal flats and the subtidal lagoon (Minero 1983). D) Image of TQ quarry, which exposes the reef facies of El Abra Formation (Enos 1986). E) PM quarry. PM-1 (traced) exposes reef facies while PM-2 (traced) exposes interbedded skeletal rudstone and grainstone. CA is the abandoned Cementos Anahuac (CA) quarry (Enos 1982; Minero et al. 1983). BP is a borrow-pit exposing San Felipe Formation, which is overstepped by Méndez Formation at the foot of the El Abra escarpment in CA (Enos 1982; Minero et al. 1983, p. 18). F) PM-1 section. The length of section (dashed line) is 42 m.

supports this proposition and suggests that El Abra rocks were exposed on the Cretaceous sea floor as late as Cenomanian time. The absence of Upper Cretaceous cover locally on the Sierra El Abra could reflect non-deposition and/or erosion, presumably submarine, perhaps localized by an elevated platform rim or local upwarp, as postulated by Smith (1986, p. 120). Alternatively, Carrillo-Bravo (1971) and Aguayo (1978, p. 110) suggested that unconsolidated deposits covering El Abra platform may have 'slid' eastward into the basin to form a turbidite wedge (Tamuín Member) recognized locally within the basal Méndez Formation. The Late Cretaceous-Paleocene Laramide Orogeny deformed El Abra Platform, creating the gentle, asymmetrical Sierra El Abra anticline (1-3º W dips; 5-8º E dips; Enos 1982; Minero et al. 1983, p. 16ff, Enos 1986, p. 162). Later post-Oligocene uplift exhumed and breached El Abra reservoir (Minero 1988; Yurewicz et al. 1997; Brennan 1999).

Post-Abra Disconformity

A disconformity is widely recognized between the mid-Cretaceous shallow-water platform carbonates and Late Cretaceous deep-water deposits on the Valles-San Luis Potosi platform (Smith 1986). The duration of the hiatus has been estimated at 5 to 24 Ma, depending on which strata overlie El Abra Formation at a given location (Smith 1986). Smith (1986, p. 120) estimated the hiatus at 17 million years in the Sierra El Abra study area, based on Méndez Shale pinching out against the El Abra Formation at the base of the escarpment. However, the Sierra El Abra was apparently submerged during most of this interval, based on the lack of subaerial exposure features on top of El Abra Formation, apparently continuous pelagic deposition in the surrounding basins and adjacent platform from Turonian through Maastrichtian time, and 'palimpsest' planktonic fossils within the uppermost El Abra Formation. There is evidence of a late Cenomanian disconformity elsewhere on the platform of varying duration as reported by

Smith (1986). A late Cenomanian hiatus in the Sierra El Abra probably lasted no more than 3 million years, approximate duration of late Cenomanian and part of middle Cenomanian, and likely involved some subaerial exposure. This is the apparent time of major dissolution, creating megaporosity, perhaps in a regional meteoric aquifer in El Abra Formation or in migrating mixing zones. This secondary porosity was reduced by isopachous, presumably marine, cement (RFC-2), locally overlain by pelagic internal sediment containing Cenomanian planktonic Foraminifera (Enos 1986, p. 169). Sediment containing late Turonian planktonic foraminifers (Aguayo 1978) apparently further reduced large secondary porosity, indicating pores tens of meters below, but connected to, the seafloor, during the Turonian transgression. The absence of subaerial-exposure features on the top of El Abra Formation remains a conundrum, probably best explained by relatively brief duration of exposure.

METHODS

Four stratigraphic sections were measured across the platform margin in the Sierra El Abra (Fig. 2-1A-F, 2-3, 2-4, 2-5). Two sections, CM-1 (Fig. 2-2) and CM-2 (Fig. 2-1C), measuring 72.5 m and 18 m, respectively, are inner-margin rocks at Cementos Mexicanos (CM) quarry. CM quarry cuts stratigraphically and spatially much deeper into the platform than when studied by Minero (1983) and Aguayo (1975). The quarry exposes transitions from tidally influenced, distal-margin deposits (CM-1) to the skeletal grainstone (CM-2) interpreted as marginal shoals by Minero (1983), nearly 1 km from the slope break. Two sections, PM-1 (Fig. 2-3) and PM-2 (Fig. 2-1E), measuring 42 m and 41 m thick, respectively, are in reef or shoal facies near the margin. PM-1 (Fig. 2-1F) is within 100 m of the slope break. PM-2 exposes interbedded rudstone and skeletal grainstone about 400 m behind the slope break. The measured sections provide qualitative and quantitative data on facies distributions and thicknesses,

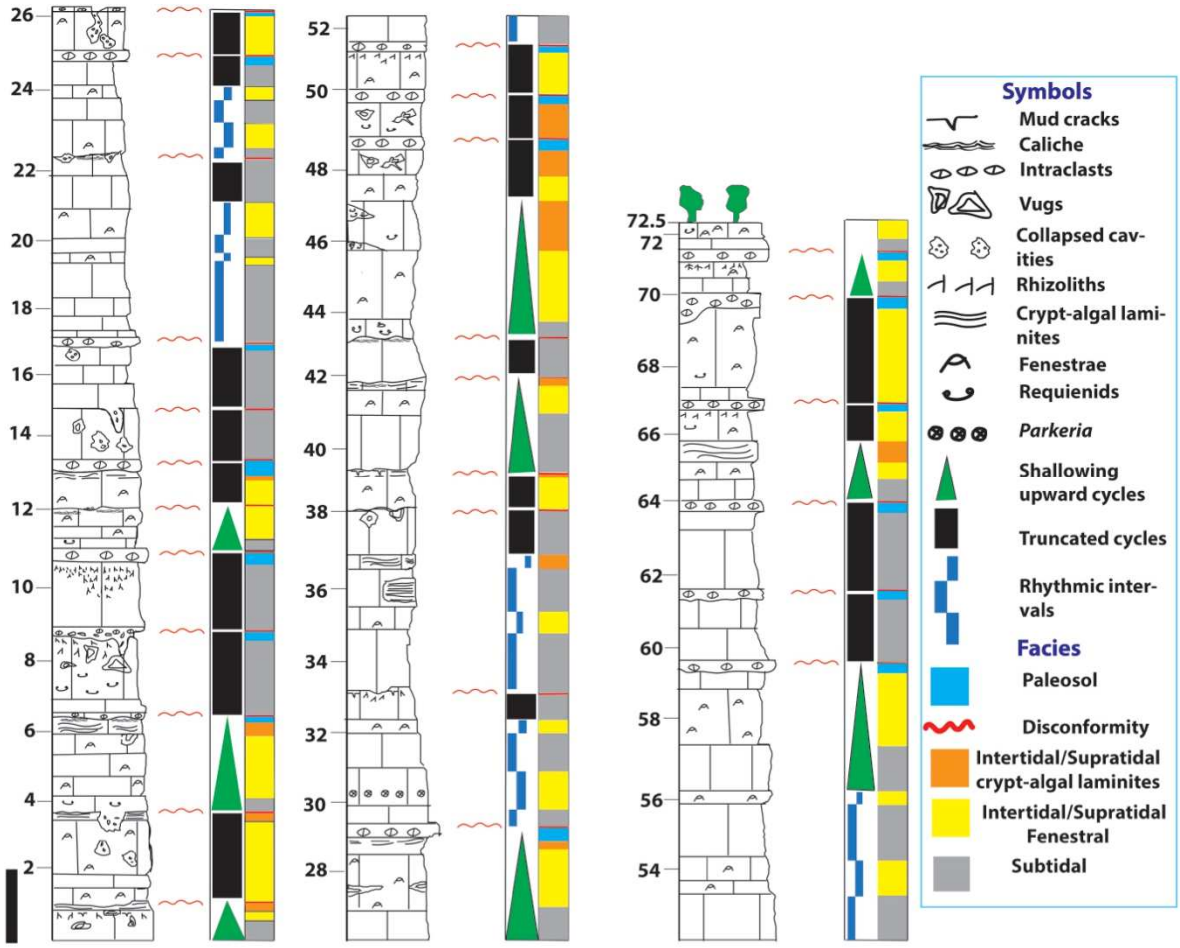

FIG. 2-2: Measured section from Cementos Mexicanos quarry (CM-1, location in Fig. 2-1B).

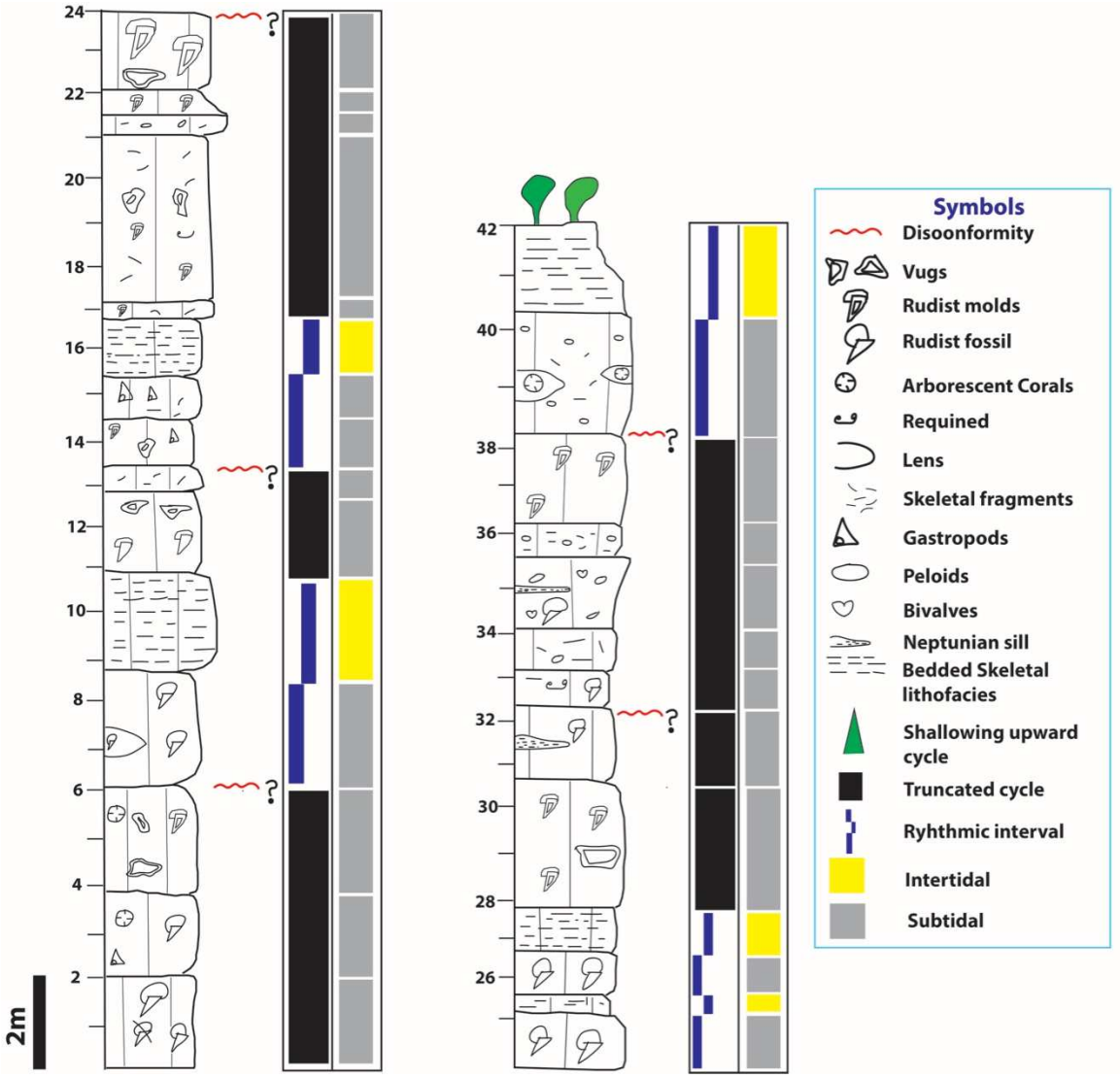

FIG. 2-3: Measured section from Las Palmas Quarry (PM-1, Fig. 2-1B).

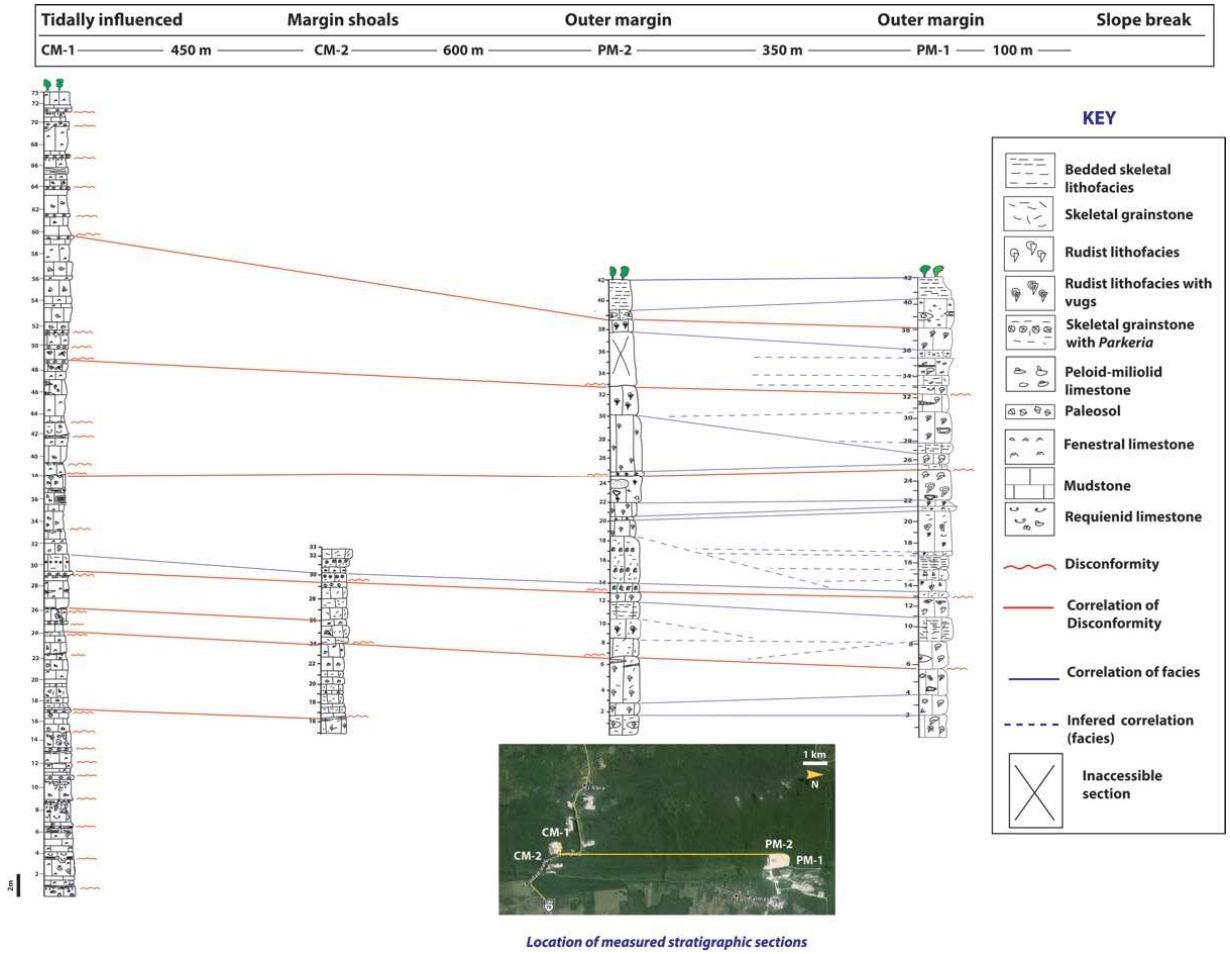

FIG. 2-4: Correlation of measured sections at the eastern margin of Valles-San Luis Potosí platform.

macroscopic diagenetic features, Dunham (1962) textures, and sedimentary structures in the cyclic, uppermost El Abra Formation. Multiple disconformities were recognized based on various subaerial-exposure features. The lateral spacing of the sections (300-400 m within CM quarry) allowed documentation of continuity or changes of depositional units, subaerial-exposure features, etc. Each CM section was sampled with an average spacing of 50 cm. Rocks at the margin (PM) were sampled with average spacing of 1 m. One hundred 2X3-in. thin sections and polished slabs of variable dimensions were prepared from oriented rock samples. Cathodoluminescence petrography was used to establish cement stratigraphy and fluid-inclusion analysis revealed compositions of cement-precipitating fluids.

LITHOFACIES IN EL ABRA FORMATION

A summary of more detailed lithofacies and their depositional environments follows.

Peloid-Miliolid Lithofacies

Peloid-miliolid lithofacies is characterized by abundant miliolid foraminifers and is predominantly wackestone or packstone. Other biota are ostracodes, gastropods, requienid rudists, and rudist skeletal fragments, in decreasing order of relative abundance. Peloids are the dominant non-skeletal grains. Bioturbation is common. Peloid-miliolid facies appear dark to light grey in outcrop, are typically oil-stained, and lack any internal stratification (Fig. 2-5A).

Diverse fauna, abundance of miliolid foraminifera and peloids, extensive bioturbation, lack of hydrodynamic structures, and abundant mud indicate that peloid-miliolid facies was deposited below mean tide. This facies is restricted to the inner margin. Minero (1983) reported peloid-miliolid facies from quarry VIII (fig 2-1B) nearly 3 km from the slope break in the Sierra El Abra (Fig. 2-1B).

Requienid Lithofacies

Requienid rudists of the genus *Toucasia* are abundant in this rock type (Fig. 2-5B), which occurs as lenses and locally in layers <1 m thick. Caprinid fragments, miliolids, and peloids are common as well. Ostracodes, whole caprinids, and gastropods are few. Typical texture in this lithofacies is packstone. Requienid lithofacies appears medium gray in outcrop, is commonly oil-stained, and lacks any internal stratification.

Ward (1979) reported requienid rudists from subtidal facies in El Doctor platform; Minero (1983) and Aguayo (1978) reported requienid rudists with major abundance in the inner margin and minor presence in the outer margin. Requienid rudists are observed in situ both sporadically and in lenses, but also as bioclasts. The abundant mud, miliolids, and bioturbation in this facies suggest semi-restricted, subtidal conditions. Minero (1983) reported lateral transitions and interlayering with peloid-miliolid lithofacies. Requienid lithofacies are absent from the outer margin, although individual requienids are sparsely scattered throughout.

Bioclastic Lithofacies

Bioclastic lithofacies is characterized by the presence of caprinids, requienids, radiolitids (few), red and green algae, miliolid forams, gastropods, and by lack of stratification (Fig. 2-5D). Peloids are also common in this lithofacies. Bioturbation is common. Packstone, wackstone, and rudstone are typical textures. Minero (1983) interpreted these facies as subtidal storm deposits, based on a diverse skeletal assemblage, abundant mud, and poor sorting.

Skeletal-Grainstone Lithofacies

Fine grains (few skeletal fragments larger than 2 mm), lack of apparent stratification and good sorting characterize skeletal grainstone (Fig. 2-5E). Skeletal fragments are typically disarticulated and difficult to recognize in the outcrop. The few large skeletal fragments include

rudists, mollusks, red algae, and gastropods. Smaller skeletal fragments are forams. Colonies of *Parkeria spaeherica* are found only in this facies. Wilmsen (2003) interpreted colonies of *Parkeria sphaerica* as benthic drifters that were rolled by ocean-bottom currents. Based on small grain size and good sorting, we interpret skeletal-grainstone lithofacies as deposits in a subtidal environment with agitated water conditions. Minero (1983, 1988) lumped bioclastic and skeletal-grainstone lithofacies into his bioclastic limestone facies.

Fenestral Lithofacies

Fenestral lithofacies is dominantly wackestone with some packstone (Fig. 2-5F). Miliolids, peloids, and ostracodes are common. Abundant fenestrae, relatively depauperate fauna and sparse bioturbation indicate deposition in the upper intertidal or supratidal environment (cf. Shinn, 1983, p. 209). Minor lime mudstones were lumped with fenestral facies.

Cryptalgal Laminite

Cryptalgal laminite forms in mudstone and wackestone; it is typically light grey and slightly dolomitic (Fig. 2-5G). Miliolids, peloids, ostracodes, and small gastropods are the main constituents. Fenestrae and desiccation cracks are common. Cryptalgal laminite was deposited in an upper intertidal or supratidal setting, based on the presence of desiccation cracks, apparent microbial influence, and paucity of open-marine biota (Shinn 1983).

Rudist-Skeletal Lithofacies

Recumbent caprinids are abundant and common as fragments (Fig. 2-5C), radiolitids occur in small lenses, arborescent corals are few, red algae are few, complete or as fragments, requienids are rare, and *Actaeonella* gastropods are common (Minero 1983). The dominant texture is floatsone with grainstone or packstone matrix. Rudist lithofacies appears cream-colored in outcrop with sporadic dark spots of oil staining. High diversity of reefal fauna, lens-

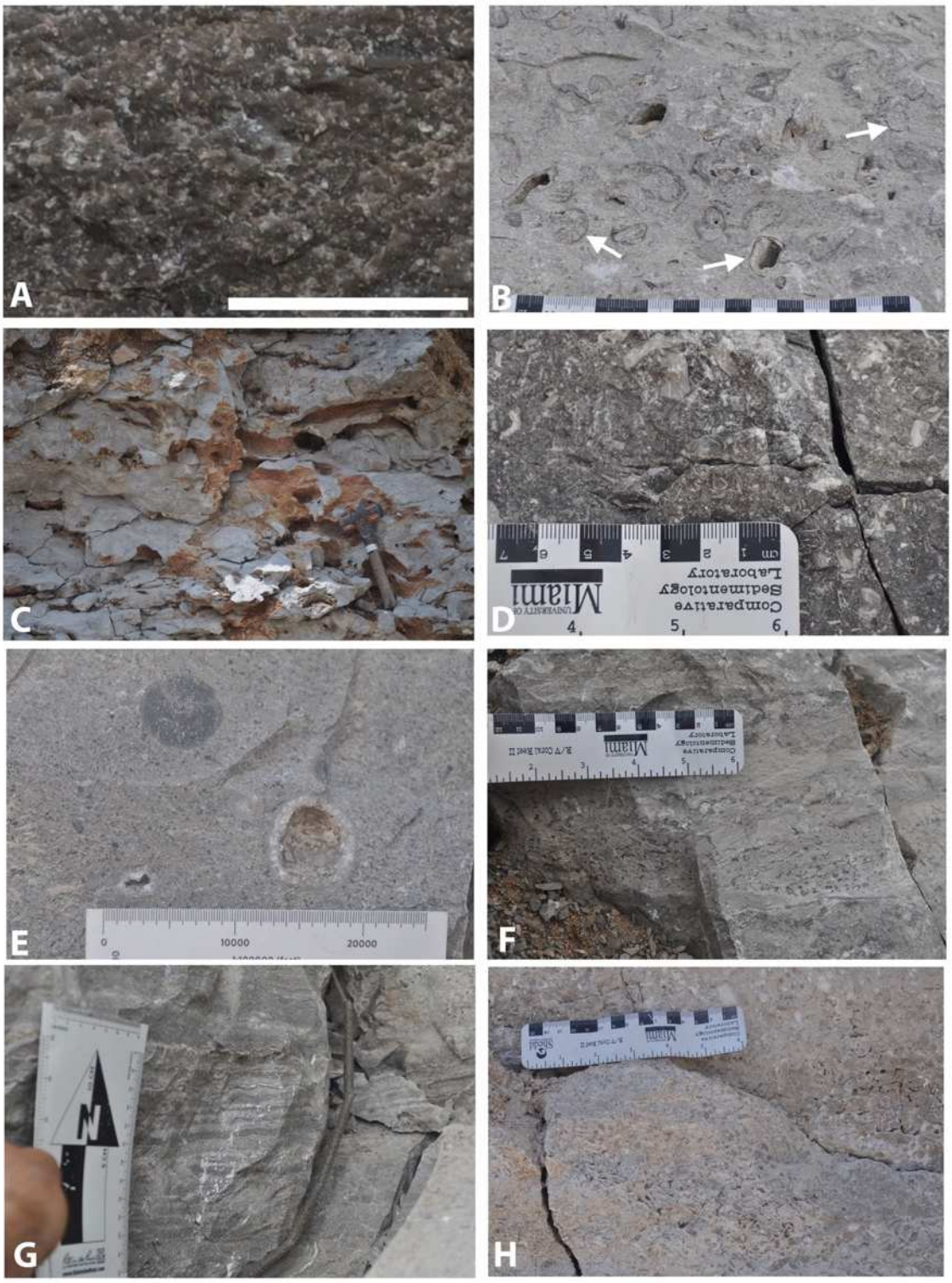

FIG. 2-5: Lithofacies in El Abra Formation. A) Miliolid-peloid lithofacies. White specks are miliolid foraminifers. Scale is 1 cm. B) Requienid lithofacies. Dark outlines (arrows) are outer layer of requienid rudist shells. C) Rudist facies. Internal cavities and molds of recumbent caprinids are dominant. For scale, note the sledgehammer (20 cm). D) Bioclastic facies. E) Skeletal grainstone with *Parkeria sphaerica* preserved as original fabric (top) and a mold. F)

Fenestral lithofacies G) Lamination in cryptalgal laminite. Note alteration of mud- and grain-rich layers. H) Bedded-skeletal grainstone with keystone vugs. Scales in centimeters (major divisions).

shaped rudist concentrations, skeletal remains, in situ arborescent corals, and little mud indicate deposition below mean tide with high energy in the outer margin.

Bedded-Skeletal Lithofacies

Rudist fragments are the most common bioclasts in this lithofacies. The dominant texture is grainstone. Bedded-skeletal facies features rounded grains, good sorting, coarse/fine layering, sub-horizontal bedding, and, locally, keystone vugs (Dunham 1970; Fig. 2-5 H) indicating beach or island deposition.

Peloid-miliolid, requienid, and bioclastic are identical to lithofacies association 1 of Minero (1983), except Minero lumped skeletal grainstone facies into his bioclastic facies. Skeletal grainstone facies are considered a separate facies from bioclastic facies based on comparatively fine-grained grainstone texture, better sorting, and the presence of colonial *Parkeria spaeherica*. Fenestral lithofacies with some minor lumped lime mudstone and cryptalgal facies match lithofacies association 2 of Minero (1983). Bedded skeletal and Rudist-skeletal facies are lithofacies association 3 of Minero (1983).

SUBAERIAL-EXPOSURE CRITERIA

Subaerial-exposure events are important for understanding sedimentology and stratigraphy of shallow-water carbonates. Exposure to meteoric fluids can enhance, degrade, or compartmentalize the pore network in carbonate rocks. Advances made by previous studies provide useful criteria in recognition of fossil subaerial-exposure surfaces (James 1972; Klappa 1979; Esteban and Klappa 1983; Goldstein 1988; Goldstein et al. 1991; Budd et al. 1995). Suites of subaerial exposure features are documented in El Abra Formation that meet the criteria, in part

or entirely, described by previous workers. The most important features are paleosols, rhizoliths, laminated caliche crusts, blackened clasts, pitted truncation surfaces, solution pipes, solution-collapse breccia, and solution porosity.

Paleosols

Paleosols are remnants of ancient soil, formed by exposure of sediment or rock for an extended period of time. Rhizoliths circumgranular cracks, and intraclasts of the underlying rocks, commonly deposited or reworked on an eroded surface, characterize paleosols in El Abra Formation (Fig. 2-6). Desiccation and wetting associated with paleosols led to formation of circumgranular cracks and to autoclastic brecciation. Circumgranular desiccation cracks within this unit are filled with greyish clay-size carbonate and equant calcite cement. The resulting intraclasts are highly variable in size, ranging up to 20 cm (Fig. 2-6B); larger ones are typically associated with thicker paleosol horizons. Seventeen paleosols are recognized in section CM-1 of El Abra Formation (Fig. 2-2). Thickness averages 20 cm and is quite variable within individual units. All of the paleosol horizons extend ~400 m across depositional dip from CM-1 to -2 and traced as much as 800 along quarry walls. No paleosol horizons are documented in PM quarry, which comprises the outer-margin rudstone facies. Paleosol horizons are numerous, but less well-developed in Sierra El Abra quarries further towards the platform interior (Minero 1983).

Rhizoliths

Rhizoliths are defined as organosedimentary structures resulting in the preservation of traces of the roots of higher plants in mineral matter (Klappa 1980). They are sinuous to cylindrical tubes that may be filled with internal sediment or cement (Fig. 2-6A, C-D) (Klappa 1980; Goldstein 1988). Many El Abra rhizoliths are oil stained (Fig. 2-6A and D). Rhizoliths can be discriminated from burrows by their downward tapering, relatively variable sizes, and

downward branching, with accompanying decrease in diameter (Fig. 2-6D). They trend vertically but have various orientations, including horizontal. Diameters average about 2 cm and lengths are highly variable, with maximum about 20 cm. Rhizoliths are common with well-developed paleosols in the CM quarry, but were not observed in PM sections.

FIG. 2-6: Subaerial exposure features from CM-1 section. A) Rhizoliths extending beneath a paleosol horizon (at 11 m in CM-1, Fig. 2-2). Note downward tapering and branching (arrows) B) Close-up of the paleosol horizon in A. Boundary of a clast is traced. C) Rhizoliths extending beneath a poorly developed soil breccia (at 67.3 m in CM-1, Fig. 2-2) D) Abundant, locally branching (arrows), rhizoliths in a float block in CM-1 section (black arrow points to the stratigraphic up).

Laminated Crusts

Laminated crusts are common features of calcareous paleosols (Read 1976; Wright 1989). Crusts were observed along 6 surfaces of subaerial exposure in CM quarry (Fig. 2-2), but are absent from the PM sections. Laminated crusts form irregular surfaces of variable thickness composed of multiple laminae of micrite and sparry calcite that follow paleokarst surfaces (Fig.

2-7A). Laminated crusts are typically associated with brecciated horizons (Fig. 2-7A-C). They are observed to coat walls of some paleocavities in CM-1 to depths reaching nearly 1 m beneath an exposure surface.

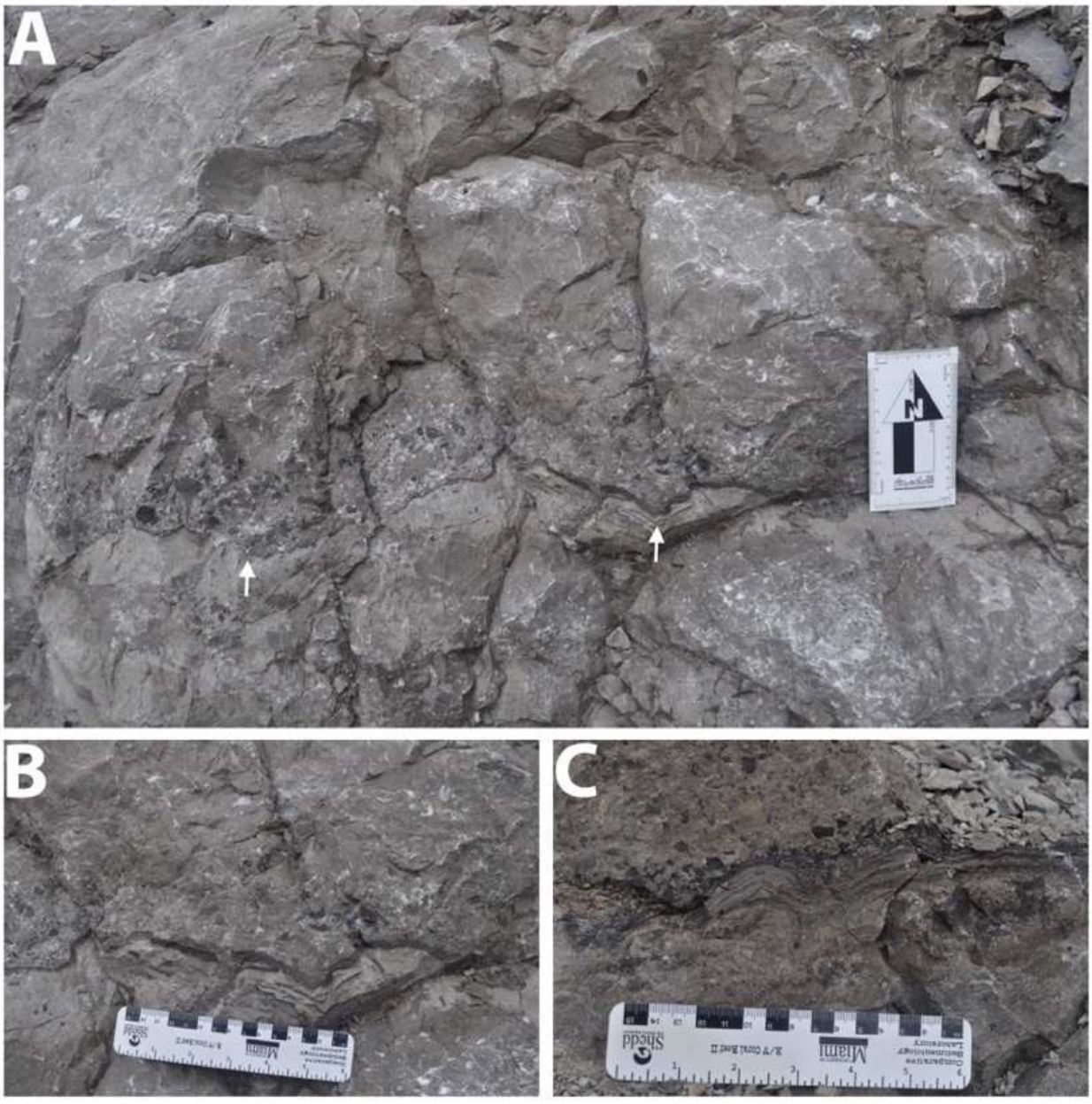

FIG. 2-7: Laminated crusts beneath disconformity. A) Laminated crust (arrows) developed on a solution-modified surface beneath a soil breccia (6.5 m, Fig. 2-2, CM-1). B) Close up of A**.** C) Blackened breccia clasts overlying a laminated crust at a disconformity (12 m, Fig. 2-2, CM-1). Note blackened grains in A and B, as well.

Blackened Clasts

Blackened clasts are a common feature in CM sections (Fig. 2-7 B-C), but are entirely absent from PM sections. The black color can be due to the preservation of sulfides (Goldstein 1988) or charred organic matter in the clasts (Shinn and Lidz 1988). They are not diagnostic exposure features, as they form in other environments as well (Strasser 1984; Shinn and Lidz 1988), but they can provide useful clues to finding an exposure surface.

Crystalline Internal Sediment

Crystalline internal sediment (CIS) reduces both primary and secondary porosity in carbonate rocks. CIS consists of silt-size sediments, some coarse rock fragments (up to sand size), and rare skeletal fragments that are leached from the host rock. CIS is essentially the vadose silt described by Dunham (1969); however, the term CIS is used here to include sand-sized clasts and fossils. CIS is easily recognized along exposure surfaces by a typical grayish appearance in the rock (Fig. 2-8B). Rarely, it is brown, perhaps due to oxidation of contained iron. CIS is voluminous in the Sierra El Abra and occurs beneath most disconformities. Its distinctive texture, color, presence of leached host rock fragments and solution-liberated crystals, occurrence in secondary pores, and greater abundance within 1 m below a disconformity suggests a subaerial origin.

Pitted Truncation Surfaces

Pitted truncation surface in El Abra Formation are a series of connected pits and highs with typical relief of about 20 cm (Fig. 2-8A and C). Some pits penetrate the underlying rock as much as 1 m (Fig. 2-10D). Minero (1983, 1988) interpreted these features as microkarst surfaces. Pits are typically filled with dissolution residue, clasts of the underlying rock, or

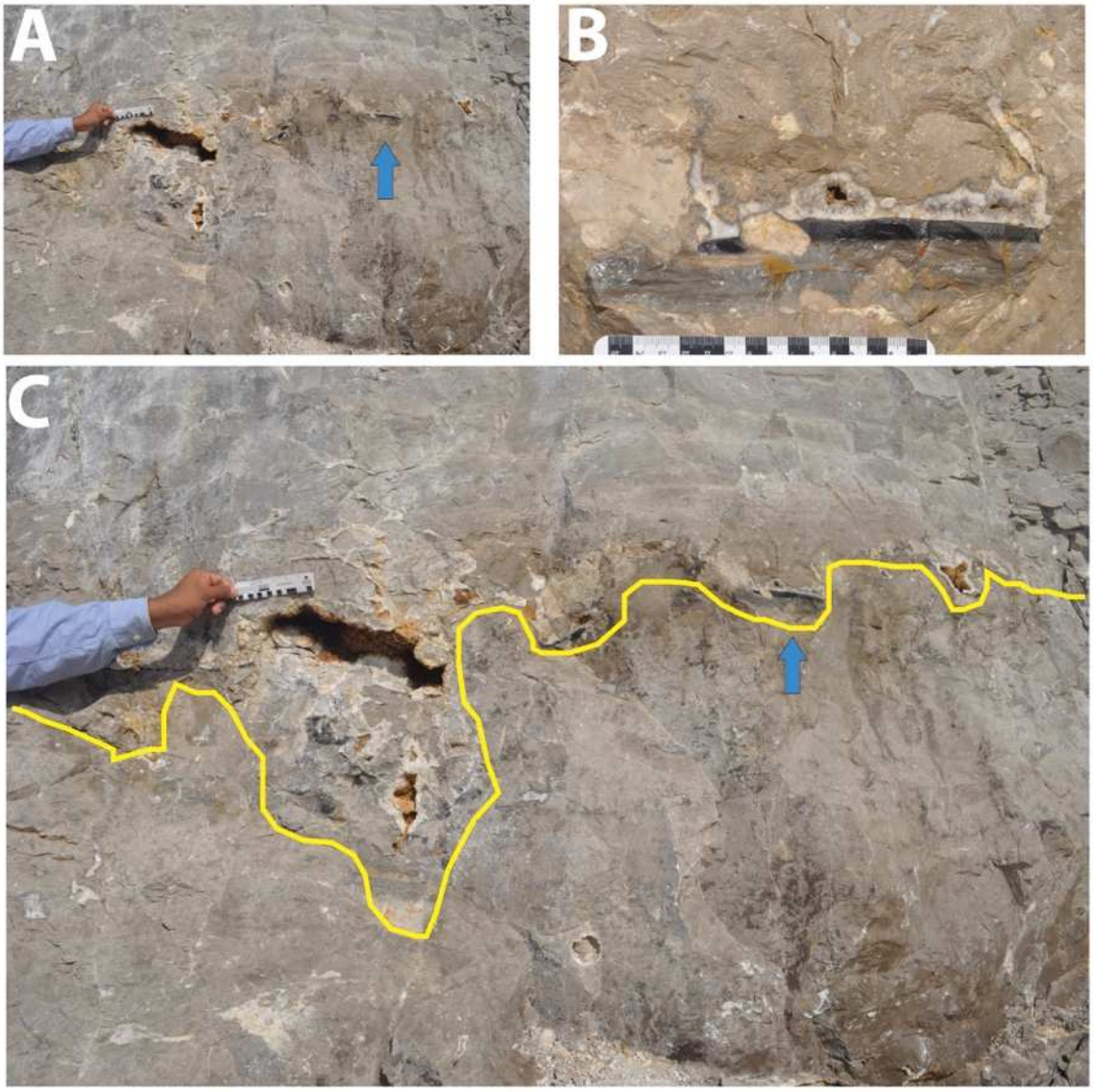

FIG. 2-8: Dissolution and disconformity at 38 m in section CM-1. A and C) Pitted truncation surface (traced) with a bowl-and-funnel morphology. The bowl (beneath scale) is filled in with residue clasts that leached outer later during a major episode of dissolution to form a vug. B) CIS and LEC reduced bowl (arrow in A). The upper part of the CIS is oil stained.

sediment from the overlying cycle (Fig. 2-8 C). Large vugs, molds, paleocavities now filled with lithified sediment and breccia clasts are generally abundant within 1 m below microkarst surfaces, which aids in identifying these microkarst surfaces. Estimated dissolution rates of 16 mm/1000 years (Corbel 1959) and 10.4 mm/1000 years (Land et al. 1967) of limestone in warm humid climate can be cautiously applied to El Abra Formation; a karst surface with the average

relief of 20 cm could then form in 12,000 to 19000 years (using Corbel 1959 and Land et al. 1967 values, respectively).

Solution Pipes

Solution pipes are prominent indicators of karst activity associated with subaerial exposure. Vertical pipes are common in section CM-1; some extend more than a meter, to an underlying unconformity (Fig. 2-9, 2-10A). The pipes are filled with breccia, internal sediment, isopachous cement crusts, and LEC (Fig. 2-9C, 2-10A). Some solution pipes cut several lithologies, resulting in polymictic breccia fill.

Solution-Collapse Breccia

Solution-collapse breccia is the result of removal of underlying carbonate rock that leads to collapse into a vug or cavern, forming a diagnostic feature associated with subaerial exposure (Estaban and Klappa 1983). Solution-collapse breccias fill many cavities of various sizes and shapes within 2 m below an unconformity in CM quarry (Fig. 2-9). The cavities are filled by monomict clasts of the host rock, internal sediment, and cements. Some cavities were filled exclusively with marine sediment making recognition difficult.

Solution Porosity

Carbonate rocks and sediments, upon exposure, are generally subjected to undersaturated meteoric fluids that dissolve the host carbonate to reach solution equilibrium (Bathurst 1976). Molds and vugs are the dominant resulting pores in El Abra Formation (Fig. 2-10A-C and E), concentrated in the first meter or two beneath exposure surfaces. Molds of bivalves and green algae are the most common. The interior aragonite layer of rudist bivalves is the largest-scale victim. Solution enlargement of molds or primary pores results in vugs. Large vugs are most

common in the laterally extensive rudist grainstone and rudstone of the outer margin (Fig. 2-11). Non-fabric-selective dissolution of the matrix results in paleocavities that later collapse or is filled with internal sediments, intraclasts, and cements. Minor solution pores include solution-enlarged fenestrae and rhizomolds. Distribution of solution porosity aids in identifying surfaces of subaerial-exposure in the outcrop.

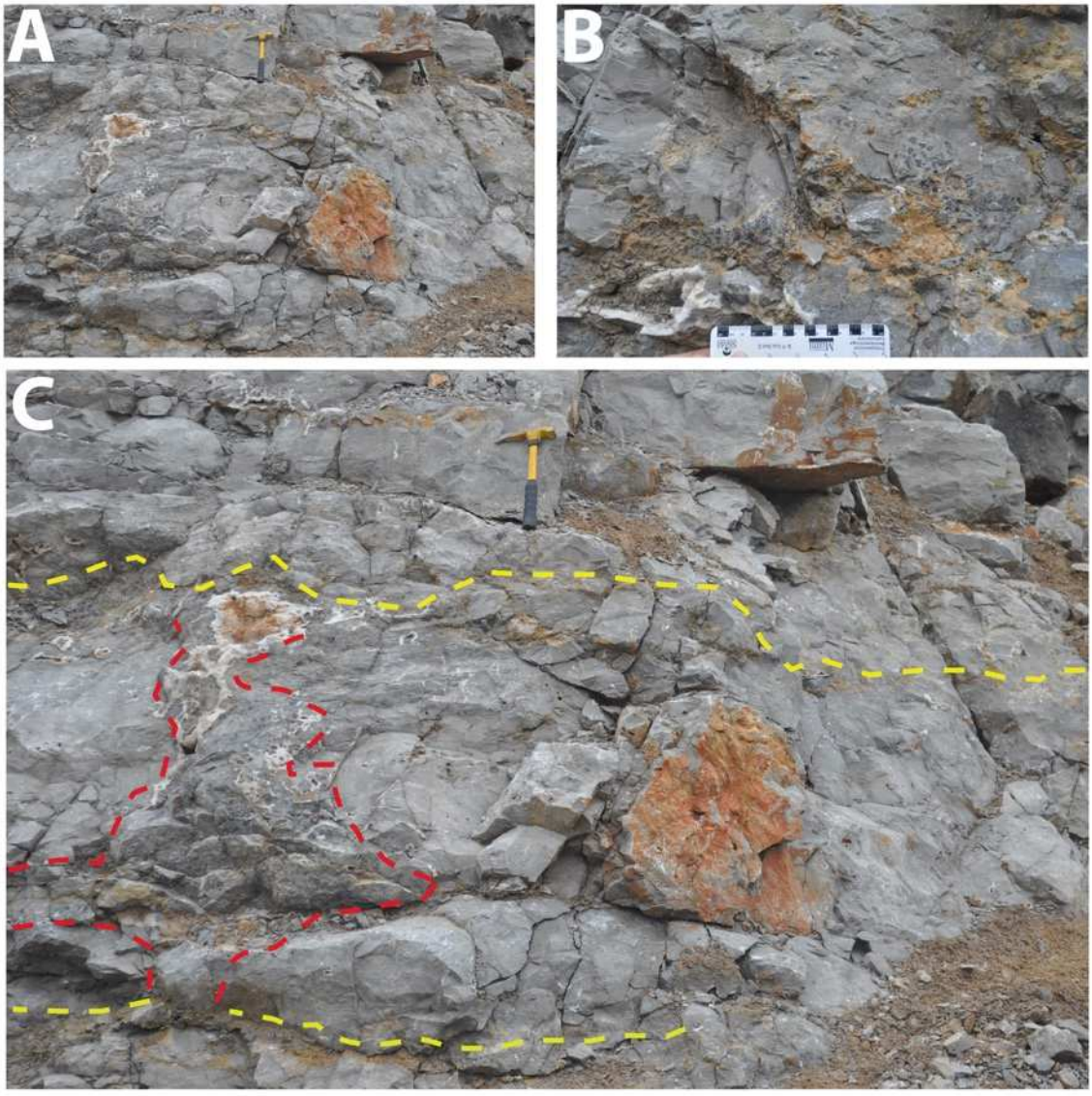

FIG. 2-9: Solution pipes and solution-collapse breccia. A) Solution pipe extends from disconformity (26.2 m, CM-1, Fig. 2-5) above to the underlying disconformity (24.8 m) Details in C). B) Solution-collapse cavity filled with breccia and late equant cement. C) Solution pipes (red) and disconformities (yellow) in A are traced. The pipe is filled with breccia clasts from the overlying lithology. Reddish staining resulted from Holocene weathering.

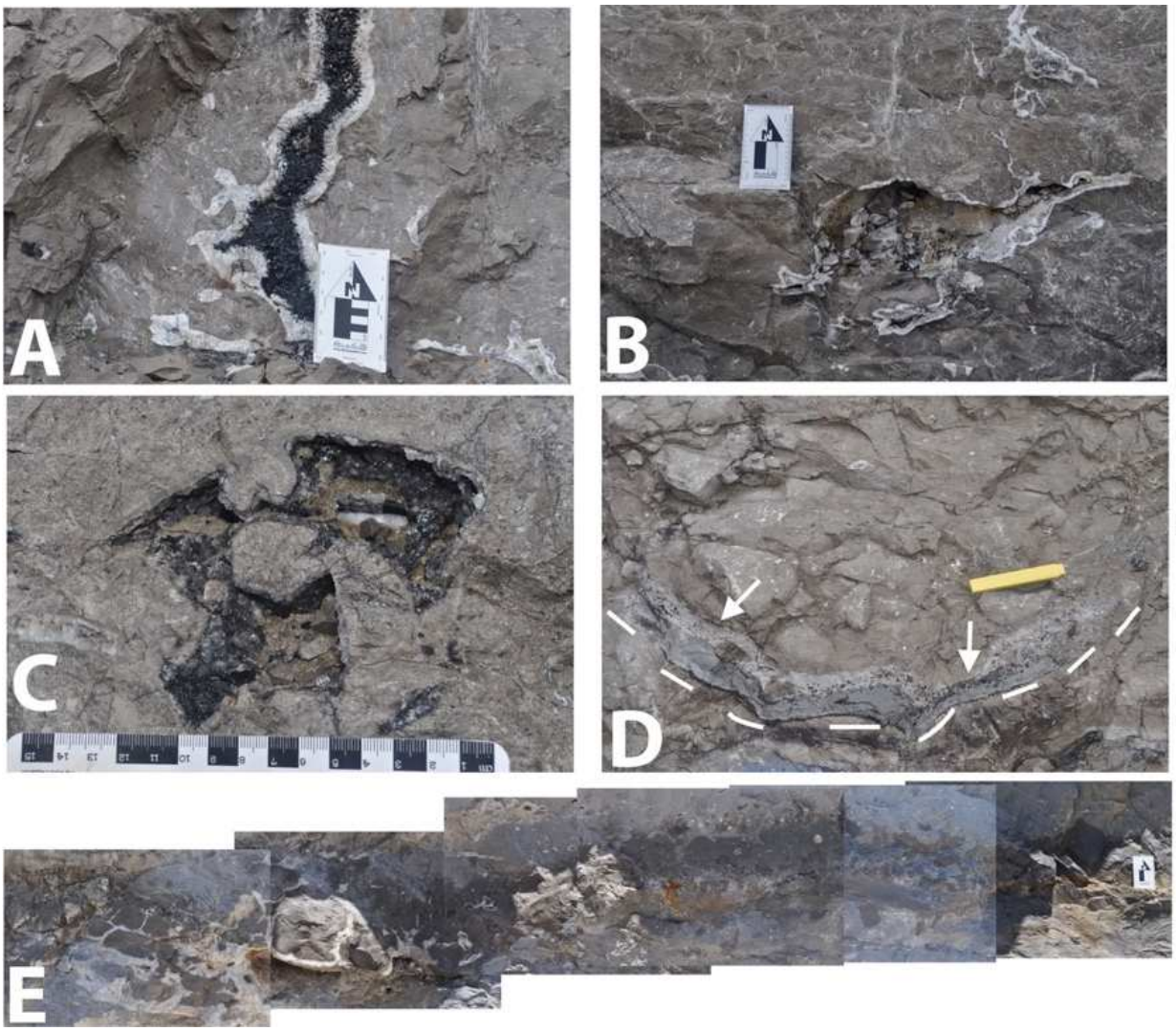

FIG. 2-10: Microkarst surfaces and secondary porosity in CM-1. A) Channel pore reduced by late equant cements and oil residue in the center of the pore (22 cm, CM-1) B) Mega-vug (Choquette and Pray 1970) is 30 cm in length, is only slightly reduced by late equant cement (7.2 cm, CM-1). C) Rudist mold partially reduced by coarsely crystalline, late equant cement (8 cm, CM-1). D) A karst surface (15 m, CM-1) (dashed) truncates the underlying strata to a depth of 1 m. Residue from dissolution overlies the surface. Marine sediment fills depression (arrows) and is underlain by clasts that formed from erosion of the underlying bed. Scale is 30 cm. E) Disconformity (29.3 m, CM-2) with poorly developed soil breccia and associated solution porosity. Scale is 20 cm.

FIG. 2-11: Extensive moldic and vuggy porosity in the reef facies of El Abra Formation in PM-1 section, 22-24 m. Solution enlarged Fractures (SxFR of Choquette and Pray 1970) are modern weathering. Length of hammer is 30 cm.

END MEMBERS AND SPATIAL VARIATION OF SUBAERIAL EXPOSURE

Two end members of subaerial-exposure expression (Esteban and Klappa 1983, p. 5) terminate cycles in El Abra Formation. First, karst surfaces overlie cycles at different points in their evolution and develop varying magnitudes of truncation (Figs. 2-7, 2-8, 2-9, and 2-10D). In some examples vertical voids and solution pipes extend down to a depth of nearly 1 m beneath the exposure surface (Fig. 2-10A). Second, paleosol horizons also developed during different stages of the cycle evolution in El Abra cycles at CM-1 section (Fig. 2-2). A paleosol penetrated by roots is the typical expression of subaerial exposure (Fig. 2-6 A, C-D), but other features such laminated crusts and blackened clasts also contribute to pedogenic expression of subaerial exposure (Fig. 2-7). Combination of the end member processes, i.e. dissolution and pedogenic

processes, also occur. An example is laminated caliche crust overlying a solution-modified surface (Fig. 2-7 and 2-10D-E).

The morphology of the steep-sided Valles-San Luis Potosí (V-SLP) platform resulted in spatially variable subaerial conditions upon emergence, recognizable by variations in the distribution of subaerial exposure features. The tidally influenced deposits of CM-1 section are transected by 27 surfaces of subaerial exposure that are laterally continuous throughout the 800-m expanse of the quarry. In contrast, very few and equivocal features of subaerial-exposure were observed in the outer margin (PM) (Fig. 2-3). However, stratigraphic intervals with extensive solution porosity make a subtler, yet compelling, case for subaerial exposure. Five such intervals occur in PM sections (Fig. 2-3) and can be correlated to CM sections, suggesting that some surfaces of subaerial exposure extended across the margin and exposed the outer margin to meteoric diagenesis (Fig. 2-4). The varied suites and distribution of subaerial exposure features have implications in understanding the paleomorphology of the carbonate platform, as discussed later in this paper.

PUNCTUATED CYCLIC SEDIMENTATION

The paradigm for cyclic sedimentation was established in classic works of Sander (1936, 1951), Schwarzacher (1948, 1954), and A.G. Fischer (1964, 1975) on the Upper Triassic Lofer cyclothems in the Dachstein Limestone of the Northern limestone Alps. Equivalents of Fisher's (1964) dABC units and the B1/B2 subdivisions of Goldhammer et al. (1990) are recognized in El Abra Formation, so this terminology was adopted. Briefly Fisher (1964) interpreted unit C as subtidal, B as tidal, A as soil, and d as disconformity. Goldhammer et al. (1990) formalized B1, laminated loferite, and B2, homogeneous loferite, as subfacies, following the layering distinction

already noted by Fischer (1964). “Loferite” was Fischer’s designation for rocks riddled by fenestrae and desiccation cracks.

Unit C

Unit C in sections CM-1 and CM-2 of El Abra Formation consists of unstratified beds with diverse biota, extensive bioturbation, abundant mud, and a predominance of miliolid foraminifera and peloids. Miliolid-peloid, requienid, rudist, bioclastic, and skeletal grainstone lithofacies comprise unit C. Unit C forms 36% of the total thicknesses of section CM-1, with a calculated mean of 1.0 m (Fig, 2-12A). In sections PM, unit C is composed mainly of rudist floatstone and rudstone facies to nearly 80% of total thickness.

Unit B

Unit B in El Abra Formation is essentially the cryptalgal-laminite, fenestral, and bedded-skeletal lithofacies. Subunit B1 is characterized by cryptalgal laminite, 30 cm thick on average in section CM-1, and 5.8% of the total section. In CM-2 section, B1 units are present, but not measured, due to difficulties in accessibility of the vertical wall. B1 is absent from the outer margin (Fig. 2-3). Subunit B-2 is the fenestral lithofacies in El Abra Formation. It comprises 32 % of the CM-1 section, with average thickness of 80 cm. In the CM-2 section, B-2 was observed; however, accessing a vertical wall limited its quantitative measurement. No B-2 unit was deposited on the outer margin. A subunit B-3 is introduced here to distinguish the bedded-skeletal facies that have abundant keystone vugs, indicating deposition on a beach or sand island. B-3 is only documented in the outer margin, where it comprises nearly 20 % of the PM-1 section and 12 % of the PM-2 section.

Goldhammer et al. (1990, p. 552) explicitly considered subunit B2 overlain by subunit B1 to represent a shoaling-up vector, with some support from their analysis of stacking patterns.

However, the main distinction between B1 and B2, lamination, is not an infallible indicator of deposition relative to high tide, commonly expressed in terms of intertidal and supratidal. In the sub-humid climate of the Bahamas, algal laminites occupy the uppermost intertidal and lower supratidal zone (Shinn et al. 1965; Ginsburg et al. 1977), but in the arid climate of the Arabian Gulf and Western Australia, they are confined to the upper intertidal zone (Logan et al. 1974). Fenestrae, along with other shrinkage cracks, the definitive character of "loferites," (Fischer 1964) are also restricted to supratidal and upper intertidal settings (Shinn 1968). All subunits within B are thus deposited in the upper intertidal or supratidal zones. Therefore, attempting to distinguish intertidal from supratidal facies or derive a shoaling vector from B1 and B2 sequences appears highly questionable. The importance of this distinction - rather, the lack thereof – is apparent in considering cycles and rhythms in El Abra Formation.

Unit A

Unit A in El Abra Formation consists of paleosols and laminated caliche crusts, found in 17 cycles in the inner margin. No units A were recognized in the outer margin sections (Fig. 2-3). The thickness of paleosol horizons is variable, however most are locally at least 20 cm thick. Paleosols typically contain intraclasts eroded from the underlying unit (Fig. 2-6B).

Disconformity (d)

Disconformities in El Abra Formation are associated with karst features or paleosols (unit A). In CM-1 section 27 disconformity surfaces have been documented with an average spacing of 2.7 m (Fig. 2-2, 2-12 B). Seventeen disconformity surfaces are marked by well-developed soil horizons, and ten by karst features with variable amounts of relief (Fig. 2-2). In PM-1 and PM-2 sections only five probable disconformities are recognized (Fig. 2-3, 2-4). No merging or bifurcation of disconformities was noted in tracing surfaces laterally within the quarries. Fischer

(1964) placed the disconformity at the base of his idealized cycle, to be overlain in gradational sequence by units A, B, and C, i.e. a deepening-upward cycle. This generalization has been little noted nor long remembered by the innumerable sedimentologists who have related Fischer's seminal work to other cyclothems worldwide, invariably interpreted as shoaling upward, correctly in most cases, it appears. Whether a disconformity is considered to lie at the base of a paleosol or at the top seems rather arbitrary, but where a subtidal unit (C) overlies a paleosol, the common case in El Abra, it seems clear that the depositional vector changes with the deepening event marked by that contact, so this is the logical disconformity horizon. By the same reasoning, in the sequence …CdABC…, Fischer's idealized cycle, the vector reversal is at the C\A contact, so this is where d should be placed; in this case, beneath the paleosol.

Cycles and Rhythms in El Abra Formation

Sediments of El Abra Formation were deposited in three different stacking patterns: shoaling-upward cycles, truncated cycles, and rhythms (Fig. 2-2. 2-3). The cycles in El Abra Formation differ from Fisher's (1964) idealized deepening-upward cycle (dABCd). All cycles that have a depth vector show shallowing-upward trends, e.g. CBAd (Fig. 2-2, 2-3). Nine shoaling-upward cycles, 20 truncated cycles, and 10 rhythms were logged in CM-1. Five truncated cycles and 5 rhythms are logged at PM-1 (Fig. 2-3, 2-4).

Shoaling-Upward Cycles.—— Shoaling-upward cycles in El Abra Formation start with subtidal unit C, which is conformably overlain by unit B or B1, or both, in varying order, and terminated by unit A (paleosol) and/or a paleokarst surface, d. The thicknesses of shoaling-upward cycles range from 1.4 m to 4 m at CM-1. No shoaling-upward cycles were recorded in the outer margin.

Truncated Cycles.—— Truncated cycles in El Abra formation are cut by disconformities at various stages of the cycle, before completion of the ideal shoaling-upward cycle. Such punctuated sedimentation is recognized in 20 cycles at CM-1, ranging in thickness from 1 to 4 m, and 5 cycles in PM-1m 2.5 to 7.2 m thick. Fourteen out of the twenty one cycles in CM-1 are truncated by paleosol horizons and karst surfaces truncated 7 cycles (Fig. 2-2). Disconformities that truncate cycles in PM-1 are subtle; they are underlain by concentrations of secondary pores and are only tentatively correlated with disconformities with CM sections (Fig. 2-4).

Rhythms.—— Rhythms are composed of repetitions of units B and C without the intervention of a disconformity (Enos and Samankassou, 1998, p. 201). They possess no definitive depth vector i.e. they can be interpreted as deepening up (BC) as readily as shoaling up (CB). Rhythmic sedimentation in El Abra Formation deposited some of the thickest intervals in CM-1 (Fig. 2-2, 2-3), as they are composed of ten rhythmic couplets. The outer margin recorded 2 rhythmic couplets (Fig. 2-3).

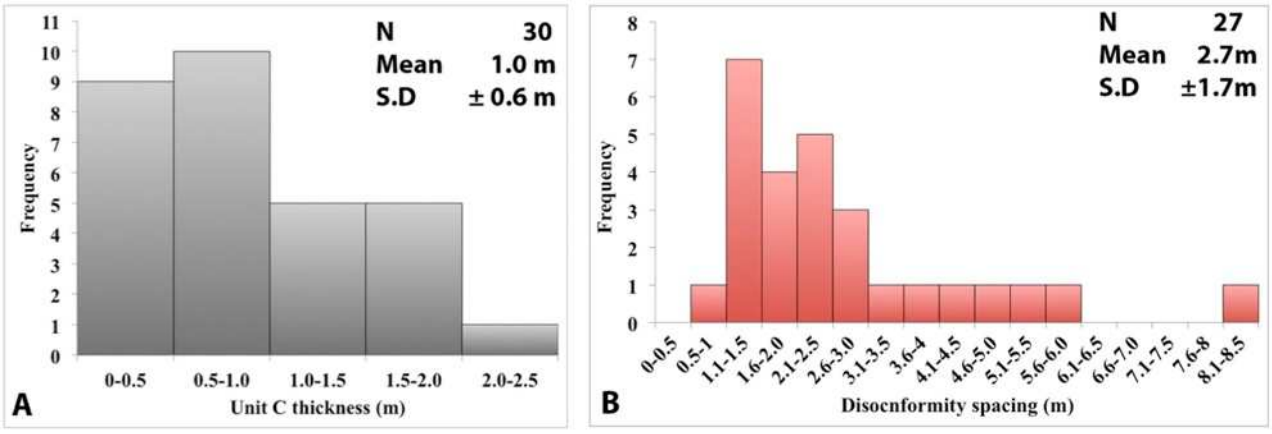

FIG. 2-12: A) Thickness of units C in CM-1. B) Spacing of disconformities in CM-1. N is number of measurements. S.D. is standard deviation.

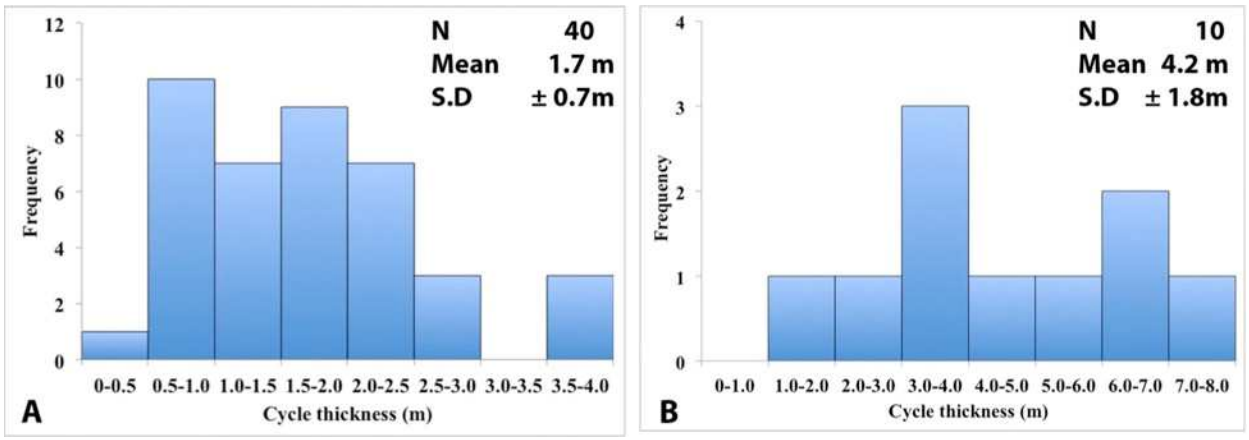

FIG. 2-13: Cycle thickness data from El Abra Formation. N is number of cycles and S.D is standard deviation. A) Cycle thickness from CM-1. B) Cycle thickness from PM-1. Shallowing upward, truncated and C-B couplets in rhythmic intervals are included in total number of cycles in both A and B.

DIAGENETIC HISTORY OF EL ABRA FORMATION

Superposed marine phreatic and meteoric diagenesis in varying order, shallow-burial diagenesis, diagenesis at elevated temperature and pressure, and diagenesis after uplift of El Abra Formation into the meteoric environment resulted in at least 21 diagenetic products, which are discussed below in order of occurrence (Fig. 2-14).

Micrite Envelopes and Micro-Borings

Micritization of skeletal grains by microbial organisms such as endolithic algae, fungi, or bacteria occurs on the sea floor, creating micrite envelopes (Bathurst 1966; Tucker and Wright 1990) (Fig. 2-15A). Thickness of micrite envelopes in El Abra Formation ranges up to about 100 μm. Micro-borings are primarily borings by sponges (Fig. 2-15B). They are filled with micrite and equant calcite cement. Large (>2mm) skeletal fragments, in particular mollusks, are extensively bored. Micro-borings and micrite envelopes are more common in the outer margin (PM) compared with the tidally influenced (CM) deposits of El Abra Formation.

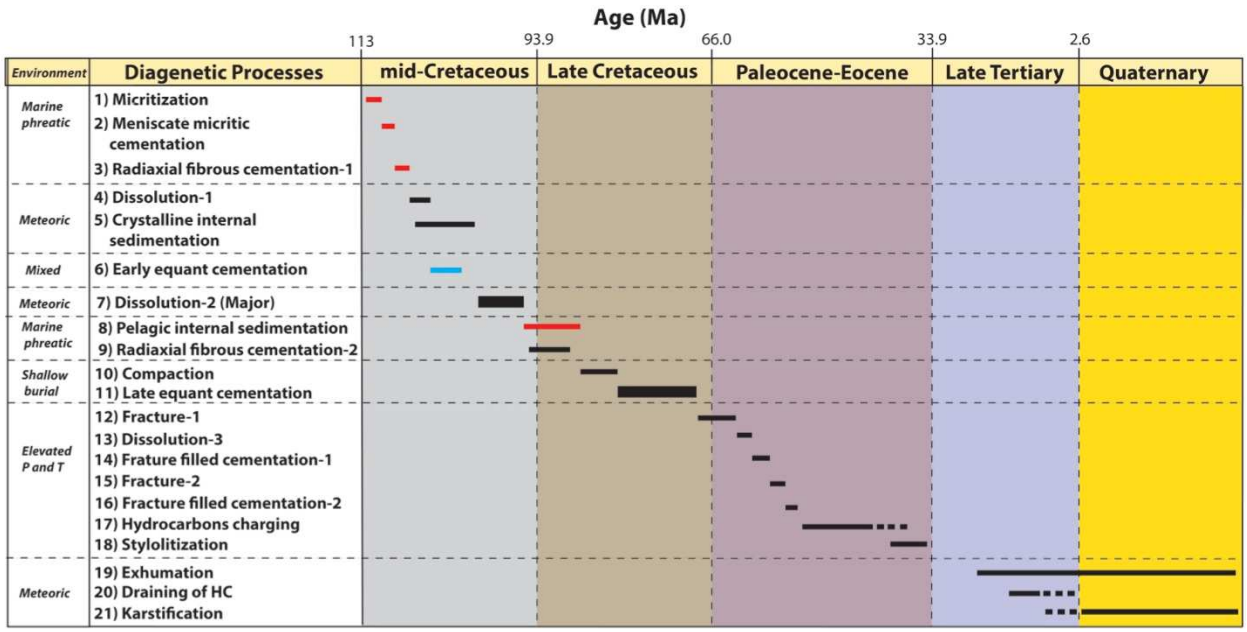

FIG. 2-14: Paragenetic sequences in El Abra Formation. Vertical axis records environments and their diagenetic products. Horizontal axis is time (Gradstein et al. 2004), not to scale. Thicker bars for products 7 and 11 emphasize the intensity of these two events; it is not a quantitative representation. Due to cyclic nature of El Abra deposition and subaerial exposure, meteoric and marine phreatic environments are juxtaposed multiple times with varying expression in inner-margin rocks. However, for simplicity only one common sequence of events is presented. RFC-1 (red bar) occurs only in outer margin and EEC (blue bar) only in inner margin. Thus they are not juxtaposed, although they must have overlapped in time, as each one kept pace with sedimentation. Meniscate micritic cements and pelagic internal sediments are restricted to the outer margin (red bars). Timing of hydrocarbon charging and drainage is based on the study of Brennan (1999) and Yurewicz et al. (1997).

Meniscate Micritic Cement

Meniscate micritic cement in El Abra Formation primarily reduced intragranular porosity and is restricted to the outer margin rocks (Fig. 2-16). Their abundance reaches to a mean of nearly 2% in the outer margin. Dunham (1971) documented meniscus fabrics in calcite cements forming in meteoric vadose environments. However, modern examples of meniscus-type micrite cements from Wood Cay, Bahamas, are interpreted as subtidal by Halligärtner et al (2001) based on their relatively uniform thicknesses, absence of pendant fabrics, associations with marine hargrounds, and lack of other vadose features such as root structures. Mensicate micritic cements in El Abra Formation also show relatively uniform crust thickness, faint laminations

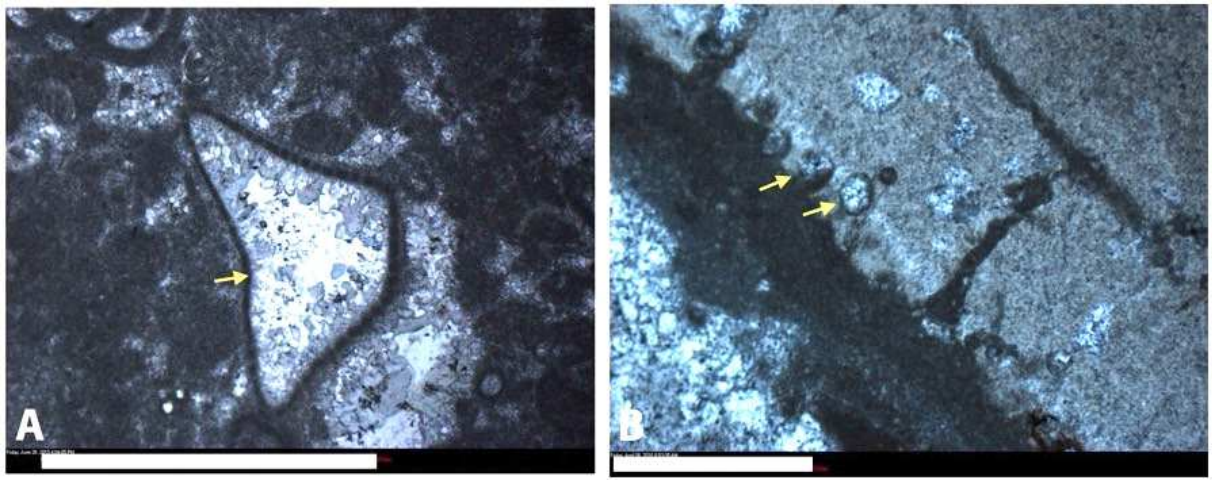

FIG. 2-15: Micrite envelope, micro-borings, and micrite cements. Scale bars are 2mm. A) Micrite envelope (arrow) preserves the mold of a skeletal fragment (51.5 m, CM-1). B) Sponge borings (arrows) in a skeletal fragment in PM-1. A dark encruster coats the skeletal fragment (6.5 m, PM-1).

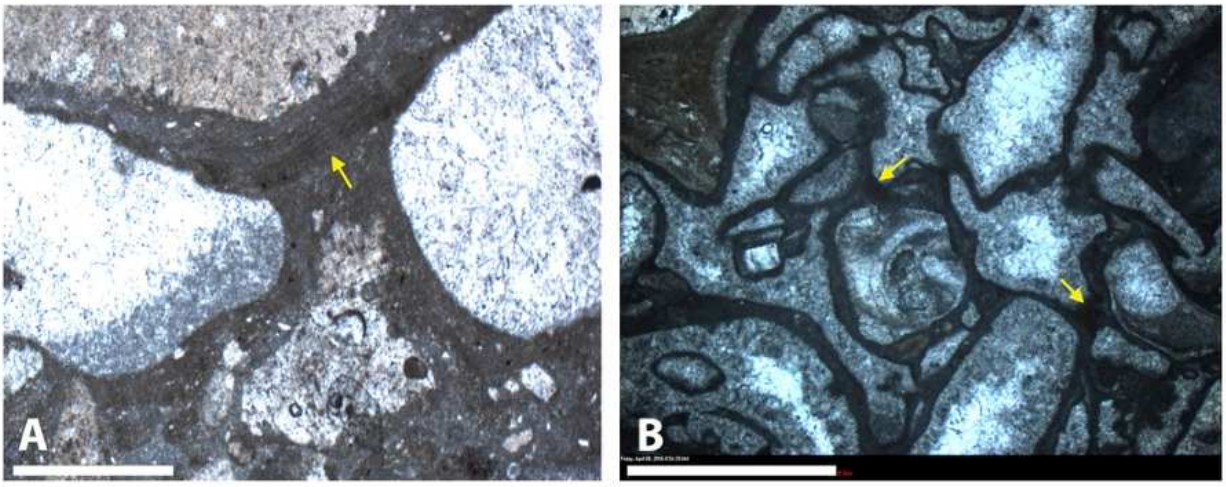

FIG. 2-16: Mensicate micritic cements in El Abra Formation. A) Meniscate micritic cements around skeletal fragments (5.0 m, PM-1). Note indistinct laminations in the micritic layer which may be microbial cement or a possible encrustation (arrow). B) Micrite cement with meniscus fabric and bridges among grains (6.5 m, PM-1). Photograph A and B are from PM-1.

(Fig. 2-16A) of probable microbial origin, and absence of pendant fabrics or root structures. Moreover, they predate RFC-1 in primary intragranular pores (Fig. 2-16B). The above observations suggest a probable marine origin of meniscate micritic cements.

Early Radiaxial Fibrous Cement (RFC-1)

Radiaxial fibrous cement forms isopachous crusts of turbid crystals characterized by concave-outward twin lamellae, optic axes that converge away from the substrate, and sub-crystals that diverge in the same direction (Kendall and Tucker 1973; Kendall 1985; Flügel 2004; Richter et al. 2011). RFC-1 is restricted to the outer margin, occurs in primary intraparticle and interparticle pores (Fig. 2-17A-B), and probably overlaps in time with intraformational dissolution, deposition of CIS, and precipitation of EEC during exposure of the inner margin. A minor variant of RFC-1 is characterized by fibrous or bladed crystals with flat terminations. The flat terminations are typical of aragonite crystals, but unknown in calcite; this suggests alteration from precursor aragonite (Tucker and Hollingworth 1986, p. 276).

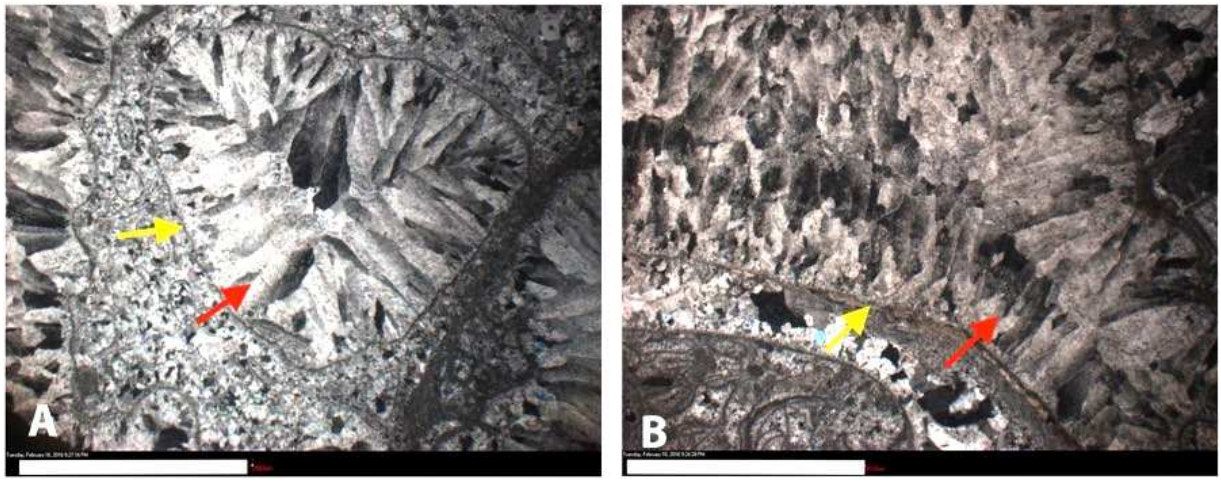

FIG. 2-17: Crossed polarized images of early generation of radiaxial fibrous cement (RFC-1) in the outer margin (10.1 m, PM-1). A & B) RFC-1 (red arrow) occludes an intragranular pore (rudist chamber, denoted by yellow arrow). Scale bar is 500 μm.

Dissolution (D-1)

Cyclic early episodes of dissolution in El Abra Formation affected rocks predominantly in the inner margin, introducing small-scale secondary porosity (sxFE, sxBP, VUG, and MO). The porosity created was later filled with CIS and EEC. This dissolution and cementation were largely restricted to the inner margin, suggesting small meteoric aquifers that developed during

intraformational subaerial exposure. The inner margin of El Abra Formation was punctuated 27 times by subaerial exposure surfaces, therefore subaerial diagenesis and marine diagenesis were superposed multiples times leading to a complex pattern of early diagenesis.

Crystalline internal sediment (CIS)

CIS in El Abra Formation reduces and locally fills some primary and small secondary pores formed during initial dissolution (D-1). CIS is also rarely observed in fenestrae and intraparticle pores. It both predates and postdates EEC in the inner margin. It overlies RFC-1 in the outer margin. It rarely contains small, unrecognizable skeletal debris and intraclasts leached from the host rock (Fig. 2-18B). It appears light grey in plan-polarized light. The sediment-cement interface of CIS is generally horizontal, producing geopetal fabrics; however, some are sloping or possess minor relief (Fig. 2-18A, C, and D), possibly reflecting deposition by currents (Dunham, 1969). The lower boundary of CIS with the pore wall is typically irregular, indicative of some prior dissolution. CIS abundance is largely determined by pore connectivity; it can be absent in the adjacent pores of same origin in the same thin section. CIS is abundant up to 2 m below a disconformity and reduces 9% of the secondary porosity (1.9% of rock volume) introduced during D-1 in the inner margin. In the outer margin CIS reduces only 1.2% of secondary porosity.

Early Equant Cement (EEC)

EEC is the first-pore filling cement in inner margin rocks (Fig. 2-19). The crystals exhibit uniform extinction. Inclusions are abundant in the small crystals at the pore walls, resulting in a cloudy appearance of the cements (Fig. 2-19B). EEC postdates successive dissolution events (D-1) that occurred during intraformational subaerial exposure. The dissolution resulted in

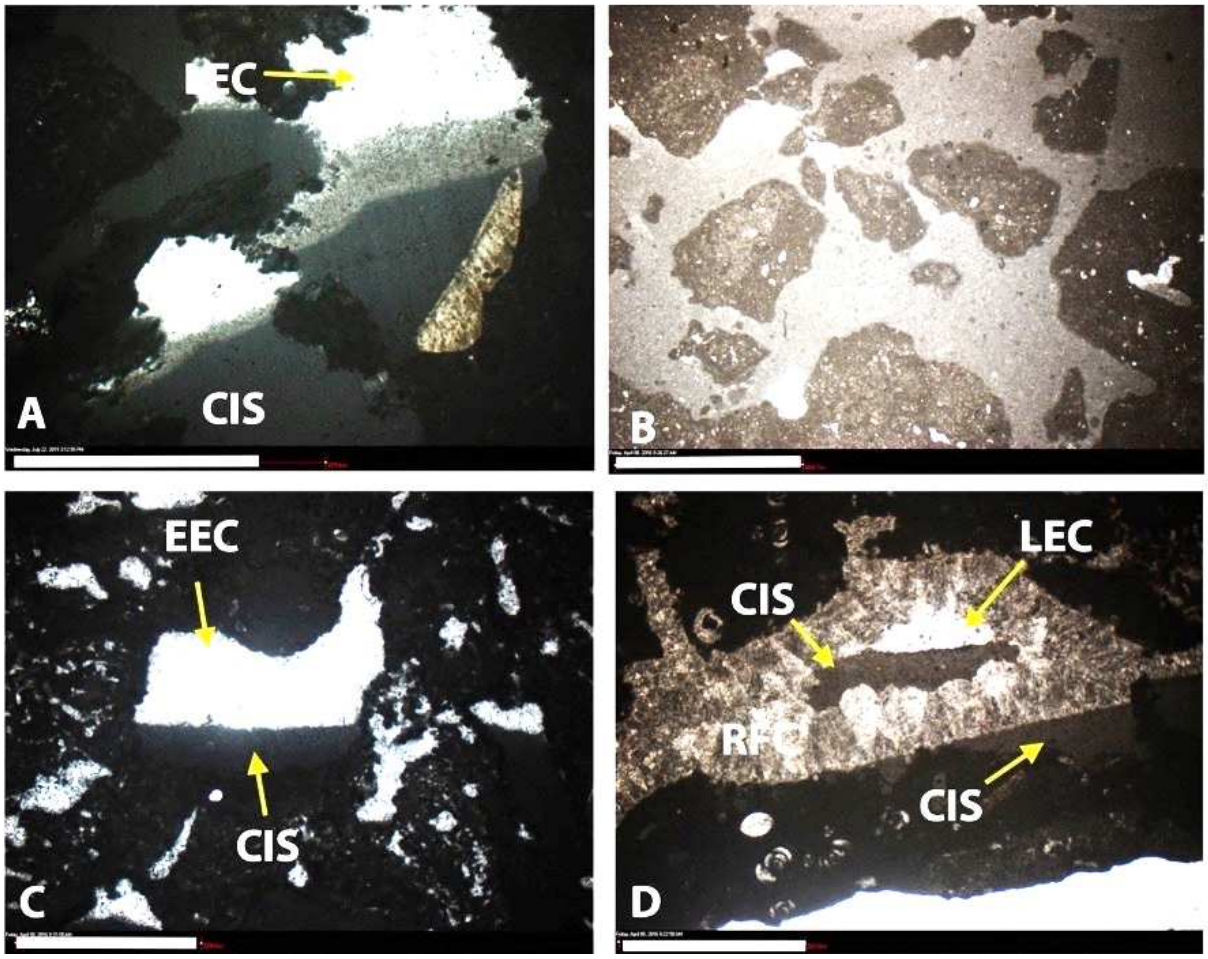

FIG. 2-18: Internal sediment from CM-1. Scale is 1 mm for all images: A) Two generations of CIS (vadose silt, Dunham, 1969) in a solution-enlarged pore is overlain by late equant cement (LEC) (4.6 m, CM-1). B) CIS in a vug with both silt-size sediment and very-coarse sand-size intraclasts (67.3 m, CM-1). The coarse sediment is leached out of the host rock. C) EEC overlies CIS in solution-enlarged fenestra (1.8 m, CM-1. D) An early generation of CIS in a large vug is overlain by RFC-2, which is overlain by a later generation of CIS (11.5 m, CM-1). LEC fills the rest of the pore space.

enlargement of primary porosity (sxFE and sxBP of Choquette and Pray 1970) and leaching of grains to create small megavugs and molds (smgVUG, smgMO). EEC also reduces paleosol porosity such as rhizoliths, desiccation cracks, and pores in conglomeratic clasts. EEC is observed only in inner-margin rocks of CM-1 section. Twenty-one growth zones are documented in EEC using cathodoluminescence petrography (Chapter III, p 23). Cathodoluminescence zones show cross-cutting relationships with disconformities, further evidence of intraformational origin

of EEC. Fluid-inclusion assemblages yielded salinity values ranging from 0 ppm to 49 ppt with clusters indicating precipitation from freshwater, evaporated water, normal seawater and various mixtures (Chapter III).

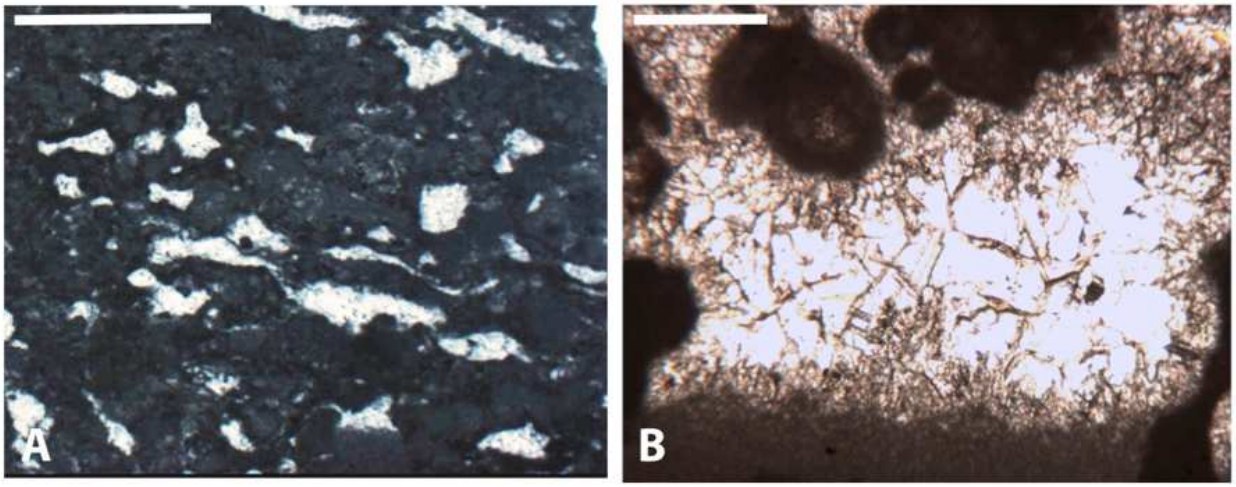

FIG. 2-19: Early equant cement in CM-1: A) EEC in fenestral pores (5.3 m, CM-1). Scale bar is 500 μm. B) EEC in sxFE, overlying crystalline internal sediments (1.8 m, CM-1). Scale bar is 200 μm.

Dissolution (D-2)

A second and more extensive episode of dissolution created large secondary pores, pervasive both in the inner and outer margin of El Abra Formation, including some cavernous porosity. A paleocave near PM-2 section, measures nearly 2 m vertically and about 4 m across; it was filled by miliolid mudstone. This episode of dissolution probably occurred during the late Cenomanian (before the Turonian transgression) in a regional meteoric aquifer, at least the size of the exposed Sierra El Abra, as it impacted both the inner and outer margins.

Pelagic internal sediment (PIS)

Pelagic internal sediment contains planktonic fossils, skeletal fragments, and lime mud (Fig. 2-20). The texture is mostly mudstone or wackstone. PIS are largely absent from small-scale secondary pores, perhaps reflecting better pore connectivity in larger pores. It is abundant

in the outer-margin quarry (PM), but missing from inner margin rocks (CM). PIS can be differentiated from CIS based on fossil abundance and type, darker appearance, relatively coarse texture and position in the paragenetic sequence. It both predates and postdates radiaxial fibrous cement (RFC-2) and predates late equant cement.

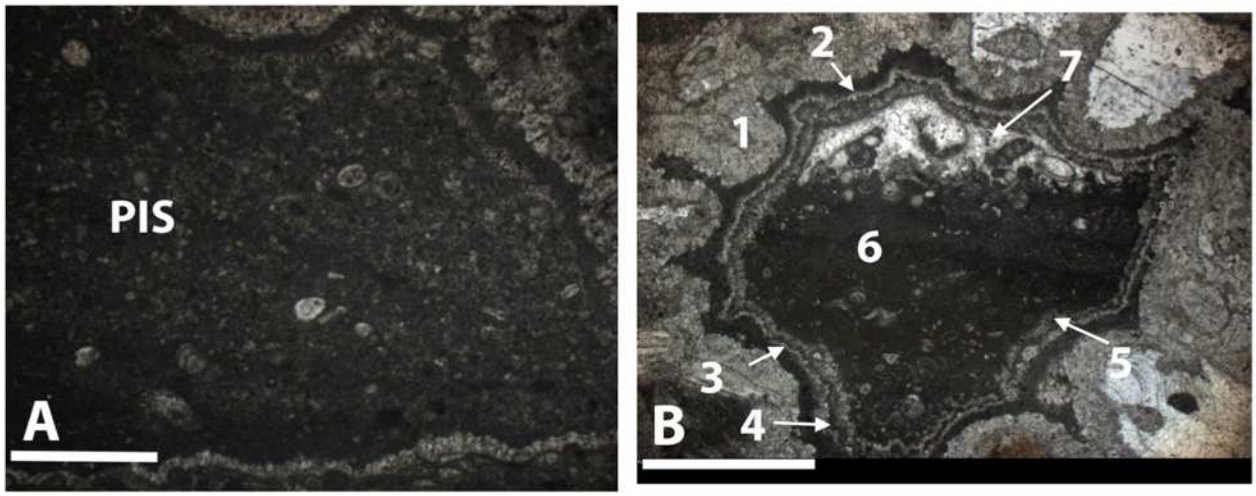

FIG. 2-20: A) Pelagic internal sediment postdates isopachous crusts of cement and reduces a large vug. B) Complex pore reduction in a vug: 1) Isopachous crust of cement (RFC-2). 2) Micrite cement with subtle meniscus ?? fabric. 3) Second banded quasi-isopachous fibrous crust. 4) A thin layer of micrite cement or micritization of second crust. 5) Third isopachous crust. Cements 1, 3, 4?, & 5 show uniform thicknesses that suggest marine phreatic origins. 6) Pelagic internal sediments reducing considerable volume of the pore space. 7) Late equant cement occluding the pore space. Scale bars are 2 mm. Photograph A and B are from PM-1 section at 16.6 m.

Late Radiaxial Fibrous Cement (RFC-2)

A second generation of radiaxial fibrous cement (RFC-2) occurs in secondary pores in both the inner and outer margin of El Abra Formation (Fig. 2-21). A more complex history appears in some samples from the outer margin (PM) where multiple generations of RFC-2 alternate with micritic cements and PIS (Fig. 2-20B). Cathodoluminescence petrography revealed splotchy luminescence in radiaxial fibrous cements (RFC-1 and -2). Such luminescence has been ascribed to neomorphic alteration of a precursor high-Mg calcite to a more stable low-Mg calcite, preserving its orignal fabric (Lohman and Myers 1977; Videtich 1985; Reinhold and

Kaufmann 2010). Marine origin of radiaxial fibrous calcite is documented by Kendall (1985), Sandberg (1985), and Saller (1986).

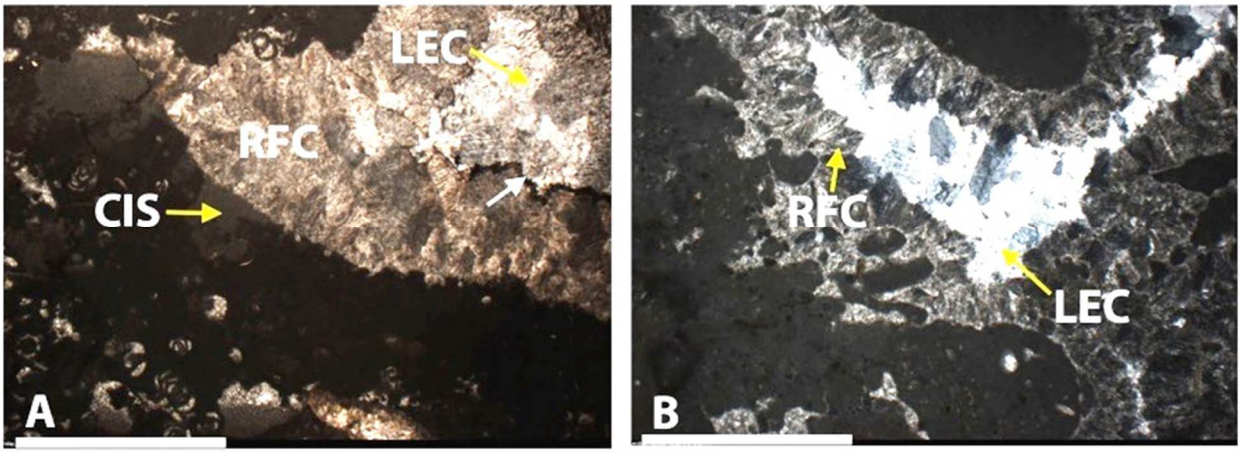

FIG. 2-21: Late radiaxial fibrous cement (RFC-2) and late equant cement (LEC) in El Abra Formation. A) RFC-2 in vug overlies crystalline internal sediment (CIS) and underlies LEC (11.5 m, CM-1). Note the blackening of crystal terminations by oil residue in stylolite that cuts crystal terminations (arrow). B) LEC overlies RFC in vug. (38.2 m, CM-1) Scale bars are 500 μm.

Physical Compaction

Physical breakage of skeletal grains (Fig. 2-22A), fractured shells (Fig. 2-22B), differential compaction of sediments in body cavities of fossils, and penetration of grains by adjacent grains provide evidence of compaction of El Abra Formation. These features of compaction in El Abra probably formed under overburdens of a few 100 m or less. Shinn and Robbin (1983) reported similar features of compaction from pressures simulating up to 1,000 ft. (300 m) of burial. They did not report results from simulation of shallower burial. There is no direct evidence that any younger rocks covered the elevated rim of El Abra Formation in the Sierra El Abra. However, Aguayo (1978, p. 110) following Carrillo-Bravo (1971) Suggested that the Tamuin member (late Campanian) of Mendez shale once covered the elevated rim of El Abra Formation may have 'slid' eastward into the basin to form a turbidite wedge. The thickness of Tamuin is 40 m at the foot of the El Abra escarpment and gradually thins out to the east (Aguayo

and Kanamori 1976). Tamuin sediments possibly resulted in physical compaction of El Abra Formation, before their postulated displacement into the basin.

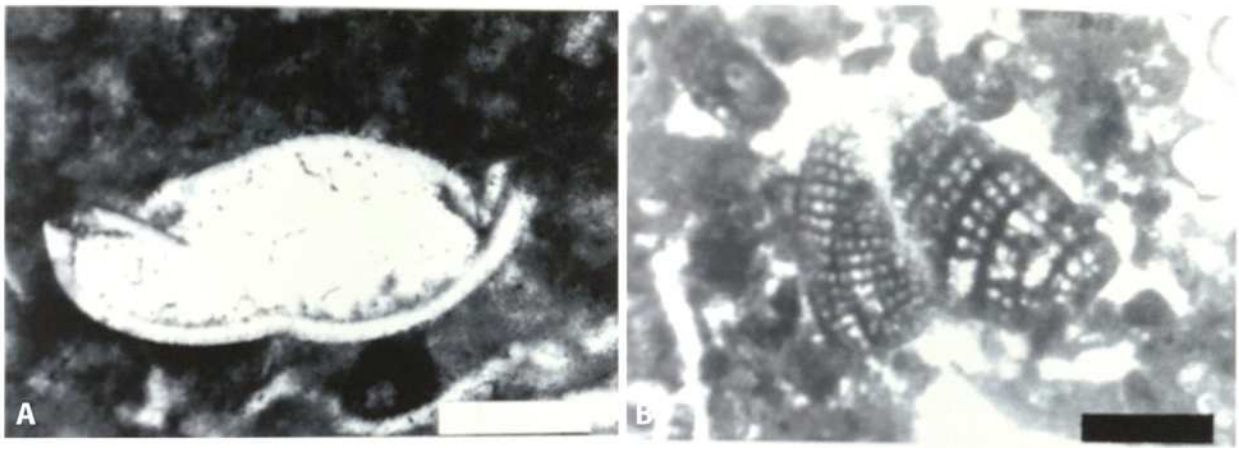

FIG. 2-22: Evidence of physical compaction in El Abra Formation. Photomicrographs are taken from Brennan (1999), p. 63. A) Late equant cement occluding intraparticle porosity after in situ deformation of an ostracode. Scale bar is 150 um. B) Foramineferal test is fractured through mechincal compaction followed by precipitation of late equant cement. Scale bar is 150 um.

Late Equant Cement (LEC)

Relatively large (typically >100 μm), clear calcite crystals are the final major episode of cementation and pore occlusion in all primary and secondary pores, excepting later fractures. (Fig. 2-22A-B). LEC is voluminous in both inner and outer margin rocks. Precipitation of late equant cement resulted in occlusion of 26% of total porosity in the inner margin and 57% in the outer margin. LEC is reported from all exposures in Sierra El Abra (Enos 1986; Minero 1988; Brennan 1999).

Fracture-Filling Calcite Cements (FFC)

Two generations of extensional fractures are documented in El Abra Formation (Fig. 2-23A-B). The first generation (FR-1) crosscuts all the above-mentioned diagenetic features, is filled with clear spary calcite (FFC-1), and is generally oil stained. FFC-1 also occludes small remnants of some large secondary pores. Later fractures (FR-2) are wider and crosscut FR-1. Spary calcite cement (FFC-2) fills FR-2, occludes some large secondary pores, and contains

abundant hydrocarbon inclusions. Cathodoluminescence petrography reveals corroded contacts between FFC-1 and LEC and between FFC-2 and FFC-1 (Chapter III, p. 20). This suggests circulation of corrosive fluids after fracturing.

Stylolites

Burial of consolidated sediment results in pressure dissolution to form seams known as stylolites. Stylolites have been recorded at burial depths as shallow as 100 meters (Schlanger 1964). Stylolites in El Abra Formation are the final diagenetic event during burial, cutting across the entire fabric. They are most common in conglomeratic soilstones. Many stylolites are oil stained (Fig. 2-23B-D). Two generation of stylolites are recognized with different stress directions. Stylolites-1 is bedding parallel with amplitudes of about 2 to 5 cm (Fig. 2-23D). Stylolites-2 are oriented 30° to 90° to bedding, indicating origin from tectonic stress (Fig. 2-23B and C). No crosscutting relationships between the two were observed, although both generations crosscut fractures.

Emplacement and Draining of Hydrocarbons and Karstification

Large volumes of hydrocarbons were generated within the Sierra Madre Oriental fold and thrust belt during the Paleocene and migrated eastward where they were trapped in Sierra El Abra prior to or during deep burial (Yurewicz et al. 1997). The presence of black bitumen in pores, oil stained fractures and stylolites, and hydrocarbon fluid inclusion in calcite cements preserves the remnants of a vanished oil pool (Brennan 1999; Yurewicz et al. 1997). Exhumation of El Abra Formation probably began in Oligocene (Yurewicz et al. 1997), eventually unroofing and draining a giant oil reservoir that may have contained over one billion barrels of oil (Pottorf et al. 1996). Karstification by surface waters produced the present caves, sinkholes, rising

streams, and vertical solution pipes, as much as a meter wide and greater than 30 meters deep, both in the inner and outer margins in El Abra Formation.

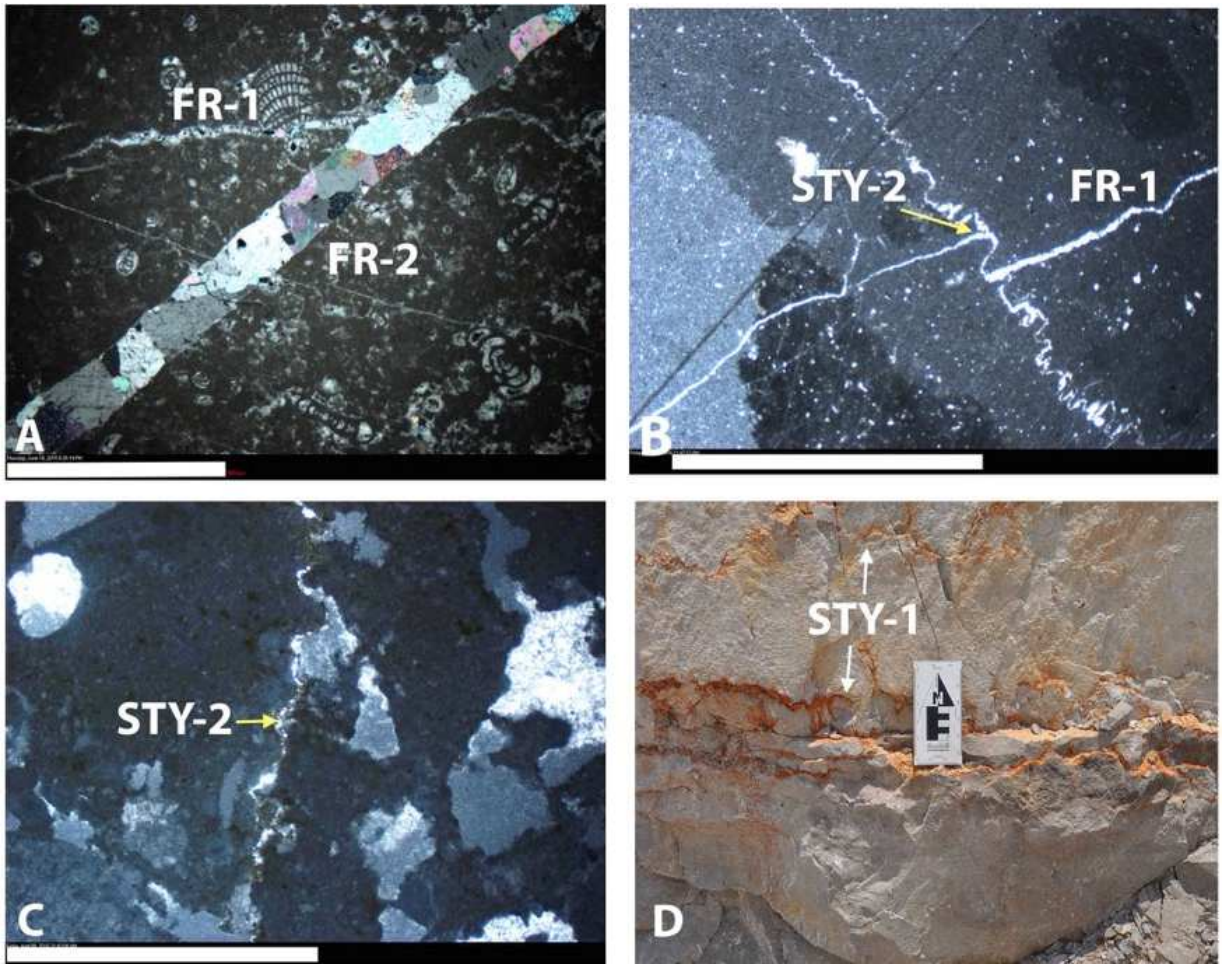

FIG. 2-23: Fractures and stylolites. A) Second-generation fracture, FR-2, offsets first generation, FR-1 (2.5 m, CM-1). Both are filled with equate cements of different generations. Scale is 500 µm. B) Stylolite oriented at 45º to bedding (horizontal in photo) offsets FR-1 (22.5 m, CM-1). Scale is 1 mm. C) Low-amplitude stylolite oriented approximately perpendicular to bedding (71.2 m, CM-1). Scale is 1 mm. D) Two bedding-parallel stylolites (PM-1). Scale is 20 cm.

INTERPRETATIONS

Cyclicity in El Abra Formation

Analysis of cyclicity in El Abra Formation yields some insight into time parameters of its deposition. Cycles and rhythm thickness in CM-1 ranges from 0.5 m to 3.6 m with a mean of 1.7 m (Fig. 2-13A). In PM-1, truncated cycle and rhythm thickness ranges from 1.5 m to 7.2 m with

a mean of 4.2 m (Fig. 2-13B). Relatively fewer and thicker cycles and rhythms in PM compared with vice versa in CM indicate that all sea level oscillations were not recorded in the PM section. According to the Sander (1936), "We cannot conclude from sequences that are not rhythmic in space that the control has been non-rhythmic in time, but we must conclude from sequences which are rhythmic in space that there has been a time-rhythmic control" (from the English translation of Sander 1936, see Sander 1951, p. 16). In more concise wording by Schwarzacher (1975), "Cyclicity in space indicates cyclicity in time but the absence of cyclicity in the stratigraphic record does not indicate the absence of cyclicity in time". It is logical to assume sea level oscillations indicated by cycles at CM-1 section are representative of the cyclicity in El Abra Formation, at least for the exposed part of Sierra El Abra. The mean thickness of subtidal units is 1.0 m, with a 'tail' of thicker units; modal thickness is 0.5-1 m (Fig. 2-12A). A subtidal unit that is approximately twice the thickness of a typical subtidal unit suggests that a sea-level oscillation failed to expose the platform and resulted in thick subtidal units.

Total thickness of El Abra Formation has been a matter of speculation; estimates include: 1800 m by Aguayo (1998), 1500 m to 2000 m by Carrillo (1971), 2098 m by Carrasco (1970) in Actopan platform, 2000 m by Guzman (1967) in the Golden Lane, and about 3000 m by Wilson (1975). Well data from the V-SLP platform (Basáñez et al. 1993, p. 52) include 2720 m in Colmena-101 and Tanchuchen-1, with an average thickness of about 2000 m over the platform. The time span for deposition of El Abra Formation is disputed as well, however; Albian to early or mid-Cenomanian is the current consensus, as reviewed in the geologic setting. Albian plus mid-Cenomanian age lasted for about 15.5 Ma. Given El Abra Formation thickness of 2000 m and mean CM-1 cycle thickness of 1.5 m (ignoring the extreme `2X` outliers i.e. 2.5 m-4.0 m in Fig. 2-13 A), the total number of cycles in El Abra Formation could be about 1334. The mean

duration of deposition for each El Abra cyclothem would be approximately 11,620 years. This proposed duration for El Abra cycles is approximately similar to sub-Milankovitch cycles (<12 ka). Non-deposition or exposure duration during low stands can be estimated at about 12,000 years (using dissolution rates of Corbel 1959) to 19,000 years (using dissolution rates of Land et al. 1967) for an average of 20 cm removal of limestone through dissolution that capped most cycles in CM-1, resulting in punctuated sedimentation in El Abra Formation.

Diagenesis in El Abra Formation

Sea level fluctuated frequently over the eastern edge of Valles-San Luis Potosí platform and exposed the deposits at the margin to subaerial conditions, recorded by numerous outcrop and petrographic and macroscopic features. Twenty-seven subaerial-exposure surfaces have been documented in CM-1 section. Five possible surfaces of subaerial exposure are documented in PM section, but no paleosols or karst surfaces are recorded. Zones of prominent solution porosity provide the only evidence of early exposure of the outer-margin rocks.

Varied diagenetic environments affected the inner-margin rocks at CM and the outer margin (PM) reef facies. Secondary porosity in the inner-margin rocks is mainly non-fabric selective creating large vugs and channels. Moldic porosity is common where there are abundant rudists in small lenses. In contrast, the outer margin contains abundant fabric-selective moldic porosity. However, beneath the possible surfaces of subaerial exposure, large vugs are observed. Evolution of early porosity is also different between the inner-margin rocks and outer-margin reefal rocks. In CM-1 section, repeated intraformational exposure led to pore-space reduction by CIS and EEC. Synchronously at PM, marine diagenesis dominated, precipitating meniscate micritic cement and extensive RFC-1. A regional episode of dissolution (D-2) created extensive megaporosity in both the inner and outer margin. RFC-2 reduced the large-scale porosity in the

inner margin, while PIS and RFC-2 reduced the large-scale secondary porosity in the outer margin. During shallow burial in the Late Cretaceous, the voluminous LEC reduced and occluded pore spaces in both the inner and outer margin.

Maximum burial may be estimated from homogenization temperatures (Th) from fluid inclusions in FFC-2, which yielded temperatures reaching 110°C, and Th from cement in stylolites indicated 115°C to 160°C (Brennan 1999). Such high temperatures, if exclusively due to burial, indicate depths of 5 km (Yurewicz et al. 1997). A 5-km overburden appears unlikely, however as Late Cretaceous strata (~1100 m) and Tertiary Chicontepec flysch (900 m) do not exceed 2 km total thickness (Bush and Govela 1978, p. 239; Brennan 1999). If we assume a geothermal gradient of 25°C/km, then an overburden of 2 km would heat El Abra to a temperature of about 75°C, certainly less than 160°C. (Brennan 1999, p. 103) suggested hydrothermal fluids as a heating mechanism. Deep-burial diagenesis played a minor role in porosity modification in El Abra Formation; however, migration of hydrocarbons during this stage charged a Billion-barrel reservoir (Yurewicz et al. 1997; Brennan 1999)

Rocks of the inner margin experienced repeated early meteoric diagenesis, attested by abundance of subaerial-exposure surfaces, precipitation of EEC, and deposition of CIS, and comparatively limited marine diagenesis, indicated by relatively less intense micritization and lack of early marine cement (RFC-1). In outer-margin rocks, in contrast, subtidal sedimentation and diagenesis predominated, reflected by thicker subtidal units, abundant micritization, and abundant RFC-1. CIS is rare and EEC absent, indicating limited exposure to meteoric conditions in the outer margin. These contrasts reflect relatively lower elevation of the outer margin.

DISCUSSION

Sub-Milankovitch cycles of Pleistocene and Holocene are linked to oceanographic and atmospheric changes induced by waxing and waning of Arctic ice caps (Broecker and Denton 1989; Bond et al. 1992; Zühlke et al 2003), which have not been undisputedly documented to date for the mid-Cretaceous. However, some recent papers support the hypothesis of contemporaneous mid-Cretaceous ice sheets (Moriya et al. 2007; Bornemann et al. 2008). Stable isotopic $\delta^{18}O$ records from the tropical Atlantic showed synchronous positive excursions for both surface and deep-ocean that indicated an ice cap half the size of modern Antarctic ice caps (Bornemann et al. 2008). Turonian facies of northern Europe, North America, and the Russian platform record a rapid rise in sea level that appears too fast and regional [global?] to be accounted for by tectonics (Haq et al. 1987, 1988; Sahagian et al. 1996; Miller et al. 2008). Biostratigraphic dating and a positive $\delta^{18}O$ isotope excursion led Maurer et al. (2013) to hypothesize a long lowstand with an amplitude of at least 50 m in the late Aptian of the Arabian plate, again invoking the idea of a cooling phase during the Cretaceous greenhouse. Koch and Brenner (2009) suggest glacio-eustatic control for large and rapid sea-level fluctuations in the Albian-Cenomanian Dakota Formation, at the eastern margin of Western Interior Seaway. Alley and Frakes (2003) reported a 2-m-thick diamictite near the base of the Cretaceous Eromanga basin in South Australia. They interpreted the diamictite as a tillite deposit directly from glacial ice, although striated bedrock surfaces are not present. These studies support mid-Cretaceous glaciation. However, unequivocal sedimentological evidence such as regional-scale ice-rafted debris or high-resolution $\delta^{18}O$ data from well-preserved foraminifera is lacking. Large ice caps, if present during the mid-Cretaceous, could drive the high frequency oscillations recorded in El Abra Formation. Disproving the presence of ice caps is equally problematic. Mid-Cretaceous

glaciation is obviously not universally accepted, but it would provide the most acceptable driving mechanism for the high-frequency sea-level oscillations in the Albian-Cenomanian. Tectonics does not appear a plausible mechanism for cyclicity in El Abra Formation. If tectonics were a factor, one would expect large variances in subsidence rates, which would result in cycle thickness ranging from 1 to 10s of meters (Goldhammer et al. 1990). Such large variations in thickness are not observed in El Abra Formation (Fig. 2-13).

Subaerial-exposure features and early diagenetic trends provided useful clues to understanding the paleomorphology of V-SLP platform. The tidally influenced rocks at CM-1 section preserve repeated (27) and closely spaced (average 2.7 m) exposure surfaces with unequivocal evidence. The more distal rocks (Quarry IV, V, and VII of Minero 1983; Fig. 2-1) also record unequivocal subaerial exposure features such as microkarst surfaces; however, they lack well developed paleosols. In comparison, the outer margin (PM and TQ) rocks have relatively few and equivocal exposure features. Enos (1986) reported 9 exposure surfaces with equivocal evidence of subaerial exposure in 45 m of reef and grainstone facies (TQ quarry, Fig. 2-1). In PM sections five intervals of early (D-1) secondary porosity are prominent. This indicates freshwater lenses formed in the outer margin during relative sea-level falls. The stratigraphic intervals with early solution porosity are tentatively correlated with rocks in CM-1 section (Fig. 2-4). The contrasting degree and type of diagenetic modification between inner and outer margin is strong evidence that the tidal-flat facies at CM were deposited on a relatively elevated surface, compared with rocks at PM (Fig. 2-24). This is also consistent with Minero's (1983) concept that skeletal rudstones in CM quarry formed rubble islands.

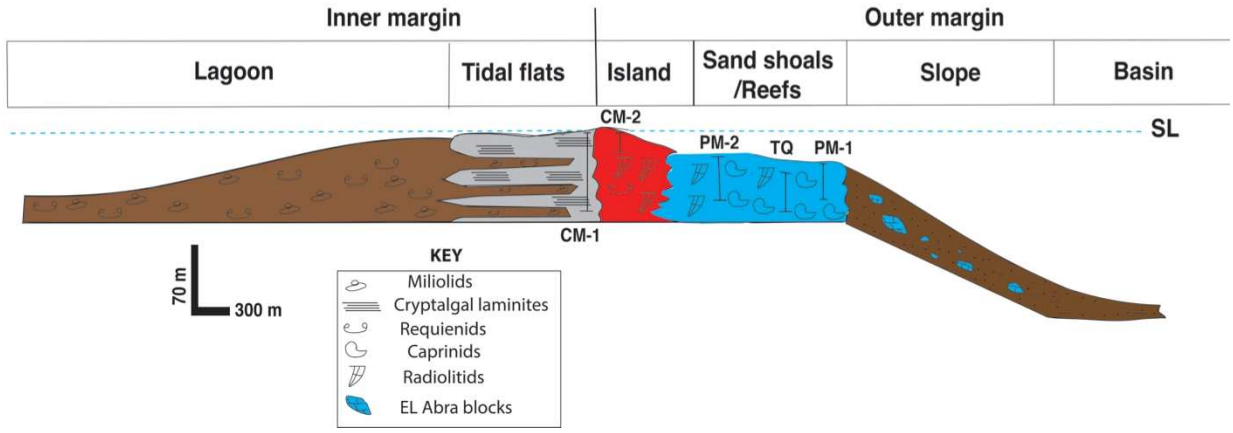

FIG. 2-24: Conceptual environmental model of El Abra platform exposed in Sierra El Abra, based on field observations and petrography. The sea level is shown close to CM sections, which include tidalites (CM-1) and skeletal grainstones with extensive meteoric diagenesis that suggest the existence of rubble islands (CM-2; Minero 1983). Only a muted record of subaerial exposure was documented at PM and TQ (This study; Enos 1986).

CONCLUSIONS

El Abra Formation exposed in the Sierra El Abra is composed of shallowing-upward cycles, truncated cycles and rhythms. Cyclothems average 1.7 m thick and record a time span that is approximately similar to sub-Milankovitch cycles (<12 ka). The El Abra platform missed some sea-level oscillations possibly above the platform top resulting in relatively thick subtidal units. Evidence for mid-Cretaceous glaciation is equivocal and controversial, but this seems the most probable mechanism for driving high-frequency and low-amplitude cycles. High frequency and low amplitude (<10 m) sea-level oscillations introduced alternating subaerial and subtidal conditions during El Abra deposition. Early diagenetic features helped in elucidating the paleo-morphology of the platform margin. Paleosols, microkarst surfaces, rhizoliths, blackened clasts, and voluminous solution porosity indicate repeated emergence of the inner margin of the Valles-San Luis Potosí platform. The tidally influenced rocks in the inner margin setting experienced more subaerial exposure than the rest of El Abra platform, suggesting relatively higher elevation on the platform as tidal flats. Marine-phreatic diagenesis dominated the outer margin, as shown by abundant micritization, meniscate micritic and early radiaxial fibrous cement, during the time

that meteoric diagenesis prevailed in the inner margin. The products of intraformational meteoric diagenesis (D-1), e.g. small secondary porosity, abundant crystalline internal sediments, and early equant cements are comparatively more abundant in the inner-margin than in the outer-margin rocks. A regional meteoric aquifer developed in the late Cenomanian resulting in large-scale secondary porosity (D-2), later reduced by pelagic internal sediments (outer margin only) and a later generation of radiaxial fibrous cement. Late equant calcite cement, the last major episode of porosity reduction, grew during shallow burial. Porosity evolution during Laramide orogeny and deeper burial were insignificant.

REFERENCES CITED

AGUAYO-CAMARGO, J.E., 1975, Sedimentary environments and diagenetic implications of the El Abra Limestone at its type locality, east Mexico: Unpublished M.S. Thesis, University of Texas at Dallas, 159 p.

AGUAYO-CAMARGO, J.E., 1978, Sedimentary environments and diagenesis of a Cretaceous reef complex, eastern Mexico: Anales Centro Ciencias del Mar Limnologia., Universidad Nacional Autonoma, Mexico, v. 5, p. 83-140.

AGUAYO-CAMARGO, J.E., 1993, The middle Cretaceous EI Abra Limestone at its type locality and Laguna Colorada, east-central Mexico, *in* Alencaster, Gloria, and Buitron, B. E., eds., Universidad Nacional Autonoma de Mexico, Instituto de Geologia: Third International Conference on Rudists, Mexico, D.F., Nov. 20-28, Guidebook for field trip "A", 43 p.

AGUAYO-CAMARGO, J.E., 1998, The middle Cretaceous El Abra Limestone at its type locality (facies, diagenesis and oil emplacement), east-central Mexico: Revisita Mexicana de Ciencias Geológicas, v. 15, p. 1-8.

AGUAYO, C. E., AND KANAMORI, K., 1976, The Tamuin Member of the Méndez Shale along the eastern flank of the Sierra de El Abra. San Luis Potosí, east Mexico: Boletin de la Sociedad Geologica Mexicana, v. 37, p. 11-17.

ALENCASTER, G., 1984, Late Jurassic-Cretaceous molluscan paleogeography of the southern half of Mexico: Geological Association of Canada Special paper, v. 27, p. 77-88.

ALLEY, N. F., AND FRAKES, L. A., 2003, First known Cretaceous glaciation: Livingston Tillite member of the Cadna□owie Formation, South Australia: Australian Journal of Earth Sciences, v. 50, p. 139-144.

BASÁÑEZ-LOYOLA, M.A., FERNÁNDEZ-TURNER, R., AND ROSALES-DOMÍNGUEZ, C., 1993, Cretaceous platform of Valles-San Luis Potosí, northeastern central Mexico: American Association of Petroleum Geologists, Memoir, 56, p. 51-51.

BATHURST, R. G. C., 1966, Boring algae, micrite envelopes and lithification of molluscan biosparites: Geological Journal, v. *5*, p. 15-32.

BATHURST, R. G. C., 1974, Marine diagenesis of shallow water calcium carbonate sediments: Annual Review of Earth and Planetary Sciences, v. 2, p. 257.

BATHURST, R. G. C., 1976, Carbonate sediments and their diagenesis: Elsevier scientific publishing company, Amsterdam, 2nd ed, 658 p.

BOND, G.C., HEINRICH, H., AND BROECKER, W., 1992, Evidence for massive discharges of icebergs into the North Atlantic Ocean during the last glacial period: Nature, v. 360, p. 245–249.

BORNEMANN, A., NORRIS, R. D., FRIEDRICH, O., BECKMANN, B., SCHOUTEN, S., DAMSTÉ, J. S. S., & WAGNER, T., 2008, Isotopic evidence for glaciation during the Cretaceous super greenhouse: Science, v. 319, p.189-192.

BRENNAN, S.T., 1999, Impact of fluid and thermal history on reservoir properties of El Abra Limestone, Sierra el Abra, Mexico: Unpublished Master Thesis, University of Kansas, Lawrence, 183 p.

BROECKER, W.S., AND DENTON, G.H., 1989, The role of ocean-atmosphere reorganizations in glacial cycles: Geochimica et Cosmochimica Acta, v. 53, p. 2465–2501.

BUDD, D.A., SALLER, A.H., AND HARRIS, P.M., 1995, Unconformities and porosity in carbonate strata: American Association of Petroleum Geologists, Memoir, 63, 301 p.

BUSH, A. D., AND GOVELA, S., 1978, Stratigraphy and structure of Chicontepec Turbidites, Southeastern Tampico-Misantla Basin, Mexico: American Association of Petroleum Geologists, Bulletin, v. 62, p. 235-246.

CARRASCO, B., 1970, Formacion El Doctor en la platforma Valles-San Luis Potosí: Revista del Instituto Mexicano del Petróleo, v. 2, p. 97-99.

CARRILLO-BRAVO, J., 1971, La Plataforma Valles-San Luis Potosí: Boletín de la Asociación Mexicana de Geólogos Petroleros, v. 23, p. 1-113.

CHOQUETTE, P.W., AND PRAY, L.C., 1970, Geologic nomenclature and classification of porosity in sedimentary carbonates: American Association of Petroleum Geologists, Bulletin, v. 54, p 207-250.

CORBEL, J., 1959, Erosion en terrain calcaire (vitesse d'érosion et morphologie): In Annales de geographie, v. 68-366, p. 97-120.

DIENI, I., TUNSEK, D., 1979, Parkeri spaherica Carter, 1877 (Hudrozoan) in the Varconian (Lower Cretaceous) of Orosei (Sardinia): Bollettino della Societa Paleontologica Italiana, v. 18, p. 200-206.

DUNHAM, R. J., 1971, Meniscus cement. Carbonate Cements: Johns Hopkins University: Studies in Geology, p. 297-300.

DUNHAM, R.J., 1962, Classification of carbonate rocks according to depositional texture: *in* Ham, W.E., ed., Classification of carbonate rocks: American Association of Petroleum Geologists, Memoir 1, p. 108-121.

DUNHAM, R.J., 1969, Early vadose silt in Townsend Mound (Reef), New Mexico: *in* Friedman, G. M., eds., Depositional Environments in Carbonate Rocks: Society of Economic Paleontologists and Mineralogists, Special Publications, v. 14, p. 139-

181.

DUNHAM, R.J., 1970, Keystone Vugs in Carbonate Beach Deposits (abs.): American Association of Petroleum Geologists, Bulletin, v. 54, p. 845-845.

ENOS, P., 1974, Reefs, platforms, and basins of middle Cretaceous in northeast Mexico: American Association of Petroleum Geologists, Bulletin, v. 58, p. 800-809.

ENOS, P., 1977, Tamabra limestone of the Poza Rica trend, Cretaceous, Mexico: *in* Cook, H. E., and Enos, P., eds., Deep-water Carbonate Environments: Society of Economic Paleontologists and Mineralogists, Special Publications, v. 25, P. 273-314.

ENOS, P., 1982, Basin-to-platform transition, mid-Cretaceous, Mexico (abstract): American Association of Petroleum Geologists, Bulletin, v. 66, p. 567.

ENOS, P., 1983, Late Mesozoic paleogeography of Mexico: *in* Reynolds M.W., Dolly E.D., eds., Mesozoic paleogeography of west-central United States: Society of Economic Paleontology and Mineralogy, Rocky Mountain Sect, Symposium 2, p. 133-157.

ENOS, P., 1986, Diagenesis of mid-Cretaceous rudist reefs, Valles platform, Mexico, *in* Schroeder, J.H. and Purser, B.H., eds., Reef diagenesis: Springer-Verlag, Berlin, p. 160-185.

ESTEBAN, M., AND KLAPPA, C.F., 1983, Subaerial exposure, *in* Scholle, P.A., Bebout, D.G., and Moore, C.H., eds., Carbonate depositional environments: American Association of Petroleum Geologists, Memoir, 33, p. 1-63.

FISCHER, A. G., 1964, The Lofer cyclothems of the alpine Triassic: State Geological Survey Kansas, Bulletin, 169, v. 1, p. 107-148.

FISCHER, A.G., 1975, Tidal deposits, Dachstein limestone of the north-alpine Triassic, Tidal deposits: Springer Berlin Heidelberg, p. 235-242.

FLÜGEL, E., 2004, Microfacies of carbonate rocks: analysis, interpretation and application: Springer-Verlag Berlin Heidelberg, Germany, 976 p.

GINSBURG, R.N., HARDIE, L.A., BRICKER, O.P., GARRETT, PETER, AND WANLESS, H.R., 1977. Exposure index: A quantitative approach to defining position within the tidal zone, *in* Hardie, L.A., ed., Sedimentation on the modern carbonate tidal flats of northwest Andres Island, Bahamas: Johns Hopkins University Studies in Geology, no. 22, p. 7-11.

GOLDHAMMER, R. K., P. A. DUNN, AND L. A. HARDIE., 1990, Depositional cycles, composite sea-level changes, cycle stacking patterns, and the hierarchy of stratigraphic forcing: examples from Alpine Triassic platform carbonates.": Geological Society of America ,Bulletin 102, v. 5, p. 535-562.

GOLDSTEIN, R. H., ANDERSON, J. E., AND BOWMAN, M. W., 1991, Diagenetic responses to sea-level change: integration of field, stable isotope, paleosol, paleokarst, fluid inclusion, and cement stratigraphy research to determine history and magnitude of sea-level fluctuation: Sedimentary Modeling, p. 139-162.

GOLDSTEIN, R., 1988, Paleosols of Late Pennsylvanian cyclic strata, New Mexico: Sedimentology, v. 35, p. 777-803.

GRADSTEIN, F.M., OGG, J.G., AND SMITH, A.G., 2004, A geologic time scale Cambridge University Press, London, 488 p.

GUZMAN, E.J., 1967, Reef type stratigraphic traps in Mexico: 7th world Petroleum Congress proceeding, v. 2, p. 461-470.

HAQ, B. U., HARDENBOL, J., AND VAIL, P. R., 1987, Chronology of fluctuating sea levels since the Triassic: Science, v. 235, p. 1156-1167.

HAQ, B.U., HARDENBOL, J., VAIL, P.R., 1988, Mesozoic and Cenozoic chronostratigraphy and cycles of sea-level changes, *in* Wilgus, C.K., Hastings, B.S., Kendall, C.G.St.C., Posamentier, H.W., Ross, C.A., Van Wagoner, J.C. eds., Sea-Level Changes — An Integrated Approach: Society of Economic Paleontologists and Mineralogists, Special Publications, v. 42, p. 71–108.

HILLGÄRTNER, H., DUPRAZ, C., AND HUG, W., 2001, Microbially induced cementation of carbonate sands: are micritic meniscus cements good indicators of vadose diagenesis? : Sedimentology, v. 48, p. 117-131.

JAMES, N. P. AND CHOQUETTE, P. W., 1984, Limestones - The meteoric diagenetic environment: Geoscience Canada, v. 11, no. 4, p. 785-799.

JAMES, N. P., 1972, Holocene and Pleistocene calcareous crust (caliche) profiles: criteria for subaerial exposure: Journal of Sedimentary Research, v. 42, p. 817-836.

KENDALL, A. C., AND M. E. TUCKER., 1973, Radiaxial fibrous calcite: A replacement after acicular carbonate: Sedimentology, v. 20, p. 365-389.

KENDALL, ALAN C., 1985, Radiaxial fibrous calcite: a reappraisal, *in* Schneidermann, N., Harris, P.M., eds., Carbonate Cements: Society of Economic Paleontologists and Mineralogists, Special Publications, v. 36, p. 59–77.

KLAPPA, C.F., 1979, Lichen stromatolites: criterion for subaerial exposure and a mechanism for the formation of laminar calcretes (caliche): Journal of Sedimentary Research, v, 49, p. 387-400.

KLAPPA, C.F., 1980, Rhizoliths in terrestrial carbonates; classification, recognition,

genesis and significance: Sedimentology, v. 27, p. 613-629.

KOCH, J. T., AND BRENNER, R. L., 2009, Evidence for glacioeustatic control of large, rapid sea-level fluctuations during the Albian-Cenomanian: Dakota Formation, eastern margin of western interior seaway, USA: Cretaceous Research, v. 30, p. 411-423.

LAND, L.S., T., MACKENZIE, F.REID, AND GOULD, S.J., 1967, Pleistocene history of Bermuda: Geological Society of America, Bulletin, v. 78, p. 993-1006.

LANGORIA, J.F., 1975, Estatigrafia de le Sierra Comancheana del Noreste de Mexico: Boletin Sociedad Geologia Mexicana, v. 36, p. 31-59.

LOGAN, B. W., P. HOFFMAN, AND C.D., GEBELEIN, 1974, Algal mats, cryptalgal fabrics, and structures, Hamelin Pool, Western Australia: *in* Logan, B. W., J. F. Read, G. M. Hagan, P. Hoffman, R. G. Brown, P. J. Woods, and C. D. Gebelein, Evolution and diagenesis of Quaternary carbonate sequences, Shark Bay, Western Australia: American Association of Petroleum Geologists, Memoir, 22, p. 140-194.

LOHMAN, K. C., MEYERS, W. J., 1977, Microdolomite inclusions in cloudy prismatic calcites: a proposed criterion for former high-magnesium calcites: Journal of Sedimentary Petrology, v. 47, p. 1078–1088.

MAURER, F., VAN BUCHEM, F. S., EBERLI, G. P., PIERSON, B. J., RAVEN, M. J., LARSEN, P. H., AND VINCENT, B., 2013, Late Aptian long□lived glacio□ eustatic low stand recorded on the Arabian Plate: Terra Nova, v. 25, p. 87-94.

MCBRIDE, E. F., WEIDIE, A. E AND WOLLEBEN, J. A., 1975, Deltaic and associated deposits of Difunta Group (Late Cretaceous to Paleocene), Parras and La Popa

basins northeastern Mexico, in M. L. S. Broussard, ed., Deltas: Houston Geological Society, p. 485-522.

MILLER, K. G., WRIGHT, J. D., KATZ, M. E., BROWNING, J. V., CRAMER, B. S., WADE, B. S., AND MIZINTSEVA, S. F., 2008, A view of Antarctic ice-sheet evolution from sea-level and deep-sea isotope changes during the Late Cretaceous–Cenozoic, Antarctica: a keystone in a changing world, p. 55-70.

MINERO, C.J., 1983, Sedimentary environments and diagenesis of the El Abra Formation (Cretaceous), Mexico: Unpublished Ph.D. dissertation, State University of New York at Binghamton, 367 p.

MINERO, C.J., 1988, Sedimentation and diagenesis along an island-sheltered platform margin, El Abra Formation, Cretaceous of Mexico, *in* James, N.P. and Choquette, P.W. eds., Paleokarst: Springer-Verlag, Berlin, p. 385-405.

MINERO, C.J., ENOS, P., AND AGUAYO-CARMAGO, J.E., 1983, Sedimentation and diagenesis of mid-Cretaceous platform-margin east-central Mexico, with accompanying field guide: Dallas Geological Society, Dallas, 168 p.

MORIYA, K., WILSON, P. \A., FRIEDRICH, O., ERBACHER, J., AND KAWAHATA, H., 2007, Testing for ice sheets during the mid-Cretaceous greenhouse using glassy foraminiferal calcite from the mid-Cenomanian tropics on Demerara Rise: Geology, v. 35, p. 615-618.

PESSAGNO, E. A., JR., 1969, Upper Cretaceous stratigraphy of the Western Gulf Coast Area of Mexico, Texas and Arkansas: Geological Society of America, Memoir 111, p. 139.

POTTORF, R.J., GRAY, G.G., KOZAR M.G., FITCHEN W.M., RICHARDSON, M., CHUCHLA, R. J., AND D.A., YUREWICZ, 1997, Hydrocarbon generation and migration in the Tampico Segment of the Sierra Madre Oriental fold-thrust belt: evidence from an exhumed oil field in the Sierra de El Abra (abs): Memoir del V Congreso Latinoamericano de Geoquimica Organica, p. 100-101.

READ, J.F., 1976, Calcretes and their Distinction from Stromatolites: Developments in Sedimentology, v. 20, p. 55-71.

REINHOLD, C., KAUFMANN, B., 2010, Sea-level changes as controlling factor of early diagenesis: the reefal limestones of Adnet (Late Triassic, Northern Calcareous Alps, Austria): Facies, v. 56, p. 231–248.

RICHTER, D.K., NEUSER, R.D., SCHREUER, J., GIES, H., AND IMMENHAUSER, A., 2011, Radiaxial-fibrous calcites: A new look at an old problem: Sedimentary Geology, v. 239, p. 23-36.

SAHAGIAN, D., PINOUS, O., OLFERIEV, A., AND ZAKHAROV, V., 1996, Eustatic Curve for the Middle Jurassic--Cretaceous Based on Russian Platform and Siberian Stratigraphy: Zonal Resolution: American Association of Petroleum Geologists, Bulletin, v. 80, p. 1433-1458.

SALLER, A.H., 1986, Radiaxial calcite in Lower Miocene strata, subsurface Enewetak Atoll: Journal of Sedimentary Petrology, v. 56, p. 743–762.

SANDBERG, P., 1985, No skeletal aragonite and pCO2 in Phanerozoic and Proterozoic, *in*: Sundquist, E., Broecker, W., eds., The Carbon Cycle and Atmospheric CO2: Natural Variations, Archean to Present: American Geophysical Union Monograph,

Washington, D.C, p. 585–594.

SANDER, B., 1936, Beitrage zur Kenntnis der Ablagerungsgefiige (rhythmische Kalke und Dolomite aus der Trias), -Tschermaks Mineralogische und Petrographische Mitteilungen, v. 48, p. 27-139

SANDER, B., 1951, Einftihrung in die Gefugekunde als geologischer Korper, 2. Tell. Die Korngefhgemerkmale: Wien Springer, 409 p.

SCHALNGER, S. E., 1964, Petrology of the limestones of Guam: United State Geological Survey, Professional paper, v. 403 D, p. 1-52.

SCHWARZACHER, W., 1948, fiber sedimentare P, hythmik des Dachsteinkalkes am Lo fer.- Verhandlungen dcr Geologischen Bundesanstalt. 1947. (Heft 10-12), p. 176-188.

SCHWARZACHER, W., 1954, Die Grossrhythmik des Dachstein Kalkes yon Lofer.Tschermaks Mineralogische und Petrographtsche Mitteilungen: Leitgzig, p. 44-54

SCOTT, R. W., 1990, Models and stratigraphy of mid-Cretaceous reef communities, Gulf of Mexico: Society of Economic Paleontologists and Mineralogists, Special Publications, Tulsa, p. 102.

SHINN, E. A., 1983, Tidal flat environment, *in*, Scholle, P.A., Bebout, D.G., and Moore, C.H., eds., Carbonate depositional environments: American Association of Petroleum Geologists Tulsa, Memoir, 33, pp. 171-210.

SHINN, E. A., AND LIDZ, B. H., 1988, Blackened limestone pebbles, fire at subaerial unconformities, *in* James, N.P. and Choquette, P.W. eds., Paleokarst, Springer-Verlag, Berlin, p. 117-131.

SHINN, E. A., GINSBURG, R. N., AND LLOYD, R. M., 1965, Recent supratidal dolomite from Andros Island, Bahamas: Society of Economic Paleontologists and Mineralogists, special publication, no. 13, p. 112-123.

SHINN, E.A., 1968, Practical significance of birdseye structures in carbonate rocks: Journal of Sedimentary Petrology, v. 38, p. 215-223.

SHINN, E.A., AND ROBBIN, D.M., 1983, Mechanical and chemical compaction in fine-grained shallow-water limestones: Journal of Sedimentary Research, v. 53, p. 595-618.

SMITH, B.A., 1986, Upper Cretaceous stratigraphy and the mid-Cenomanian unconformity of the east central Mexico: Unpublished Ph.D. dissertation, University of Texas at Austin, 190 p.

SOEGAARD, K., DANIELS, A., YE, H., AND HALIK, N., 1996, Late Cretaceous Early Tertiary Evolution Of Foreland To Sevier Laramide Fold Thrust Belt, Northeast Mexico: In Geological Society of America Abstracts with Programs, v. 28, p. A-115.

STRASSER, A., 1984, Black-pebble occurrence and genesis in Holocene carbonate sediments (Florida Keys, Bahamas, and Tunisia): Journal of Sedimentary Research, V. 54, p. 1097-1109.

TUCKER, M.E., and HOLLINGWORTH, N.T.J., 1986, The Upper Permian reef complex (EZ1) of North East England: diagenesis in a marine to evaporitic setting, In Reef diagenesis, Springer Berlin Heidelberg, p. 270-290.

TUCKER, M.E., AND WRIGHT, V.P., 1990, Carbonate sedimentology: Malden MA, Blackwell Publishing, p. 386.

VIDETICH, P.E., 1985, Electron microprobe study of Mg distribution in recent Mg calcites and recrystallized equivalents from the Pleistocene and Tertiary: Journal of Sedimentary Petrology, v. 55, p. 421–429.

WARD, J.A., 1979, Stratigraphy, depositional environments and diagenesis of the El Doctor platform, Queretaro, Mexico, unpublished Ph.D. dissertation, State University of New York, Binghamton, 172 p.

WILMSEN, M., 2003, Taxonomy, autecology and paleobiogeography of the middle Cretaceous genus *Parkeria* Carpenter, 1870 (spherical hydrozoan): Journal of Systematic Paleontology, v, 1, p. 161-186,

WILSON, J.L., 1975, Carbonate Facies in Geologic history: New York, Springer-Verlag, 471 p.

WRIGHT, V.P., 1989, Terrestrial stromatolites and laminar calcretes, a review: Sedimentary Geology, v. 65, p. 1-13.

YE, H., 1997, Sequence stratigraphy of the Difunta group in the Paras_La Popa foreland basin, and tectonic evolution of the Sierra Madre Oriental, NE Mexico: Unpublished Ph.D. dissertation, The University of Texas at Dallas, 197 p.

YUREWICZ, D.A., CHUCHLA, R.J., RICHARDSON, M., POTTORF, R.J., GRAY, G.G., KOZAR, M.G., AND FITCHEN, W.M., 1997, Hydrocarbon generation and migration in the Tampico-Misantla Basin and Sierra Madre Oriental, east-central Mexico: Evidence from an exhumed oil field in the Sierra de El Abra: AAPG Field Trip Guidebook, Dallas Geological Society and Society of Economic Paleontologists and Mineralogists, 24 p.

ZÜHLKE, R., BECHSTÄDT, T., AND MUNDIL, R., 2003, Sub-Milankovitch and

Milankovitch forcing on a model Mesozoic carbonate platform–the Latemar (Middle Triassic, Italy): Terra Nova, v. 15(2), p. 69-80.

CHAPTER III: DISCONFORMITY-CONTROLLED DIAGENESIS IN EL ABRA CARBONATE PLATFORM (MID-CRETACEOUS), MEXICO

ABSTRACT

Cyclic strata of El Abra Formation were deposited on an isolated mid-Cretaceous carbonate platform. Intraformational subaerial exposure surfaces repeatedly punctuated sedimentation in the inner margin and resulted in dissolution (D-1), deposition of crystalline internal sediment (CIS), and cementation by early equant cement (EEC). Contemporaneous marine-phreatic diagenesis resulted in micritization and precipitation of isopachous radiaxial fibrous cements (RFC-1) in the outer margin. Twenty-one cathodoluminescence zones of inner-margin early equant cements are recognized. The cement zones exhibit cross-cutting relationships indicative of intraformational conditions, i.e. early cement zones truncated at edges of intraformational conglomerates, association of cement zones with paleosol features, and termination of early zones or addition of younger cement zones up-section. Tm-ice values from fluid-inclusion assemblages in EEC yielded salinity values ranging from 0 ppt to 49 ppt seawater-salt equivalent, indicating precipitation from freshwater to evaporated seawater, including normal seawater and various mixtures. A pervasive dissolution event (D-2), probably in a regional meteoric aquifer preceding the Turonian transgression, created voluminous porosity. This porosity was reduced by a second generation of radiaxial fibrous cement (RFC-2) in the inner margin, by RFC-2 and pelagic internal sediment (PIS) in the outer margin, and ultimately by late equant cement (LEC) throughout. Four pervasive, distinctive cathodoluminescence zones in LEC indicate approximate synchronicity of cementation throughout the platform margin. Fluid-inclusions of LEC indicate precipitation from freshwater at temperature less than about 50°C. This freshwater, with depleted $\delta^{18}O$, probably infiltrated through clastic wedges developed at the

front of the rising Sierra Madre Oriental during the Late Cretaceous and passed through fractured (?) basinal rocks and porous platform limestones, to exit through the elevated rim of the platform.

INTRODUCTION

Cement stratigraphy combined with fluid-inclusion analysis is a significant method in understanding cement zones, their spatial distribution, time-stratigraphic significance, fluid compositions, diagenetic environments, and the hydrological conditions responsible for precipitation of cements (Meyers 1974, 1978, 1991; Grover and Read 1983; Dorobek 1987; Kaufman et al. 1988; Niemann and Read 1988; Goldstein 1998). Previous studies have generated numerous data on diagenesis of El Abra Formation (Aguayo 1975, 1978, 1998; Minero 1988; Enos 1986; Brennan 1999; Armstrong et al. 2011), but detailed cement stratigraphy and fluid-inclusion analysis of early and late equant cements reveals significant new information on the role of intraformational subaerial-exposure surfaces in precipitation of EEC in El Abra Formation, as well as on the origin of LEC cements. EEC precipitated from varied fluids ranging from freshwater to evaporated seawater including normal seawater and various mixtures during repeated intraformational exposure. Fluid inclusions of LEC indicate uniform precipitation from freshwater at temperature less than about 50°C. This freshwater, with depleted $\delta^{18}O$, infiltrated through the Difunta clastic wedge, entered the El Abra platform through the basin from the west, while deposition of Méndez shale continued in the basin throughout the late Cretaceous, and precipitated the voluminous LEC.

GEOLOGICAL SETTING

El Abra Formation formed on an isolated mid-Cretaceous (Albian-Cenomanian) platform in northeast Mexico surrounded by intracratonic basins (Carrillo 1971; Enos 1974, 1983). It is

spectacularly exposed in the Sierra El Abra, a low-relief asymmetric anticline, 3-5 km wide and 125 km long (Yurewicz et al. 1997), that formed a giant oil reservoir, now breached and drained. Extensive quarries provide nearly continuous, dip-parallel exposure over a total distance of 3.5 km (Fig. 3-1). Previous work by Minero (1983, 1988) documented three major lithofacies associations: 1) peloid-miliolid, requienid, and bioclastic limestone, 2) fenestral, cryptalgal laminate, and lime mudstone and 3) laminated grainstone and rudist-skeletal limestone. These facies associations represent subtidal lagoon, tidal flat, and island/beach depositional environments, respectively. Two more-generalized facies belts can be recognized in El Abra Formation within the Sierra El Abra: tidally influenced cyclic deposits in the inner platform margin and Taninul or "reef" facies of the outer margin (Aguayo 1975, 1998; Minero 1983, 1988; Enos 1986). The tidally influenced cyclic rocks comprise Minero's first two lithofacies associations. Taninul facies consists primarily of rudist-reef and rudist-debris rudstones and grainstones. Shoaling-upward cycles, truncated cycles, and rhythms are represented in El Abra Formation of the inner platform margin. Closely spaced (mean 2.7 m) disconformities punctuated inner-margin deposition. Thick soil horizons, microkarst surfaces, solution-collapse breccia and extensive solution porosity mark multiple disconformities in the inner margin. In contrast, within outer-margin rocks, only equivocal subaerial exposure indicators, such as extensive solution porosity, mark possible disconformities.

El Abra deposition on the Valles-San Luis Potosí platform began in the Albian (Carrillo-Bravo 1971; Scott 1990) and continued into the Cenomanian, as indicated by early Cenomanian ammonites in Taninul quarry (Aguayo 1993, 1998, p. 4) and corroborated by Foraminifera (Langoria 1975) and rudists (Alencaster 1984; summarized by Scott, 1990). Colonial, spherical hydrozoans, *Parkeria sphaerica* Carter 1877, found in the platform-margin exposures (Minero et

al, 1983; this study) are reported from late Albian and early Cenomanian (Dieni and Trunsek 1979; Wilmsen 2003, p. 164). Examples of 'palimpsest' planktonic fossils in the Sierra El Abra were reported by Aguayo (1978, p. 78; Campanian) from CA quarry and Enos (1986, p. 169; Cenomanian) from TQ (Fig. 3-1). Most of the Valles-San Luis Potosí platform drowned abruptly in the Turonian and accumulated pelagic sediments throughout the Late Cretaceous including the Agua Nueva (Turonian), San Felipe (Coniacian-Santonian) and Méndez (Campanian-Maastrichtian) Formations. The Méndez Shale grades westward into clastic wedges of the Difunta Group that records the onset of the Laramide Orogeny in north-central Mexico (McBride et al. 1975; Soegaard et al. 1996; Ye 1997, p. 112). Neither Agua Nueva nor San Felipe appears to have covered El Abra Formation in the Sierra El Abra study area (Enos 1982, 1986; Minero et al. 1983; Aguayo 1998). At CA quarry, Méndez Shale oversteps the San Felipe Formation and onlaps the exhumed El Abra slope deposits. San Felipe pelagic limestone and shale overlie El Abra platform carbonates at the village of San Felipe, 5 km to the west. Very thin Aqua Nueva pelagic limestones cover El Abra platform carbonates 25 km south of Ciudad Valles (Minero et al. 1983, p. 136; Basáñez et al. 1993, p. 57) and 70 km north (in outcrop, Passagno 1969, and Perez-1 well, Basáñez et al. 1993, p. 56). It is not clear, however, whether the Méndez once covered El Abra Formation in the Sierra El Abra study area. It seems certain that the Sierra El Abra was submerged during most or all of the Late Cretaceous, as all deposits in the region are pelagic. The presence of Turonian and Campanian planktonic fossils in El Abra vugs supports this proposition. Thus the absence of Upper Cretaceous cover locally on the Sierra El Abra would reflect non-deposition and/or erosion, presumably submarine, perhaps localized by an elevated platform rim or by local upwarp, as postulated by Smith (1986, p. 120). Alternatively, Carrillo-Bravo (1971) and Aguayo (1978, p. 110) suggested that unconsolidated deposits

covering El Abra platform may have 'slid' eastward into the basin to form a turbidite wedge (Tamuín Member) recognized locally within the basal Méndez Formation. The Late Cretaceous-Paleocene Laramide Orogeny deformed El Abra Platform, creating the gentle, asymmetrical Sierra El Abra anticline (1-3º W dips; 5-8º E dips; Enos 1982; Minero et al. 1983, p. 16ff, Enos 1986, p. 162). Later post-Oligocene uplift exhumed and breached El Abra reservoir (Minero 1988; Yurewicz et al. 1997; Brennan 1999).

Post-Abra Disconformity

A disconformity is widely recognized between the mid-Cretaceous shallow-water platform carbonates and Late Cretaceous deep-water deposits on the Valles-San Luis Potosi platform (Smith 1986). The duration of the hiatus has been estimated at 5 to 24 Ma, depending on which strata overlie El Abra Formation at a given location (Smith 1986). Smith (1986, p. 120) estimated the hiatus at 17 million years in the Sierra El Abra study area, based on Méndez Shale pinching out against the El Abra Formation at the base of the escarpment. However, the Sierra El Abra was apparently submerged during most of this interval, based on the lack of subaerial exposure features on top of El Abra Formation, apparently continuous pelagic deposition in the surrounding basins and adjacent platform from Turonian through Maastrichtian time, and 'palimpsest' planktonic fossils within the uppermost El Abra Formation. There is evidence of a late Cenomanian disconformity elsewhere on the platform of varying duration as reported by Smith (1986). A late Cenomanian hiatus in the Sierra El Abra probably lasted no more than 3 million years, approximate duration of late Cenomanian and part of middle Cenomanian, and likely involved some subaerial exposure. This is the apparent time of extensive dissolution, creating megaporosity, perhaps in a regional meteoric aquifer in El Abra Formation or in


500 m
C
CM-1
CM-2
D
200 m
TQ
A
N
GOM
500 km
B
El Abra
VIII
VII
VI
V
IV
CM-1
CM-2
TQ
Sierra El Abra
PM-2
PM-1
Las Palmas
N
2 km
© 2016 Google
Image © 2016 DigitalGlobe
© 2016 INEGI
Google earth
E
PM-2
PM-1
N
CA
BP
PM-1
F

FIG. 3-1: A) Google Earth image of the location of the study area. GOM refers to Gulf of Mexico. Yellow box represents area in B. B) Location of quarries in the Sierra el Abra. Sections measured for this study were located in CM (abbreviated from Cementos Mexicanos, which owns this quarry) and PM (abbreviated after the town of Las Palmas in which this quarry is located). Roman numerals follow the identification scheme of Aguayo (1975) and Minero (1983). Dashed line traces the slope break of El Abra platform. C) Google Earth image of CM quarry is showing location of stratigraphic sections (traced). CM-1 exposes the tidally influenced cyclic rocks while CM-2 exposes the skeletal grainstone nearer the margin. The quarries west of CM (shown in B) expose rocks deposited in tidal flats and the subtidal lagoon (Minero 1983). D) Image of TQ quarry, which exposes the reef facies of El Abra Formation (Enos 1986). E) PM quarry. PM-1 (traced) exposes reef facies while PM-2 (traced) exposes interbedded skeletal rudstone and grainstone. CA is the abandoned Cementos Anahuac (CA) quarry (Enos 1982; Minero et al. 1983). BP is a borrow-pit exposing San Felipe Formation, which is overstepped by Méndez Formation at the foot of the El Abra escarpment in CA (Enos 1982; Minero et al. 1983, p. 18). F) PM-1 section. The length of section (dashed line) is 42 m

migrating mixing zones. This secondary porosity was reduced by isopachous cement (RFC-2), locally overlain by internal sediment containing Cenomanian planktonic Foraminifera (Enos 1986, p. 169). Sediment containing late Turonian planktonic foraminifers (Aguayo, 1978) apparently further reduced large secondary porosity, indicating pores tens of meters below, but connected to, the seafloor during the Turonian transgression. Despite all this record, the absence of subaerial-exposure features from top of El Abra Formation remains a curious conundrum.

METHODS

Four stratigraphic sections were measured across the platform margin in the Sierra El Abra (Fig. 3-1). Two sections, CM-1 and CM-2, measuring 72.5 m and 18 m, respectively, are in inner-margin rocks at Cementos Mexicanos (CM) quarry (Fig. 3-1B). The CM quarry is stratigraphically and spatially much deeper into the platform than when studied by Minero (1983) and Aguayo (1975, 1978). The quarry exposes transitions from tidally influenced, distal-margin deposits (CM-1) to the skeletal grainstone (CM-2) interpreted as marginal shoals by Minero (1983), nearly 1 km from the slope break. Two sections, PM-1 and PM-2 (Fig. 2.1D), measuring 42 m and 41 m thick, respectively, are in reef or shoal facies near the margin. PM-1 (Fig. 2-1F) is within 100 m of the slope break. PM-2 exposes interbedded rudstone and skeletal grainstone about 400 m behind the slope break. The measured sections provide qualitative and quantitative data on facies distribution and thicknesses, macroscopic diagenetic features, Dunham (1962) textures, and sedimentary structures in the cyclic uppermost El Abra Formation. Multiple disconformities were recognized based on various subaerial exposure features. The lateral spacing of the sections (300-400 m within CM quarry) allowed documentation of continuity or changes of depositional units, subaerial-exposure features, etc. Each CM section was sampled with an average spacing of 50 cm in the tidally influenced, cyclic rocks. Rocks at

the margin (PM) are sampled with average spacing of 1 m. One hundred 2X3-inch thin sections and polished slabs of varied dimensions were prepared from oriented rock samples. Pores were classified using the terminology of Choquette and Pray (1970). Cements zones were identified using transmitted light and cathodoluminescence petrography. Crosscutting relationships and correlation of zones between stratigraphically adjacent samples established the cement stratigraphy. Fluid inclusions in cements are studied to determine the compositions of the precipitating fluids. Doubly polished thick sections (~130 μm) were prepared for microthermometry to obtain final melting temperatures of ice (Tm ice) (Goldstein and Reynolds 1994). Petrographic criteria were used to identify primary fluid inclusions (Goldstein 2003). Thick sections containing all-liquid fluid inclusion were cut into small chips (~2 mm square) and heated overnight at 150-170°C to generate bubbles by stretching inclusions, which were then frozen. A Linkam T 95-PE heating-and-freezing stage mounted on Olympus BX53 microscope was used to conduct microthermometry. The stage was calibrated with a precision of ±0.1 °C, using synthetic fluid inclusions with known compositions. The final melting temperature of ice correlates with the percentage of salt in fluid inclusions (Potter et al. 1978; Goldstein and Reynolds 1994). Multiple freezing runs were completed for each inclusion to ensure precise documentation of the Tm-ice values.

CEMENTS OF EL ABRA FORMATION

Cementation in El Abra Formation occurred in syndepositional, intraformational, extended surface, and shallow- and deep-burial diagenetic settings (Fig. 3-2). Early marine diagenesis resulted in precipitation of meniscate micritic cement and early radiaxial fibrous cement (RFC-1) in the outer margin. Early surficial diagenesis, repeated at most successive disconformities, created extensive dissolution porosity (D-1), reduced by crystalline internal

sediment (CIS) and early equant cement (EEC) in the inner margin. Meteoric, hypersaline, and mixed-water diagenesis precipitated EEC during successive exposure intervals. A second, pervasive episode of dissolution (D-2) in the late Cenomanian created voluminous large-scale secondary porosity, followed by flooding that produced RFC-2 in the inner margin and RFC-2 and PIS in the outer margin. Physical compaction, possibly caused by transitory Campanian sedimentary cover (Tamuín Member, Aguayo and Kanamori 1976; Aguayo 1978, p. 110; Carrillo-Bravo 1971), resulted in physical breakage of skeletal grains, followed by precipitation of large volumes of LEC. Further burial into higher temperature and pressure conditions during Laramide deformation resulted in fracturing and stylolitization, followed by hydrocarbon emplacement. Post-Oligocene uplift of the Sierra El Abra exhumed El Abra platform margin,

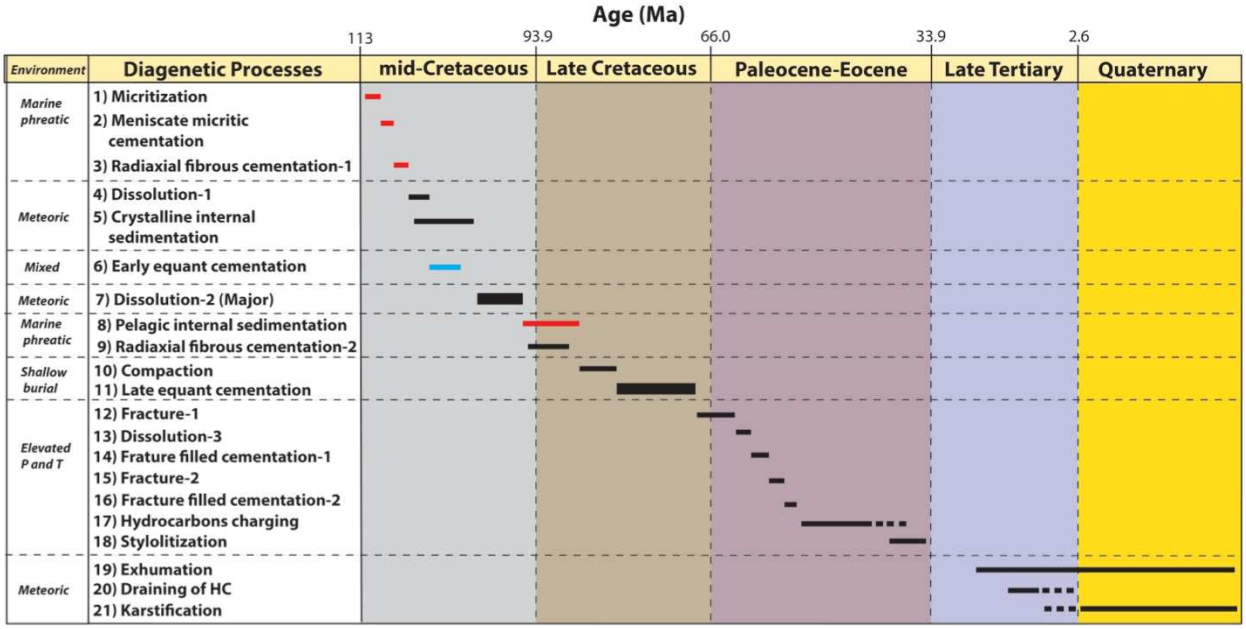

FIG. 3-2: Paragenetic sequences in El Abra Formation. Vertical axis records environments and their diagenetic products. Horizontal axis is time (Gradstein et al. 2004), not to scale. Thicker bars for products 7 and 11 emphasize the intensity of these two events; it is not a quantitative representation. Due to cyclic nature of El Abra deposition and subaerial exposure, meteoric and marine phreatic environments are juxtaposed multiple times with varying expression in inner-margin rocks. However, for simplicity only one common sequence of events is presented. RFC-1 (red bar) occurs only in outer margin and EEC (blue bar) only in inner margin. Thus they are not juxtaposed, although they must have overlapped in time, as each one kept pace with sedimentation. Meniscate micritic cements and pelagic internal sediments are restricted to the

outer margin (red bars). Timing of hydrocarbon charging and drainage is based on the study of Brennan (1999) and Yurewicz et al. (1997).

drained hydrocarbons, and introduced extensive karstification (Brennan 1999; Yurewicz et al. 1997). A brief summary of the cements follows.

Early Equant Cement (EEC)

Early equant cement occurs only in the tidally influenced rocks (CM-1) and is entirely absent from outer-margin samples. Equidimensional crystal morphology characterizes EEC, which exhibits uniform extinction under cross-polarized light. Early portions of crystals have abundant inclusions, resulting in cloudy appearance near the pore wall, whereas larger crystals toward the center of the pore are clear (Fig. 3-3 B). EEC reduces both primary (BP, WP, FE) and secondary porosity (sx-FE; MO) (Fig. 3-3 A and B).

Radiaxial Fibrous Cement (RFC)

Radiaxial fibrous cement forms isopachous crusts of turbid, inclusion-rich crystals characterized by concave-outward twin lamellae, optic axes that converge away from the substrate, and sub-crystals that diverge in the same direction, producing sweeping extinction under cross-polarized light (Kendall and Tucker 1973; Kendall 1985; Flügel 2004, p. 294; Richter et al. 2011). Two generations occur. RFC-1 is confined to primary pores in the outer margin (PM) (Fig. 3-3C). RFC-2 occurs exclusively in secondary pores in both inner and outer margin rocks (Fig. 3-3 D and E).

Late Equant Cement (LEC)

Late equant calcite cement occludes the remaining primary pores and smaller secondary pores and lines larger molds and vugs, as the last major episode of cementation in both inner- and outer-margin rocks. It forms mosaics of clear (inclusion-poor), equant crystals generally

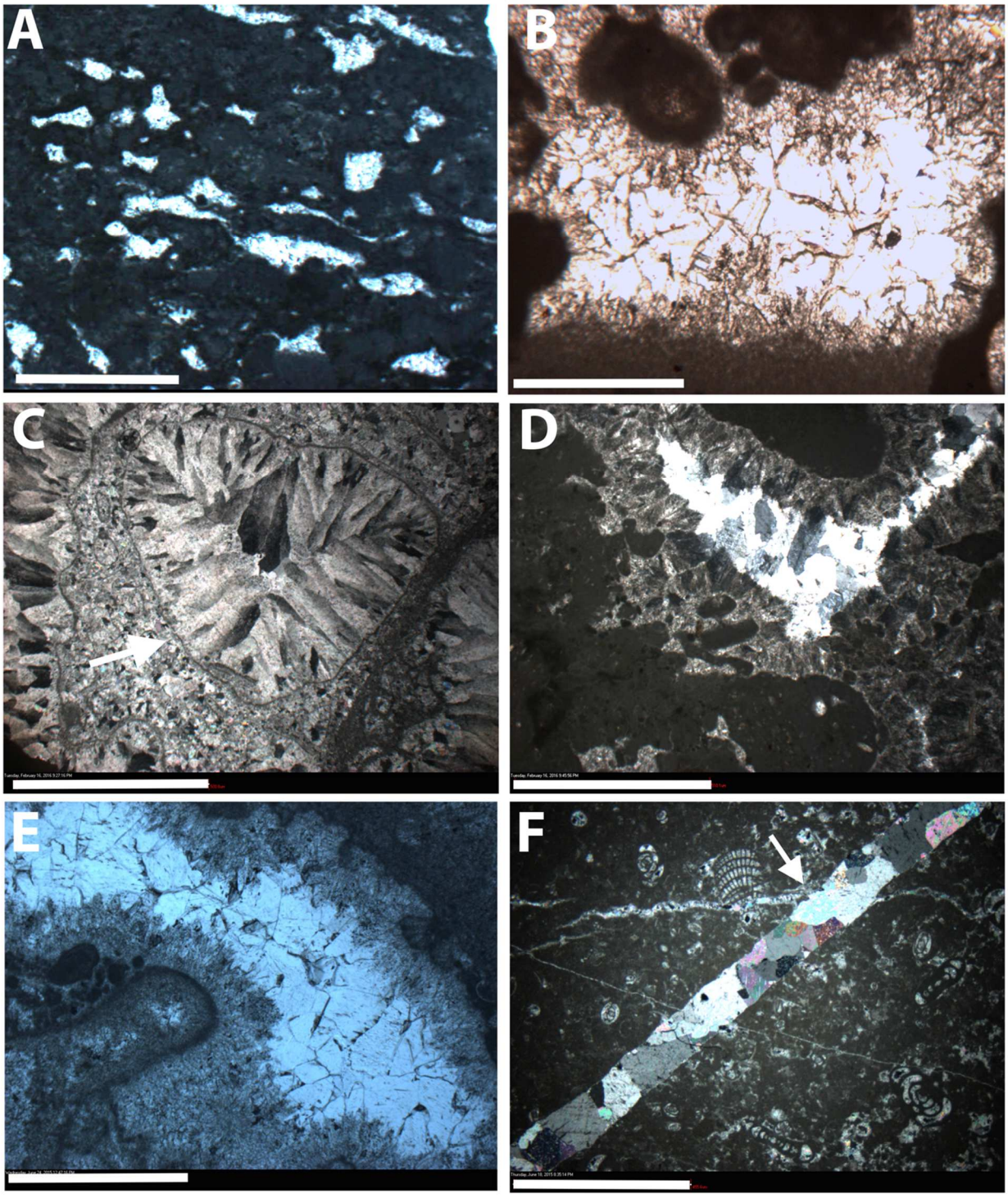

FIG. 3-3: Photomicrographs of calcite cements in El Abra Formation. Scale bars are 500 µm except in B, which is 200 µm. A) Early equant cement (EEC) in fenestrae. B) EEC in solution-enlarged fenestra. Note inclusion-rich border and the increase in crystal size towards the pore center. C) Radiaxial Fibrous cement (RFC-1) within intraparticle pore (cf-WP, arrow) of neomorphosed rudist. D) and E) Late equant cements (LEC) overlying RFC-2 in solution-

enlarged pores. F) Cement-filled fracture (FR-1, arrow) cut by FR-2. A, B, and D are from CM-1 and C, E, and F are from PM-1 section.

larger than 100 μm (Fig. 3-3 D and E). LEC is the most voluminous diagenetic product in El Abra Formation.

Fracture Filling Calcite Cement (FFC)

Two generations of fracture filling cement (FFC-1 and FFC-2) fill two generations of fractures (FR-1 and FR-2) (Fig. 3-3E). FR-2 is wider (up to 1 mm) and crosscuts FR-1. Each generation of FFC fills a minor amount of large-scale secondary porosity.

CATHODOLUMINESCENCE PETROGRAPHY

A total of 27 cathodoluminescence zones are identified from El Abra cements EEC and LEC. RFC-1 and RFC-2 displayed only blotchy luminescence lacking correlative zones. Color, brightness, pattern, and crosscutting relationships of luminescence helped distinguish among the many zones. The initial 21 zones were observed in EEC, each, with few exceptions, truncated by the succeeding intraformational disconformity. LEC contains four distinctive zones (Z-22 through Z-25), pervasive throughout the sampled portion of El Abra Formation. Luminescent zones Z-26 and Z-27 characterize cements in fractures and a few large vugs. None of the cement zones is present in every sample, although Z22-25 are nearly so.

Cathodoluminescence Zones in Early Equant Cements

Cathodoluminescence zones in EEC (Z-1 to Z-21*)* form four broad categories, based on similar luminescent characteristics. *Banded* cements are characterized by narrow, dull bands, ranging in thickness up to a few micrometers, separated by non-luminescent bands. These include Z-1, Z-3, Z-8, Z-12, Z-16, and Z-18 (Fig. 3-4 A, B and D; Fig. 3-5A and B). *Dull* luminescent cements are composed of one or several bands of dull luminescence. They differ

from banded cements in lacking non-luminescent subzones. Thickness of these zones is variable. Z-4, Z-7, Z-9, and Z-15 are dull (Fig. 3-4 B, C, and D). *Bright-orange* luminescent with tightly-spaced subzones characterizes Z-2, Z-5, Z-10, Z-13, Z-17 and Z-21 (Fig. 3-4 B and D; Fig. 3-5 A and D). Z-6, Z-11, Z-14, Z-19 and Z-20 are *non-luminescent* zones (Fig. 3-4 C; Fig. 3-5 B, C and D).

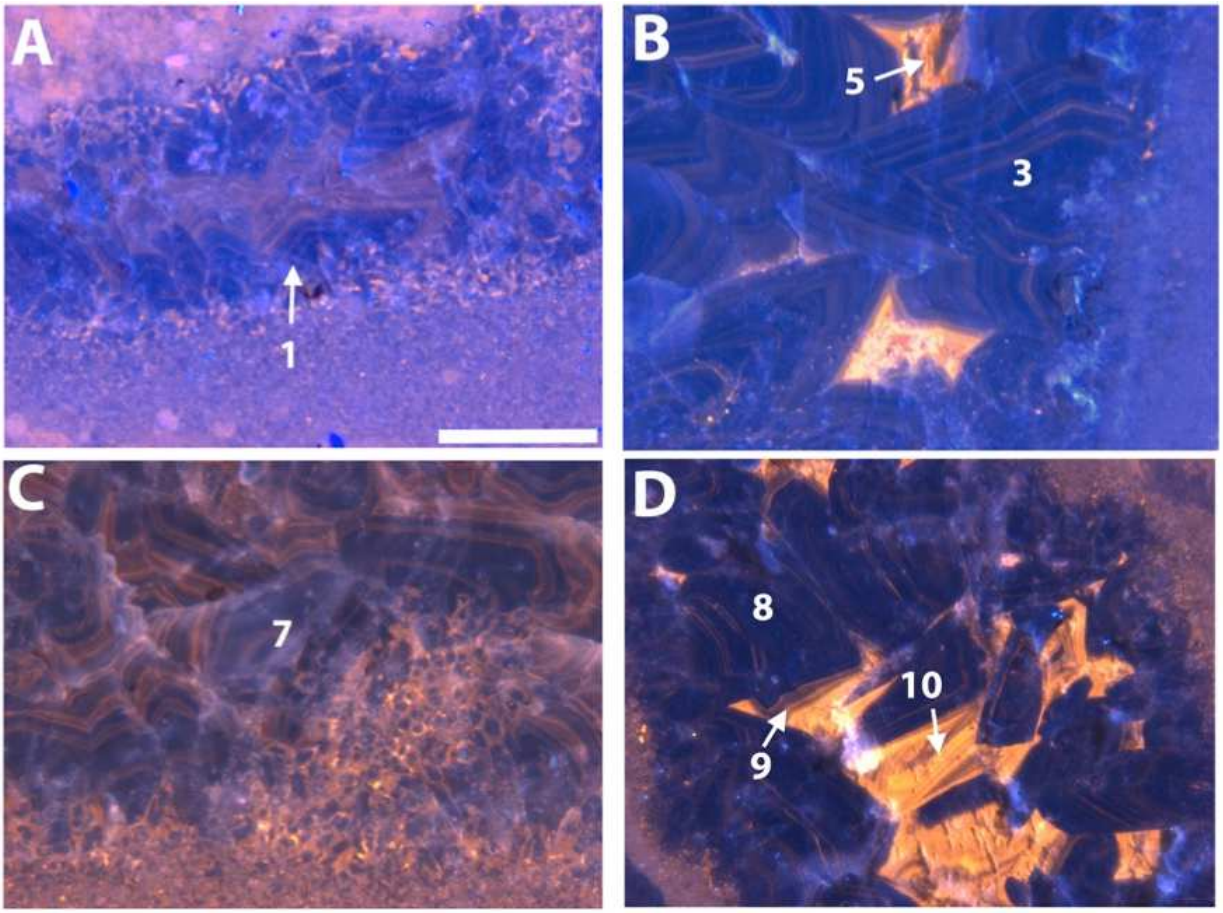

FIG. 3-4: Photomicrographs of cathodoluminescence cement zones in EEC at CM-1 section. Scale bar is 200 for all images.

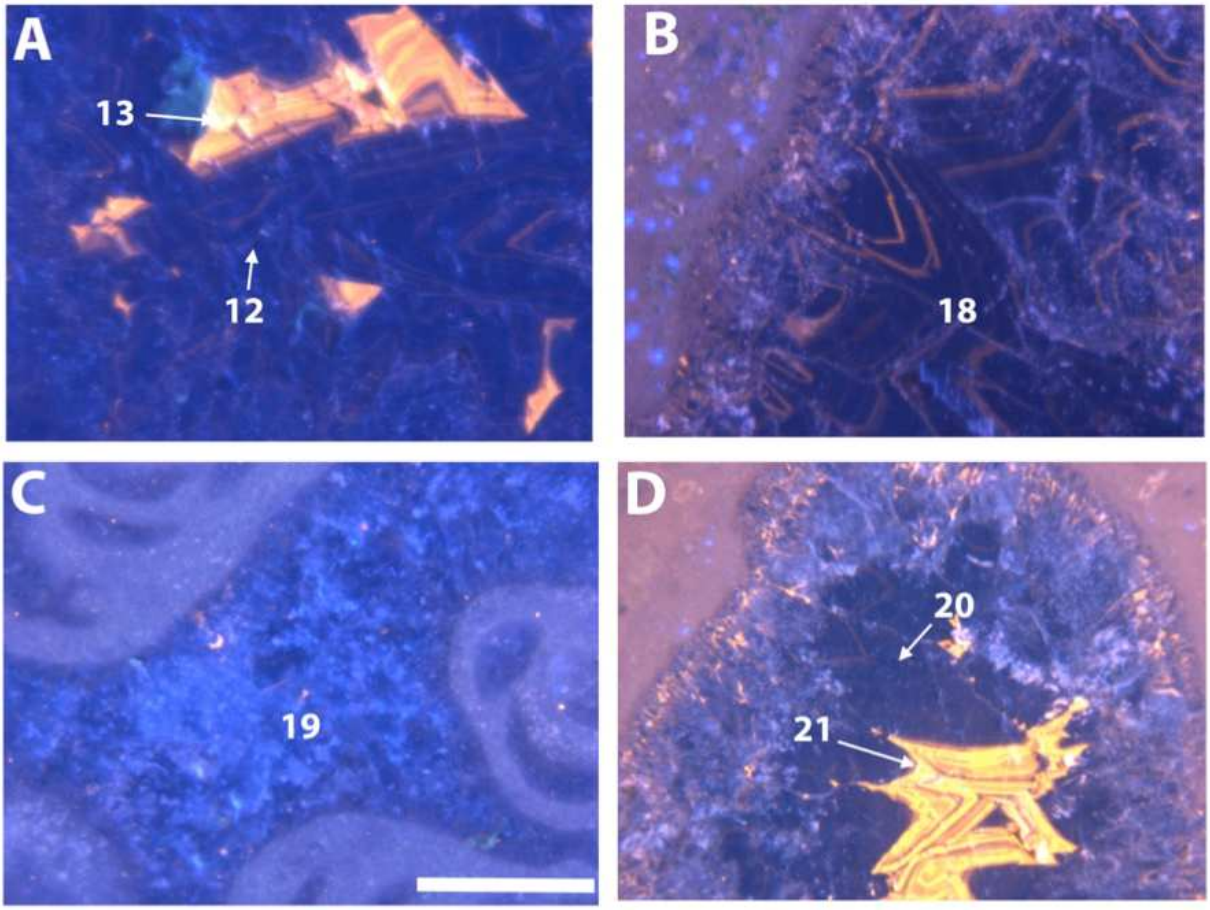

FIG. 3-5: Photomicrographs showing cathodoluminescence cement zones in EEC in CM-1 section. Scale bar is 500 μm for all photos.

Cathodoluminescence of Radiaxial Fibrous Cements (RFC-1 and -2)

Radiaxial fibrous cements (RFC-1 and -2) show a mix of bright luminescent spots with moderate to dull luminescence, resulting in a blotchy appearance. The brightest spots are typically at crystal terminations. Repetitive bands of dull to bright blotchy luminescence are common in RFC (Fig. 3-6 A and B). Such blotchy luminescence is commonly interpreted as neomorphic alteration of a precursor high-Mg calcite to a more stable low-Mg calcite, while preserving its original fabric (Lohmann and Meyers 1977; Videtich 1985; Reinhold and Kaufmann 2010). El Abra RFC contains abundant inclusions of euhedral to subhedral micro-dolomite, as reported by these authors. Luminescent zones in RFC cannot be correlated among adjacent samples, so are not useful in cement stratigraphy.

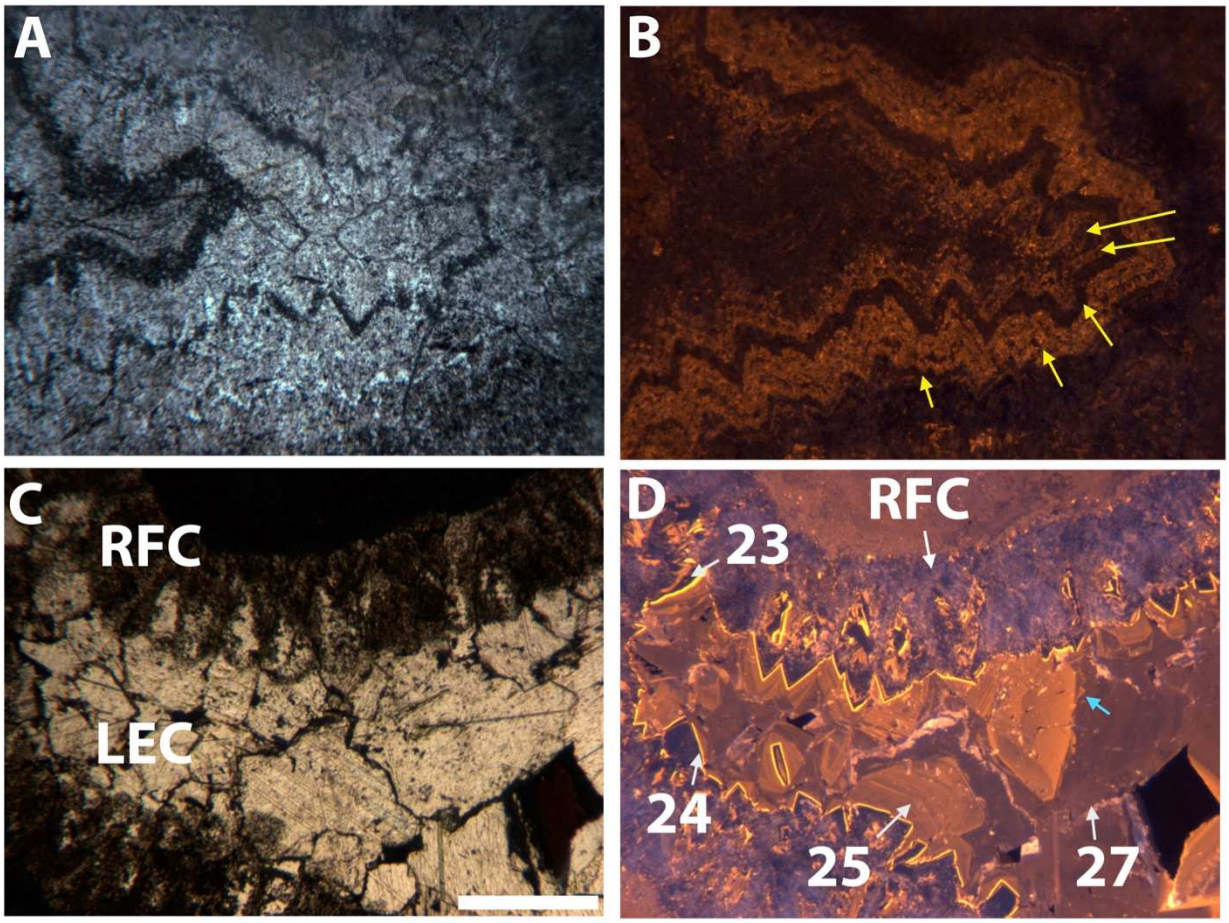

FIG. 3-6: Paired photomicrographs in transmitted light (left) and cathodoluminescence (right) showing zones in RFC and LEC. A and B) Multiple cement zones (arrows) in RFC-1 exhibiting blotchy luminescence at PM-1. C and D) RFC-2 showing blotchy luminescence is overlain by LEC, containing luminescent zones Z-23-25 in CM-1. Zone 27 is an extension of cement from an adjacent fracture (FFC-2). Note the corroded contact between Z-25 and Z-27 (blue arrow). Scale is 500 μm.

Cathodoluminescence Zones in Late Equant Cement (Z-22 to Z-25)

Four distinctive cathodoluminescence zones *(Z-22 to Z-25)* are observed in LEC. Each zone occurs throughout CM-1 and PM-1 measured sections. *Zone 22* is characterized by as many as 15 bright-orange luminescent subzones separated by hairline non-luminescent subzones. The width of this zone is variable among samples (Fig. 3-7 B and F). It fills as much as 50% of some pores. *Zone 23* is non-luminescent (Fig. 3-7 B, D, and F). Its width is uniform, which makes it easy to recognize in contrast to the other variably wide zones in LEC. *Zone 24* is uniformly very narrow, in contrast to other zones in LEC (Fig. 3-7 B, D, and F). A single or double band of

bright-orange luminescence makes this zone easy to identify. *Zone 25* is the widest luminescent zone in LEC; it exhibits faint banding in dull-orange luminescence (Fig. 3-7 B, D, and F).

Cathodoluminescence Zones in Fracture-filling Cements (Z-26 to Z-27)

First generation fractures (FR-1) are filled by cement of luminescent *Zone-26,* the brightest in El Abra Formation (Fig. 3-8). This distinctive luminescence also identifies Z-26 in some large vugs in samples cut by FR-1, where it overlies Z-25 and locally underlies Z-27 (Fig. 3-8D). The contact between Zones 25 and 26 appears corroded (Fig. 3-8 B), suggesting an intervening dissolution episode.

Cement with dark reddish-brown luminescence (Z-27) fills the second generation of fractures (FR-2) and some adjacent large vugs. Multiple nucleation sites in Z-27 resulted in a disjunctive contact between Z-26 and Z-27. This cement contains abundant 2-phase hydrocarbon inclusions, visible under UV-light. Brennan (1999) studied fluid inclusions in cements occluding meso-scale fractures (his calcite IV, most likely cements of Z-27) and obtained precipitation temperatures between 35°C in primary fluid-inclusion associations and a maximum of 110°C in secondary FIAs.

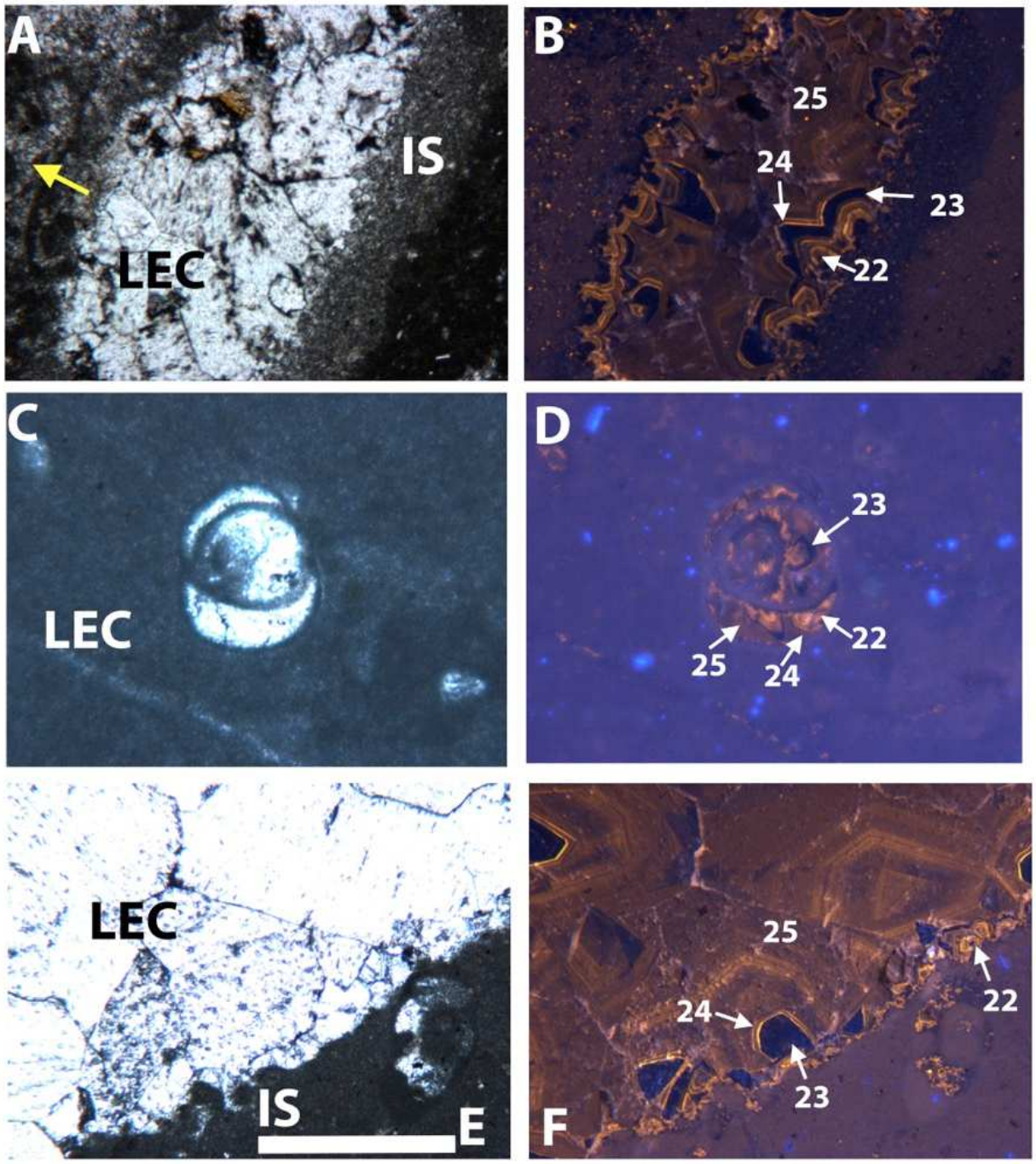

FIG. 3-7: Paired transmitted and cathodoluminescence photomicrographs showing cement zones in LEC at CM-1. Scale is 500 μm in all images. A and B) Cement zones 22 to 25 postdate internal sediments and occlude a vug (ir cf-VUG). Yellow arrow shows up-section in A. C and D) Zoned LEC occluding foraminifer chambers (cf-WP). E and F) LEC, zones 22-25, occlude a vug.

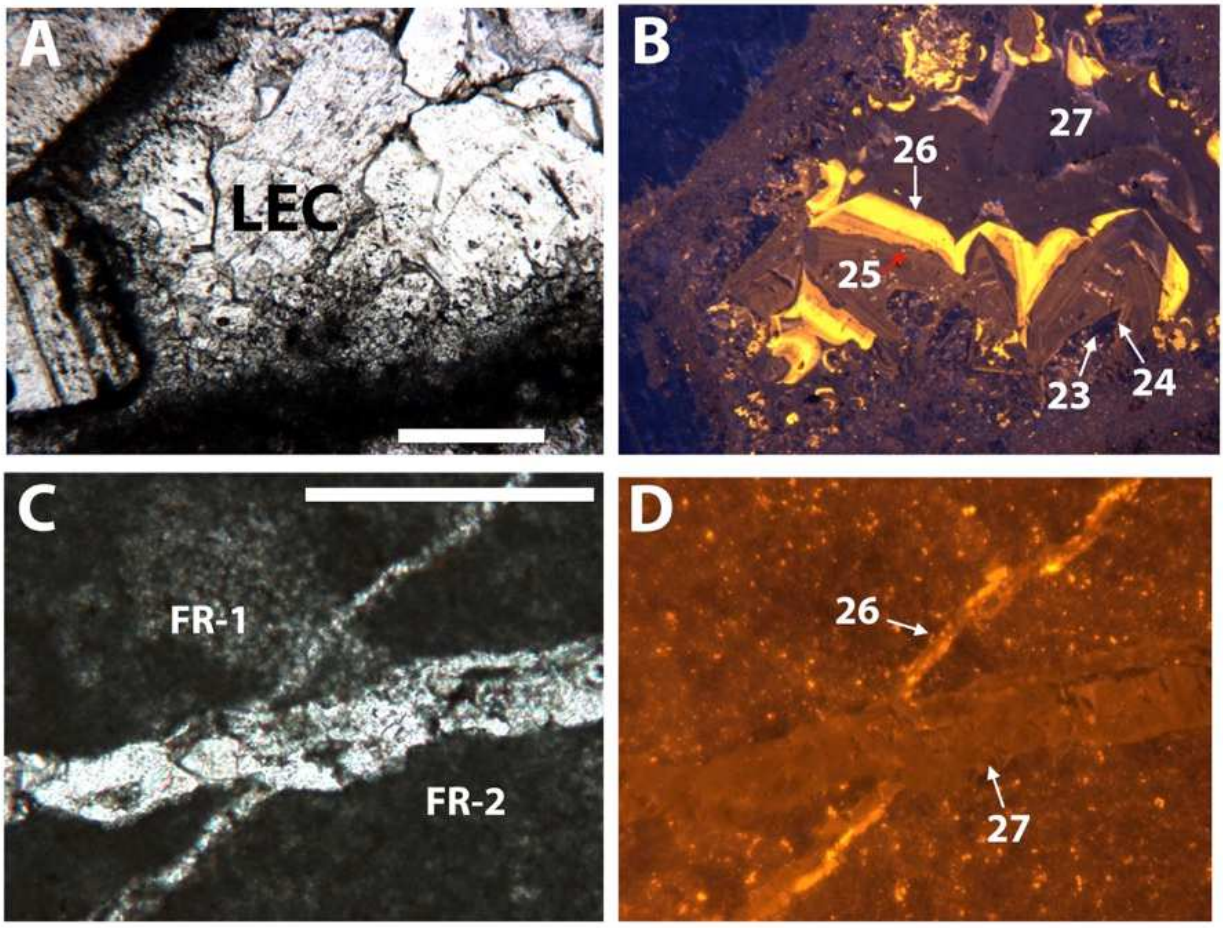

FIG. 3-8: Paired transmitted-light and cathodoluminescence photomicrographs showing cement zones in fracture-filling cements and crosscutting relationships with LEC. A and B) From PM-1 shows LEC (Z-23-25 overlain by FFC-1. FFC2 (Z-27) overlies Z-26. Scale bar is 0.5 mm. C and D) FR-2 cuts FR-1; apparent offset is merely extension. Note contrasting luminescence. Scale bars are 1mm.

RELATIVE AGES OF CEMENT ZONES

Each cement generation has a crosscutting or overgrowth relationship with the preceding generation that allows for accurate relative age dating of the various cement zones (cf. Goldstein 1998) as summarized in Table 3-1.

Intraformational Indicators

El Abra Formation in CM-1 quarry is punctuated by 27 disconformities, 17 of which have paleosol horizons. Paleosol conglomerates contain abundant clasts with pores reduced by

EEC. Where a cemented pore is truncated at the edge of the clast, precipitation of the truncated cement preceded clast deposition at the unconformity. A second criterion is pores in clasts reduced by two generations of cement, whereas the matrix pores contain only the later generation. A third scenario is an interior pore within a clast, partially reduced by early cement and then filled with internal sediment of the conglomerate matrix. In any of these scenarios, EEC predates erosion and deposition of the clasts, thus documenting intraformational origin. Laminated crusts that envelop a clast containing pores reduced by EEC indicate the intraformational origin of the cement as well. EEC reducing voids in circumgranular cracks and rhizoliths probably precipitated during soil formation (Goldstein 1998).

Post-depositional indicators

Physical breakage of grains by compaction is common during shallow burial. Cement precipitated on broken edges of grains post-dates compaction, which probably began during late Cretaceous. Two episodes of fracturing recorded in El Abra Formation probably developed during the Laramide Orogeny (Late Cretaceous-Paleogene), perhaps coincident with maximum burial (late Eocene, Yurewicz et al. 1997). Fracture-filling cements, FFC-1 and FFC-2, presumably postdate onset of the Laramide Orogeny. Two sets of stylolites, one horizontal, one inclined, which offset fracture-filling cements, probably represent maximum burial and tectonics, respectively.

	Mid-Cretaceous		Late Cretaceous	Post-Cretaceous		
	Intraformational Indicators		Post-depositional indicators			
Cement zone	1*Predates clast deposition	2*Bracketed by paleosol features	3*Postdates Initial compaction	Postdates FR-1	Postdates FR-2	Postdates stylolites
1	X	X				
2	X	X				
3	X	X				
4	X	X				
5	X	X				
6	X	X				
7	X	X				
8	X					
9	X					
10	X					
11	X					
12	X					
13	X					
14	X					
15	X	X				
16	X	X				
17	X	X				
18		X				
19	X					
20	X					
21	X					
22			X			
23			X			
24			X			
25			X			
26				X		
27				X	X	

Table 3-1: Crosscutting relationships of various cement zones that indicate relative ages of cement zones. X denotes that a cement zone is observed with the relationship described in that column. 1*: Cements truncated at margin of clasts reworked into the overlying cycle. 2* Paleosol features, e.g. laminated crust, envelops clasts with pores reduced by EEC. 3*: Cement precipitated on fractured grains.

CEMENT STRATIGRAPHY

Distribution of Cathodoluminescence Zones

EEC (luminescent zones Z-1 to Z-21) precipitated diachronously during repeated intraformational subaerial exposure that punctuated marine deposition. The vertical extent of these early cements ranges from 1 m (Fig. 3-9 at 12 m, 15 m, and 50 m) to nearly 7 m (Fig. 3-9, Z-11 at 22 m), with the majority extending <4 m below a surface of subaerial exposure. The

majority of EEC zones are confined between vertically adjacent subaerial exposure horizons (e.g. Fig. 3-9 at 4-6 m), although several extend across an underlying subaerial exposure surface (Fig. 3-9, Z-11 and Z-14). EEC is restricted to tidally influenced rocks (CM) and is entirely absent from the outer-margin samples (Fig. 3-10). If the distribution of the cements is assumed to be a record of the extent of the freshwater phreatic lens, then this limited vertical extent suggests that freshwater lenses developed at disconformities were shallow and thin, usually confined within 4 m of subaerial-exposure surfaces. Such a shallow and localized configuration of the freshwater lenses restricted the lateral distribution of early equant cements to the inner margin rocks. This shallow configuration is hardly surprising, given the assumed narrow width of exposed island belt, highly permeable sediments, and proximity to a shoreline, defined ultimately, at maximum low stands, by the very steep (>40º, Enos 1982) platform margin. Radiaxial fibrous cement (RFC-1), presumed marine cement, which occurs only in primary pores in the outer margin (PM), was syndepositional and contemporaneous to precipitation of EEC in the inner margin rocks (Fig. 3-10).

A second generation of radiaxial fibrous cements (RFC-2), also characterized by blotchy luminescence, is observed in secondary pores in quarries PM, CM, TQ (Enos 1986), and IV & V of Minero (1983) (Fig. 3-1B). Aguayo (1975, 1998) did not observe any marine cements west of quarry V (VI, VII, and VIII) and Minero (1983, p.127) recognized open vuggy pore networks in El Abra quarry (VIII). He attributed the absence of marine cements to a setting in the lee of postulated platform-margin islands and muddy tidal-flat sediments, which precluded mechanical pumping of marine water to nourish cement growth.

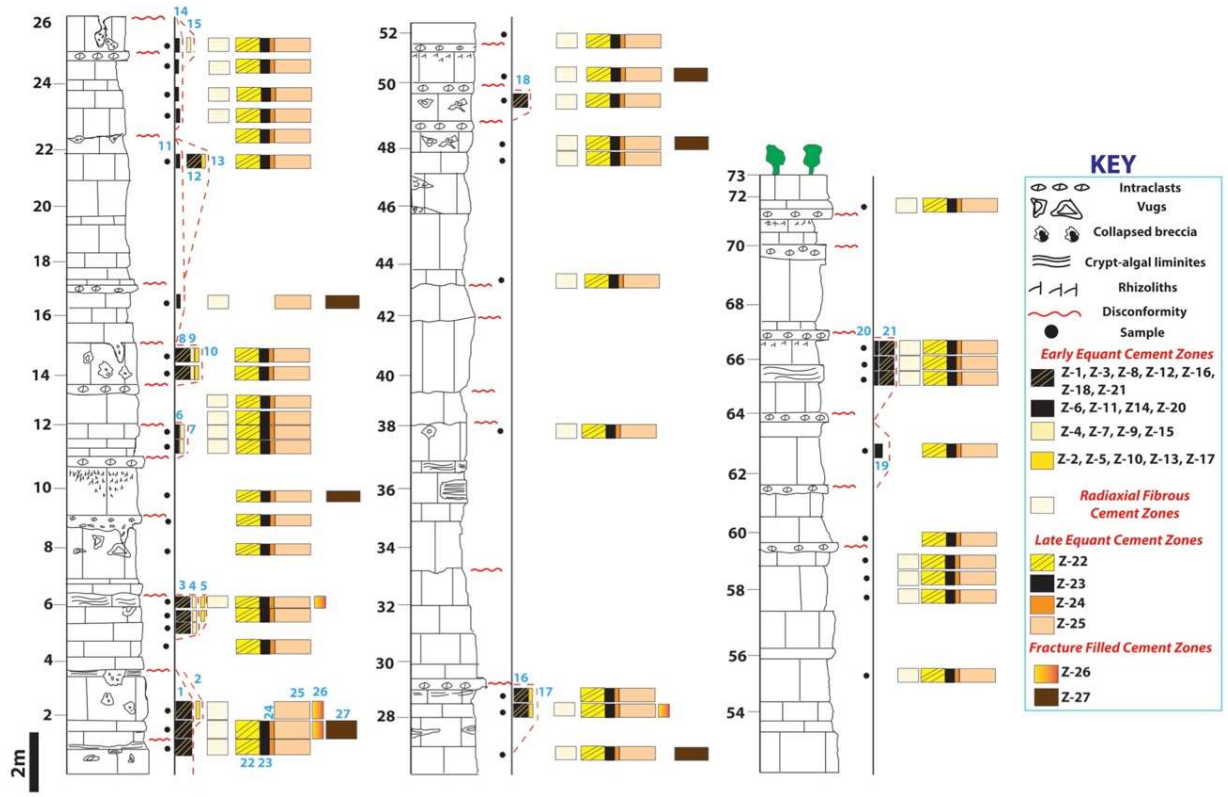

FIG. 3-9: Vertical correlations of cement zones in CM-1 section. Numbers refer to cement zones and red dashed lines trace the vertical extent of EEC zones. LEC zones persist throughout. The width of the bars approximates average relative thickness of the cement zones.

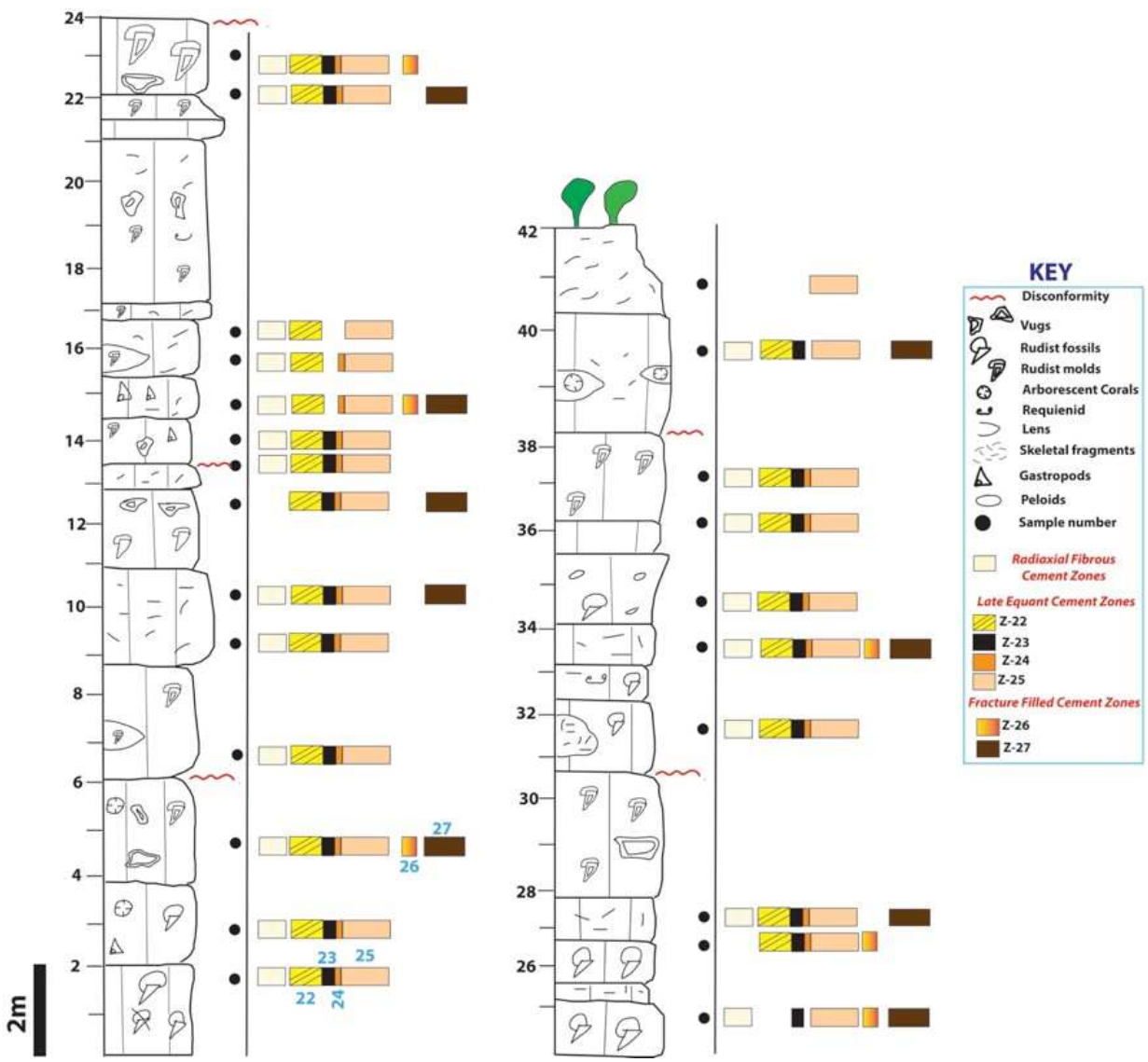

FIG. 3-10: Correlations of luminescent zones in LEC and fracture-filling cements (FFC) in PM-1 section. Bar width represents approximate average relative thicknesses of cement zones and extend essentially throughout section. Note that EEC is absent.

LEC **(**luminescent zones Z-22 to Z-25**)** postdated shallow burial (Table 1). All LEC zones are present in almost all samples from CM and PM quarries (Fig. 3-9, and 3-10). These correlations indicate that each cement zone was precipitated at about the same time throughout the intervals studied in both quarries. None of the cement zones in LEC show evidence of truncation or corrosion, except for minor corrosion of Z-25 where cements related to fracture filling overlie it. Minero (1983) and Brennan (1999) reported zones resembling Z-22, Z-23, and Z-25 from more interior sections (IV, V, & VIII) in Sierra El Abra. A rough estimate of the minimum width of the freshwater aquifer is the width of the SEA, nearly 3 km. The aquifer affected the entire stratigraphic section exposed in CM (72 m), suggesting that the freshwater lens may have followed oscillations in sea level. Fracture-filling cements (luminescent zones Z-26 and Z-27) are observed in fractures and a few large vugs, where transected by fractures.

FLUID-INCLUSION ANALYSES

Fluid-inclusion analyses of cements in El Abra Formation provide data on temperature of precipitation, salinity, and water saturation of early and late equant cements. Radiaxial fibrous cements are recrystallized, so fluid inclusions were probably altered. FFC and stylolite cements were studied in detail by Brennan (1999) to constrain the thermal history and hydrocarbon migration in El Abra Formation. Homogenization temperatures from secondary inclusions indicated temperatures of precipitation reaching 110°C for FFC and 115°C to 160°C for cements within stylolites (Brennan 1999). Such high temperatures, assuming likely geothermal gradients, indicate burial to depths of 5-6 km, consistent with the estimates of Yurewicz et al. (1997, p. 11). A 5-km overburden is, however, hard to reconcile, given the thickness of Upper Cretaceous rocks (~1100 m in the Tampico-Misantla basin; much less on the platform) and Paleogene Chicontepec flysch (900 m, again the axis of deposition was in the basin to the east) (Bush and

Govela 1978, p. 239; Brennan 1999). Bitter (1986, p. 91) tentatively concluded that numerous miliolid-bearing carbonate rock fragments and pebbles within the Chicontepec are derived from El Abra Formation exposed by Laramide uplift, a further counter-indication of 5-6 km of burial depth. Brennan (1999) suggested hydrothermal fluids as an alternative heating mechanism.

Early Equant Cement

Cement stratigraphy revealed that EEC zones Z-1 to Z-21 are intraformational in origin, precipitated during relatively brief periods of subaerial exposure. Fluid inclusions in EEC are aligned along crystallographic growth zones, are abundant in the core and deficient on the peripheries of crystals, and, rarely, include one or several inclusions much larger than the average (Fig 3-11). These are criteria for primary inclusions (Goldstein and Reynolds, 1994). Fluid inclusions in EEC include both all-liquid inclusions and two-phase inclusions, containing both liquid and vapor. No hydrocarbon inclusions are observed. There is no petrographic pairing of all-liquid and vapor-rich fluid inclusions, and some of the largest fluid inclusions are all liquid. This rules out necking down after a phase change and significant metastability. Thus, all-liquid fluid inclusions indicate entrapment at temperature less than about 50°C (Goldstein and Reynolds 1994).

Highly variable liquid-to-vapor ratios in two-phase inclusions in EEC provide insights into environment of diagenesis. The bubble size is variable and in some FIA the bubble is greater than 15 % of the inclusion volume. Such FIA with all-liquid inclusions and inclusions with large bubbles are indicative of heterogeneous entrapment in the vadose zone (Goldstein 1986a; Barker and Halley 1988; Goldstein et al. 1990). Other FIA contain large all-liquid inclusions, diagnostic of initial entrapment in a low-temperature phreatic zone (Goldstein and Reynolds 1994). This

indicates some generations of EEC precipitated in the vadose zone and others in a near-surface phreatic zone.

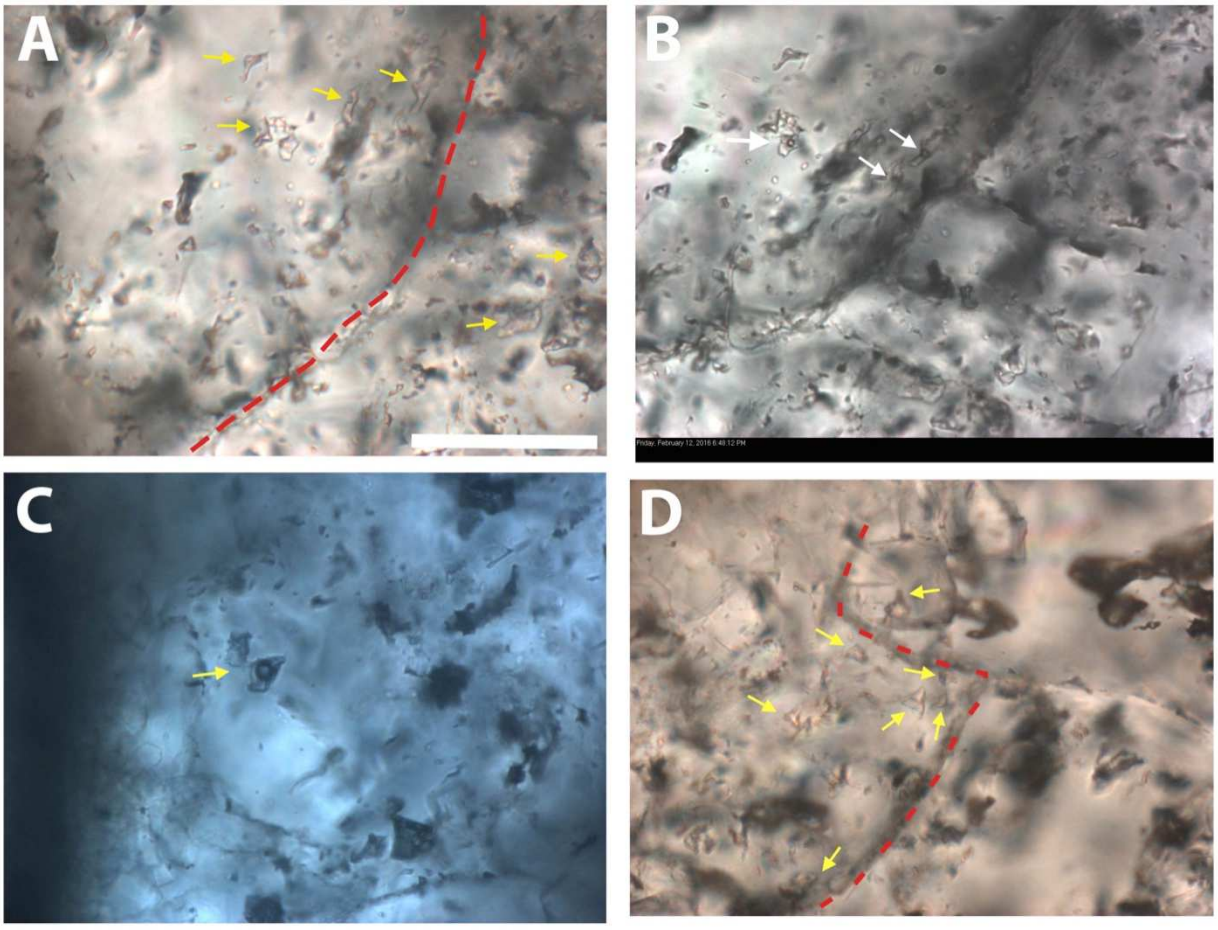

FIG. 3-11: Transmitted-light photomicrographs showing fluid-inclusion assemblages (FIAs) in early equant cement (EEC). Scale bar is 50 μm for all images A) All-liquid FIA (arrows) aligned with a crystallographic boundary, denoted by dashed red line. B) Similar view to A) after heating to generate vapor bubbles (arrows). C) Large, isolated, 2-phase inclusion. D) All-liquid FIA aligned with a crystallographic compromise boundary (dashed line).

Samples containing EEC used in microthermometry were chosen beneath four unconformities to understand the composition of fluids that existed during repeated subaerial exposure conditions in El Abra Formation (Table 3-2). The Tm ice ranged from 0.0°C to –2.6°C, corresponding to salinities ranging from 0 ppt to 49 ppt using the seawater-salt model (Goldstein and Reynolds 1994) (Fig. 3-12).

Disconformity elevation (m)	Sample elevation (m)	Tm ice (°C)	Salinity (ppt)
3.8	1.8	0.0 -0.5 -0.5 0.0	0 9 9 0
		-1.6 -1.6	30 30
		-1.6 -2.7	30 49
6.5	5.3	-1.8	33
		-1.9	35
		-2.6	47
15	14	-0.3 -0.3	6 6
		-0.3 -0.3	6 6
		-0.3	6
		-0.5	9
67.3	65.5	0.0	0
		0.0	0

Table 3-2: Fluid inclusion data of early equant cements from CM-1. Column 1 shows elevation of disconformity. Column 2 shows elevation of sample. Column 3 shows melting temperature of ice (Tm ice) in fluid inclusions. Values in red represent an FIA and values in black represent single, isolated fluid inclusions. Column 4 shows salinity values using seawater-salt model (Goldstein and Reynolds, 1994) to convert Tm ice into salinities. Notable is the wide range in salinities recorded in a single sample at 3.8 m.

Table 3-2 indicates different salinities that occurred and evolved at different disconformities. Sample CM-1.8, which is 2.0 m below a disconformity, yielded salinity values ranging from 0 ppt to 49 ppt. Sample CM-1 65.5, which underlies a disconformity by 1.8 m, yielded exclusively freshwater (0 ppt) salinity values. In sample CM-14, which underlies the disconformity by 1 m, salinity values range from 6 ppt to 9 ppt. Sample CM-5.3 yielded salinity values ranging from 33 ppt to 47 ppt at 1.2 m below a disconformity.

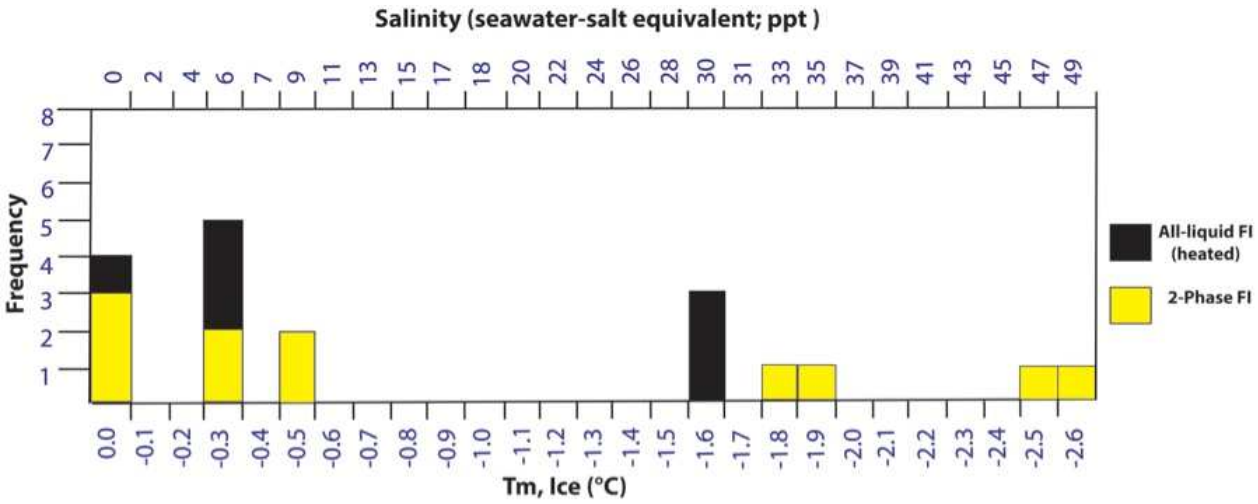

FIG. 3-12: Distribution of fluid-inclusion melting temperatures within early equant cements (EEC). Seawater-salt model (Goldstein and Reynolds 1994) is used to convert Tm ice into salinities (upper X-axis). Measurements are made on individual FI's, representing FIA's.

Fluids that precipitated EEC were extremely varied, ranging from freshwater to hypersaline including seawater (35 ppt) and various mixtures. All-liquid inclusions imply near-surface diagenetic conditions with temperatures less than about 50°C. Variable liquid-to-vapor ratios indicate cementation in the vadose zone. All-liquid or consistent liquid/vapor ratios indicate phreatic conditions. All are represented in EEC.

Late Equant Calcite Cement

The inclusions in LEC are large (Fig. 3-13), isolated, and all-liquid; they lack petrographic pairing precluding necking down or metastability. All-liquid inclusions imply near-surface phreatic conditions with temperatures less than about 50°C (Goldstein and Reynolds 1994). Eight all-liquid inclusions that generated bubbles upon artificial stretching yielded Tm ice of 0.0°C representing freshwater. Two values indicate salt contents up to 4 ppt (Fig. 3-14).

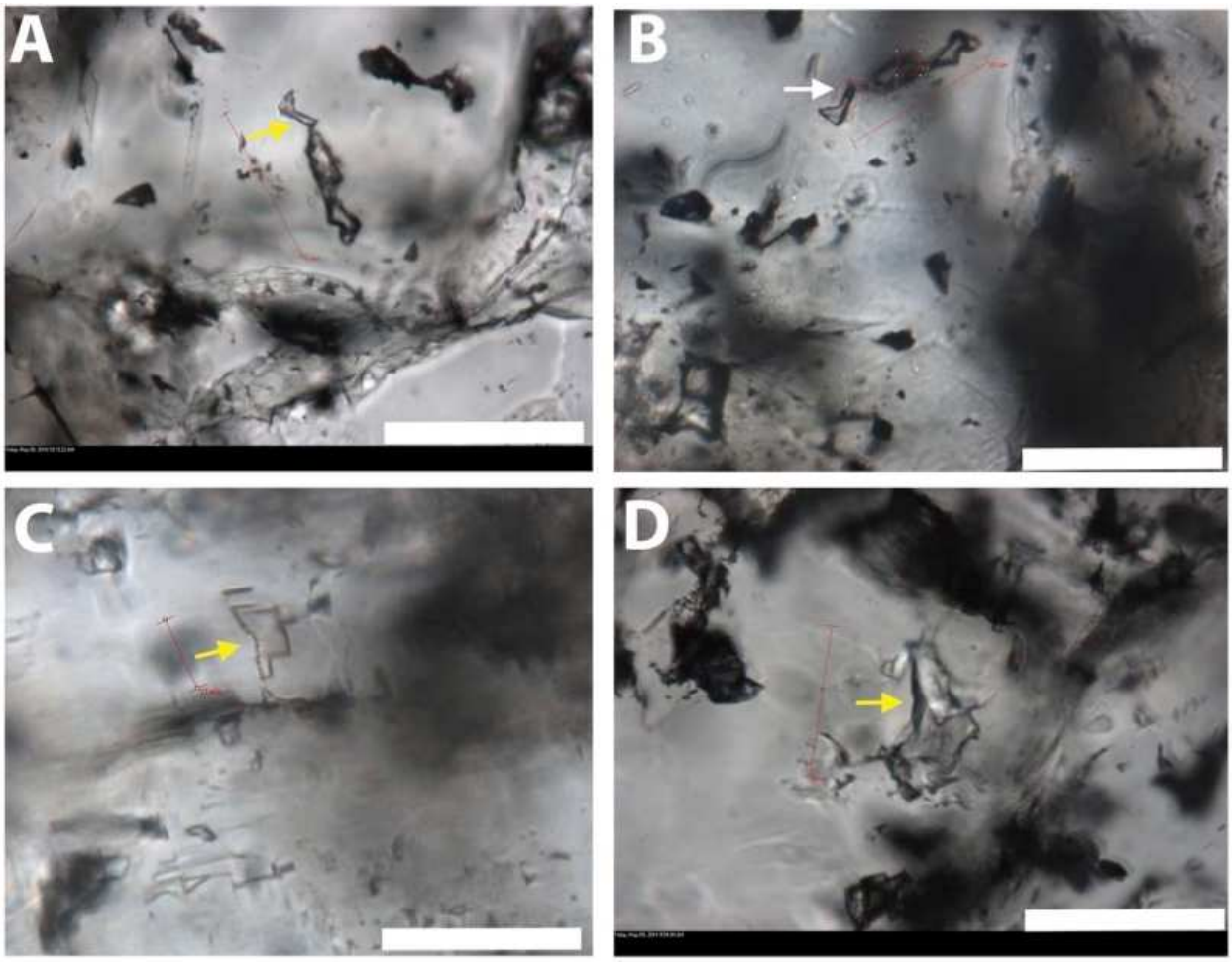

FIG. 3-13: Transmitted-light photomicrographs of fluid-inclusion assemblages (FIA) in late equant cement (LEC). Yellow arrows denote all-liquid inclusions and white arrows show 2-phase inclusions. Scale is 50 μm in all images. A) Large, isolated all-liquid inclusion. B) Same inclusion shown in A after stretching created a bubble (arrow). C and D) Large isolated all-liquid inclusions in LEC.

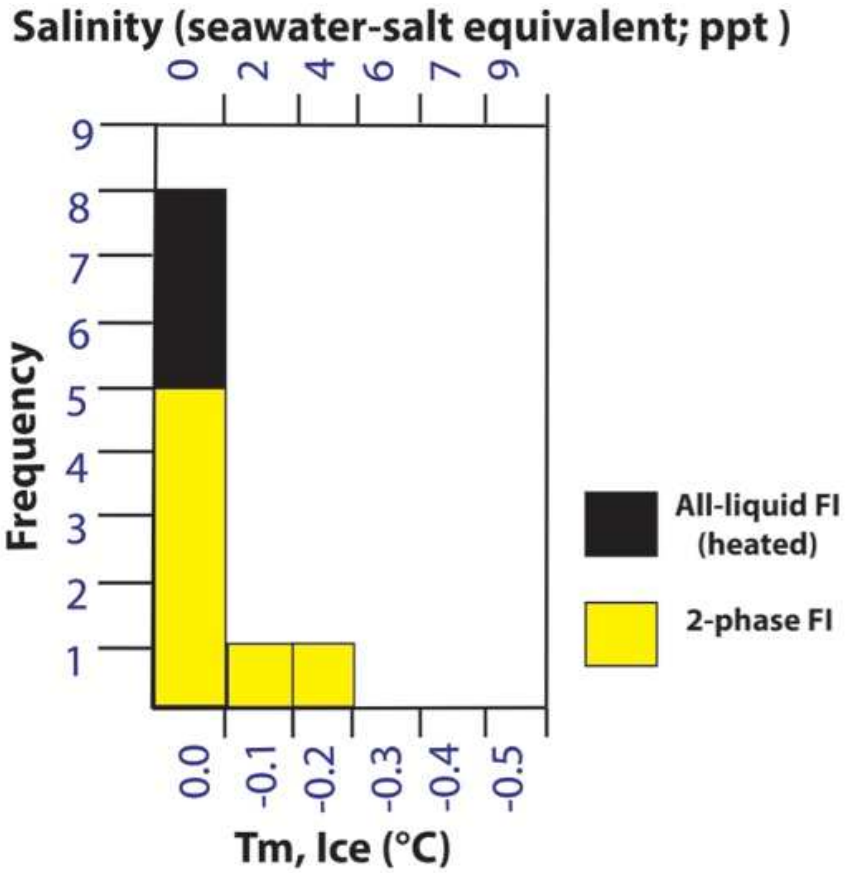

FIG. 3-14: Distribution of fluid-inclusion melting temperatures within LEC. Conventions are same as in Fig. 3-12.

DISCUSSION

Origin of Early Equant Cements

Cement stratigraphy revealed that EEC is intraformational in origin, precipitated during relatively brief periods of subaerial exposure. Thus EEC represents localized cyclic hydrologic lenses that did not pervade the entire formation. This study reported EEC from tidally influenced (CM) sections and its absence form the outer margin (PM). Minero (1983) possibly overlooked EEC from CM (his section III) section and also did not report EEC further west (Sections IV, V, and VIII). Brennan (1999) also did not report EEC from Section VIII, 3.2 km west of the slope break. Therefore, the lateral extent of EEC is apparently restricted to tidally influenced rocks (CM sections). The successive lenses that precipitated EEC had maximum widths of perhaps 450

m across dip, the distance between the inner and outer-margin quarries where EEC is absent. The vertical extent of EEC beneath disconformities is usually <4 m. This implies that relative sea level did not fall very far over the inner margin, resulting in a shallow aquifer and precipitation of EEC directly beneath disconformities. The putative disconformities at the outer margin did not trigger EEC precipitation, perhaps due to short-lived subaerial exposure, as indicated by equivocal subaerial-exposure features. The range of salinities recorded by EEC reflects evolution of the freshwater lenses developed at disconformities (Table 3-2). In small tropical islands, meteoric lenses tend to be cyclical, more developed during seasons of high rainfall and partially to completely destroyed by mixing with marine water through tidal pumping and diffusion in relatively dry seasons (Moore 1977; Budd 1984). These cycles could possibly explain the variations in salinity recorded in EEC fluid inclusions, although the range of 0 to 49 ppt measured in sample CM-1 1.8 likely required a period of evaporation lasting years, not months (Table 3-2). A likely scenario to explain lesser salinity variations is the encroachment of the mixing zone or possibly marine phreatic water during prolonged droughts.

Origin of Radiaxial Fibrous Cements

Radiaxial fibrous cements are invariably interpreted to have precipitated from marine water, by analogy to the morphology of modern isopachous marine-cement crusts. Original high-Mg calcite mineralogy is indicated by the presence of microdolomite inclusions following neomorphism (Kendall and Tucker 1973; Sandberg 1985; Lohmann and Myers 1977). RFC-2 interlayered with PIS in TQ quarry and isotopic compositions compatible with other marine components (Enos 1986) is further evidence of marine origin. The splotchy luminescence and microdolomite inclusions observed in radiaxial fibrous cements have been ascribed to

neomorphic alteration of a precursor high-Mg calcite to more stable calcite, preserving vestiges of original fabric (Lohman and Myers 1977; Videtich 198; Reinhold and Kaufmann 2010).

Origin of Late Equant Cement

Voluminous late equant cement is spread uniformly throughout the exposed El Abra platform margin with persistent cathodoluminescence zonation. Fluid inclusions from LEC yielded freshwater values and temperatures <50°C. This indicates precipitation in a single pervasive aquifer with episodic variations in redox potential and/or trace-element concentrations to produce zonation, but very stable salinity, essentially fresh water, as shown by fluid-inclusion analysis. What is a likely source of such a large volume of freshwater? Aguayo (1975), Minero (1983, 1988), and Brennan (1999) speculated on origins of fluids that precipitated LEC. Aguayo (1975) postulated that El Abra platform was emergent and karstified from late Turonian to early Campanian, during LEC precipitation. Minero (1983; 1988) also attributed LEC to this period of emergence. This hypothesis is problematic. There is little evidence of subaerial exposure on the top of El Abra Formation, in contrast to the abundant features observed at intraformational disconformities. The Late Turonian to Santonian-Campanian boundary spans ~6 Ma (Gradstein et al. 2004); Smith (1986) estimated 17 Ma of exposure. As intraformational exposure of short duration (12000-19000, see Ch2) repeatedly produced unequivocal evidence, exposure lasting millions of years should leave some evidence as well. Brennan (1999) postulated that the fluids precipitating LEC were either meteoric with depleted ^{18}O or mixed marine-meteoric water. He suggested that freshwater could have entered El Abra platform from the west, through the Difunta clastic wedge, which signals the onset of the Laramide Orogeny, perhaps as early as the Campanian (McBride et al. 1975). He assumed that the eastern margin of the platform was not covered by sediment until the basin was filled by Méndez Shale (Campanian to Maastrichtian).

So ambient marine water could mix with freshwater from the west. However, fluid-inclusion data from LEC in this study indicate precipitation from freshwater to slightly brackish.

Brennan's (1999) postulate of freshwater entering through the Difunta clastic wedge and precipitating the volumetrically significant LEC in a regional aquifer is appealing. Sierra El Abra was probably continuously flooded from Turonian through Maastrichtian based on apparently continuous pelagic deposition in the adjacent basin and on parts of the platform. Depleted $\delta^{18}O$ values of LEC (Table 3-3) could result from an elevated inland source of water and a slight increase in temperature from shallow burial. An alternative or complementary hypothesis for depleted $\delta^{18}O$ is the probable increase in altitude and inland location of the recharge area, the proximal Difunta clastic wedge (Brennan 1999).

Reference	Mean $\delta^{18}O$ ‰ PDB	Standard deviation
Brennan (1999)	-3.73	1.12
Enos (1986)	-5.70	3.29
Minero (1983)	-3.95	0.39

Table 3-3: $\delta^{18}O$ from late equant cements in the literature.

A hydrological model for precipitation of LEC must meet a number of criteria: 1) A freshwater recharge area 2) at an elevation sufficient to generate a hydraulic head to drive water through the basin into El Abra Formation, 3) a confining layer to prevent leakage or mixing, and 4) an exit for the fluids to allow continuous circulation of the very large volumes of water required (Fig. 3-15). The Difunta Group in the proposed recharge area is a series of synorogenic fluvio-deltaic and shallow-marine clastic wedges building into the foreland basin of the Sierra Madre Oriental in northern Mexico (Murray et al. 1962; McBride et al. 1975, Ye 1997), as early as Campanian. The conglomerate beds in Difunta group contain clasts of volcanic and hypabassal rocks from the highland area to the west (~ 300 km) apparently transported into the

shallow-marine depositional environment by streams (Baker 1970; Crawley 1975; McBride et al. 1975; Ye 1997). Elevation in the highland and orographic rainfall could create the hydraulic head necessary to drive meteoric fluids through the basin. The Difunta clastic wedges grade laterally into Méndez Shale in the basin (Ye 1997; McBride et al. 1975). The Méndez would confine the aquifer in the basin and the interior of the rimmed Valles-San Luis Potosí platform. The limestone and shale of the San Felipe Formation, possibly fractured near the source area, and El Abra limestones are the most likely conduits to the eastern platform margin. Extensive secondary porosity, only partly reduced by post-submerging marine cement (RFC-2) and internal sediment, provided permeable fluid pathways through the platform margin and possibly the interior. There is no clear evidence that Upper Cretaceous rocks in the Sierra El Abra covered the elevated rim of El Abra Formation. However, Aguayo (1978, p. 110) espousing Carrillo-Bravo (1971) suggested that the Tamuin member (late Campanian) of Mendez shale once covered the elevated rim of El Abra Formation and may have 'slid' eastward into the basin to form a turbidite wedge. The thickness of Tamuin is 40 m at the foot of the El Abra escarpment and gradually thins out to the east (Aguayo and Kanamori 1976). Tamuin sediments possibly resulted in physical compaction of El Abra Formation, before their postulated displacement into the basin, providing an exit route for the cementing artesian water. Comparable models for introducing freshwater into deep marine basins have been suggested in a number of studies. Dorobek (1987) described cementation by freshwater from a tectonically uplifted hinterland in the Siluro-Devonian Heldelberg Group in Virginia. Grover and Read (1983) proposed a similar mechanism of freshwater injection into a deeply buried confined aquifer in the middle Ordovician carbonates in Virginia. These examples share the phenomena of fresh water sourced

in the tectonic hinterland, largely in siliciclastics, flowing through a buried, confined aquifer, and precipitating pervasive calcite cements.

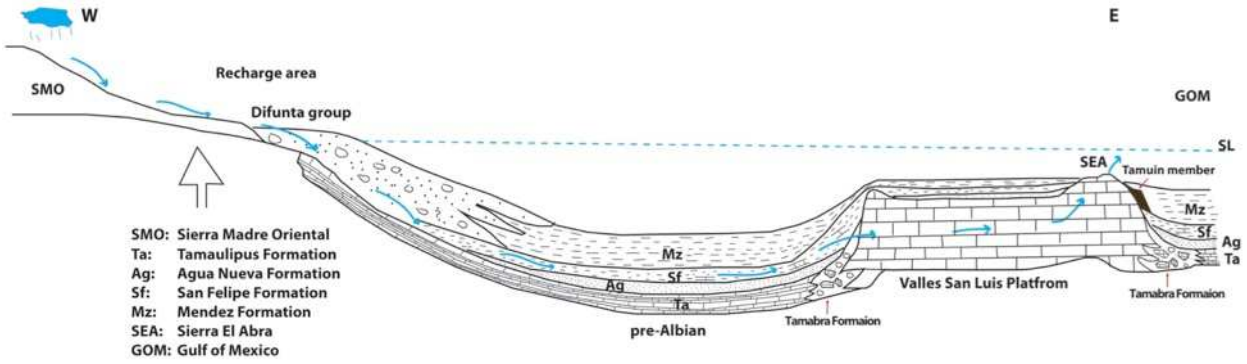

FIG. 3-15: Conceptual representation of the confined-aquifer hypothesis. Freshwater enters through Difunta clastic wedges in the elevated hinterland. The fluids migrate through (fractured?) limestone and shale of San Felipe Formation, confined by impermeable deep-water shale of Méndez Formation, and exit through the El Abra Formation locally exposed on the sea floor. Distance between the recharge and exit is about 250 km.

CONCLUSIONS

Petrography, cement stratigraphy, and fluid-inclusion analyses of the calcite cements in El Abra platform margin provide insights into cement distribution and timing and suggest a feasible hydrological scenario for cement precipitation. Crosscutting relationships document informational origin of early equant cement, with cyclic cementation alternating with deposition beneath successive disconformities in the inner margin. Salinities of the precipitating fluids ranged from freshwater to evaporated seawater, including normal seawater and various mixtures. Contemporaneous marine-phreatic diagenesis resulted in precipitation of a first generation of marine cements in the outer margin. A pervasive dissolution event (D-2) occurred probably in a regional meteoric aquifer in the late Cenomanian, creating voluminous megaporosity, which was reduced by a second generation of marine cement following the Turonian transgression. Late equant cements, the most voluminous cements in the Sierra El Abra, were deposited following shallow burial, in approximate synchronicity throughout the platform margin, as indicated by

continuity of four distinctive cathodoluminescence zones. Precipitation was from freshwater at temperatures less than 50°C. This freshwater may have infiltrated clastic wedges developed at the front of the rising Sierra Madre Oriental, passed through fractured (?) basinal rocks and porous platform limestones, to exit through the elevated rim of the Valles-San Luis Potosí platform onto the Campanian seafloor.

REFERENCES CITED

AGUAYO-CAMARGO, J.E., 1975, Sedimentary environments and diagenetic implications of the El Abra Limestone at its type locality, east Mexico: Unpublished M.S. Thesis, University of Texas at Dallas, 159 p.

AGUAYO-CAMARGO, J.E., 1978, Sedimentary environments and diagenesis of a Cretaceous reef complex, eastern Mexico: Anales Centro Ciencias del Mar Limnologia., Universidad Nacional Autonoma, Mexico, v. 5, p. 83-140.

AGUAYO-CAMARGO, J.E., 1993, The middle Cretaceous EI Abra Limestone at its type locality and Laguna Colorada, east-central Mexico, *in* Alencaster, Gloria, and Buitron, B.E., eds., Universidad Nacional Autonoma de Mexico, Instituto de Geologia, Third International Conference on Rudists, Mexico, D.F., Nov. 20-28, Guidebook for field trip "A", 43 p.

AGUAYO-CAMARGO, J.E., 1998, The middle Cretaceous El Abra Limestone at its type locality (facies, diagenesis and oil emplacement), east-central Mexico: Revisita Mexicana de Ciencias Geológicas, v. 15, p. 1-8.

AGUAYO, C.E., AND KANAMORI, K., 1976, The Tamuin Member of the Mendez Shale along the eastern flank of the Sierra de El Abra, San Luis Potosí, Mexico: Boletin de la Sociedad Geologica Mexicana, v. 37, p. 11-17.

ALENCASTER, G., 1984, Late Jurrasic-Cretaceous molluscan paleogeography of the southern half of Mexico: Geological Association of Canada Special paper, v. 27, p. 77-88.

ARMSTRONG-ALTRIN, J.S., MADHAVARAJU, J., SIAL, A.N., KASPER-ZUBILLAGA, J.J., NAGARAJAN, R., FLORES-CASTRO, K., AND RODRÍGUEZ, J.L., 2011, Petrography and stable isotope geochemistry of the cretaceous El Abra Limestones

(Actopan), Mexico: Implication on diagenesis, Journal of the Geological Society of India, v, 77, p. 349-359.

BAKER, R.A., 1970, Stratigraphy and sedimentology of the Canon del Tule Formation (Upper Cretaceous), Parras basin, NE Mexico: Unpublished Ph.D. dissertation, Austin, Texas, The University of Texas at Austin, 322 p.

BARKER, C.E., AND HALLEY, R.B., 1988, Fluid inclusions in vadose cement with consistent vapor to liquid ratios, Pleistocene Miami Limestone, southeastern Florida: Geochimica et Cosmochimica Acta, v. 52, p. 1019-1025.

BASÁÑEZ-LOYOLA, M.A., FERNÁNDEZ-TURNER, R., AND ROSALES-DOMÍNGUEZ, C., 1993, Cretaceous platform of Valles-San Luis Potosí, northeastern central Mexico: American Association of Petroleum Geologists, Memoir, 56, p. 51-51.

BITTER, M.R., 1986, Sedimentology and petrology of the Chicontepec formation, Tampico-Misantla Basin, eastern Mexico: Unpublished M.S. Thesis, University of Kansas, Lawrence, 174 p.

BRENNAN, S.T., 1999, Impact of fluid and thermal history on reservoir properties of El Abra Limestone, Sierra el Abra, Mexico: Unpublished M.S. Thesis, University of Kansas, Lawrence, 183 p.

BUDD, D.A., 1984, Freshwater Diagenesis of Holocene Ooid Sands, Schooner Cays, Bahamas: Unpublished Dissertation, The University of Texas at Austin, Texas, 491 pp.

BUSH, A.D., AND GOVELA, S., 1978, Stratigraphy and structure of Chicontepec Turbidites, Southeastern Tampico-Misantla Basin, Mexico: American Association of Petroleum Geologists, Bulletin, v. 62, p. 235-246.

CARRILLO-BRAVO, J., 1971, La Plataforma Valles-San Luis Potosí: Boletín de la Asociación Mexicana de Geólogos Petroleros, v. 23, p. 1-113.

CHOQUETTE, P.W., AND PRAY, L.C., 1970, Geologic nomenclature and classification of porosity in sedimentary carbonates: American Association of Petroleum Geologists, Bulletin, v. 54, p 207-250.

CRAWLEY, R.A., 1975, Stratigraphy and sedimentology of the Cerro Grande Formation (Upper Cretaceous), Parras Basin, northeastern Mexico: Unpublished Ph.D. dissertation, Austin, Texas, The University of Texas at Austin, 282 p.

DIENI, I., TUNSEK, D., 1979, Parkeri spaherica Carter, 1877 (Hudrozoan) in the Varconian (Lower Cretaceous) of Orosei (Sardinia): Bollettino della Societa Paleontologica Italiana, v. 18, p. 200-206.

DOROBEK, S.L., 1987, Petrography, geochemistry, and origin of burial diagenetic facies, Siluro-Devonian Helderberg Group (carbonate rocks), central Appalachians: American Association of Petroleum Geologists, Bulletin, v. 71, p. 492-514.

DUNHAM, R.J., 1962, Classification of carbonate rocks according to depositional texture, *in* Ham, W.E., eds., Classification of carbonate rocks: American Association of Petroleum Geologists, Memoir 1, p. 108-121.

DUNHAM, R.J., 1969, Early vadose silt in Townsend Mound (Reef), New Mexico, *in* Friedman, G.M., eds., Depositional Environments in Carbonate Rocks: Society of Economic Paleontologists and Mineralogists, Special Publications, v. 14, p. 139-181.

ENOS, P., 1974, Reefs, platforms, and basins of middle Cretaceous in northeast Mexico: American Association of Petroleum Geologists, Bulletin, v. 58, p. 800-809.

ENOS, P., 1982, Basin-to-platform transition, mid-Cretaceous, Mexico (abstract): American Association of Petroleum Geologists, Bulletin, v. 66, p. 567.

ENOS, P., 1983, Late Mesozoic paleogeography of Mexico, *in* Reynolds M.W., Dolly E. D., eds., Mesozoic paleogeography of west-central United States, Society of Economic Paleontology and Mineralogy, Rocky Mountain Section Symposium 2, p.133-157.

ENOS, P., 1986, Diagenesis of mid-Cretaceous rudist reefs, Valles platform, Mexico, *in* Schroeder, J.H., and Purser, B.H., eds., Reef diagenesis: Springer-Verlag, Berlin, p. 160-185.

FLÜGEL, E., 2004, Microfacies of carbonate rocks: analysis, interpretation and application. Springer-Verlag Berlin Heidelberg, Germany, 976 p.

GOLDSTEIN, R.H., 1986A, Integrative carbonate diagenesis studies: fluid inclusions in calcium carbonate cement; paleosols and cement stratigraphy of Late Pennsylvanian cyclic strata. New Mexico: Unpublished Ph.D. dissertation, University of Wisconsin, Madison, Wisconsin, 343 p.

GOLDSTEIN, R.H., 1988, Cement stratigraphy of Pennsylvanian Holder Formation, Sacramento Mountains: American Association of Petroleum Geologists, Bulletin, v. 72, p. 425-438.

GOLDSTEIN, R.H., 2003, Petrographic analysis of fluid inclusions, Fluid Inclusions: Analysis and Interpretation, v. 32, p. 9-53.

GOLDSTEIN, R.H., AND REYNOLDS, T.J., 1994, Systematics of Fluid Inclusions in Diagenetic Minerals Society of Economic Paleontologists and Mineralogists, Short Course 31, 199 p.

GOLDSTEIN, R.H., FRANSEEN, E.K., AND MILLS, M.S., 1990, Diagenesis associated with subaerial exposure of Miocene strata, southeastern Spain: Implications for sea-level

change and preservation of low-temperature fluid inclusions in calcite cement: Geochimica et Cosmochimica Acta, v. 54, p. 699-704.

GRADSTEIN, F.M., OGG, J. G., AND SMITH, A G., 2004, A geologic time scale Cambridge University Press, London, 488 p.

GROVER JR, G., AND READ, J., 1983, Paleoaquifer and deep burial related cements defined by regional cathodoluminescent patterns, Middle Ordovician carbonates, Virginia: American Association of Petroleum Geologists, Bulletin, v. 67, p. 1275-1303.

KAUFMAN, J., CANDER, H. S., DANIELS, L.D., AND MEYERS, W.J., 1988, Calcite cement stratigraphy and cementation history of the Burlington-Keokuk Formation (Mississippian), Illinois and Missouri: Journal of Sedimentary Research, v. 58, p. 312-326.

KENDALL, A.C., 1985, Radiaxial fibrous calcite: a reappraisal, *in* Schneidermann, N., and Harris, P.M., eds., Carbonate Cements: Society of Economic Paleontologists and Mineralogists, Special Publication, v. 36, p. 59-77.

KENDALL, A.C., AND TUCKER, M.E., 1973, Radiaxial fibrous calcite: a replacement after acicular carbonate: Sedimentology, v. 20, p. 365-389.

LANGORIA, J.F., 1975, Estatigrafia de le Sierra Comancheana del Noreste de Mexio: Boletin Sociedad Geologia Mexicana, v. 36, p. 31-59.

LOHMAN, K.C., MEYERS, W.J., 1977, Microdolomite inclusions in cloudy prismatic calcites: a proposed criterion for former high-magnesium calcites: Journal of Sedimentary Petrology, v. 47, p. 1078–1088.

MCBRIDE, E.F., WEIDIE, A.E AND WOLLEBEN, J.A., 1975, Deltaic and associated deposits of Difunta Group (Late Cretaceous to Paleocene), Parras and La Popa basins northeastern Mexico, *in* M. L. S. Broussard, eds., Deltas: Houston Geological Society, p. 485-522.

MEYERS, W.J., 1974, Carbonate cement stratigraphy of the Lake Valley Formation (Mississippian) Sacramento Mountains, New Mexico: Journal of Sedimentary Research, v. 44, p. 837-861.

MEYERS, W.J., 1978, Carbonate cements: their regional distribution and interpretation in Mississippian limestones of southwestern New Mexico: Sedimentology, v. *25*, p. 371-400.

MEYERS, W.J., 1991, Calcite cement stratigraphy: An overview, *in* Barker, C.E., and Kopp, D.C., eds., Luminescence Microscopy: Quantitative and Qualitative Aspects: Society of Economic Paleontologists and Mineralogists, short Course, v, 25. p. 133-148.

MINERO, C.J., 1983, Sedimentary environments and diagenesis of the El Abra Formation (Cretaceous), Mexico: Unpublished Ph.D. dissertation, State University of New York at Binghamton, 367 p.

MINERO, C.J., 1988, Sedimentation and diagenesis along an island-sheltered platform margin, El Abra Formation, Cretaceous of Mexico, *in* James, N.P. and Choquette, P.W. eds., Paleokarst: Springer-Verlag, Berlin, p. 385-405.

MINERO, C.J., ENOS, P., AND AGUAYO-CARMAGO, J.E., 1983, Sedimentation and diagenesis of mid-Cretaceous platform-margin east-central Mexico, with accompanying field guide: Dallas Geological Society, Dallas, 168 p.

MOORE, C.H., 1977. Beach rock origin: some geochemical, mineralogical and petrographic considerations. Geoscience and Man, v. 18, p. 155-163.

MURRAY, G.E., WEIDIE JR, A.E., BOYD, D.R., FORDE, R.H., AND LEWIS JR, P.D., 1962, Formational divisions of Difunta Group, Parras Basin, Coahuila and Nuevo León, Mexico: American Association of Petroleum Geologists, Bulletin, v. 46, p. 374-383.

NIEMANN, J.C., AND READ, J., 1988, Regional cementation from unconformity-recharged aquifer and burial fluids, Mississippian Newman Limestone, Kentucky: Journal of Sedimentary Research, v. 58, p. 688-705.

PESSAGNO, E. A., JR., 1969, Upper Cretaceous stratigraphy of the Western Gulf Coast Area of Mexico, Texas and Arkansas: Geological Society of America, Memoir 111, p. 139.

POTTER, R.W., CLYNNE, M.A., AND BROWN, D.L., 1978, Freezing point depression of aqueous sodium chloride solutions: Economic Geology, v. 73, p. 284-285.

REINHOLD, C., AND KAUFMANN, B., 2010, Sea-level changes as controlling factor of early diagenesis: the reefal limestones of Adnet (Late Triassic, Northern Calcareous Alps, Austria), Facies, v. 56, p. 231–248.

RICHTER, D.K., NEUSER, R.D., SCHREUER, J., GIES, H., AND IMMENHAUSER, A. 2011, Radiaxial-fibrous calcites: A new look at an old problem, Sedimentary Geology, v. 239, p. 23-36.

SANDBERG, P., 1985, Nonskeletal aragonite and pCO2 in Phanerozoic and Proterozoic, *in* Sundquist, E., Broecker, W., eds., The Carbon Cycle and Atmospheric CO2: Natural Variations, Archean to Present, 32. American Geophysical Union Monograph, Washington, D.C, p. 585–594.

SCOTT, R.W., 1990, Models and stratigraphy of mid-Cretaceous reef communities, Gulf of Mexico: Society for Sedimentary Geology (SEPM), Concepts in Sedimentology and Paleontology, no. 2, 102 p.

SMITH, B.A., 1986, Upper Cretaceous stratigraphy and the mid-Cenomanian unconformity of the east central Mexico: Unpublished Ph.D. dissertation, University of Texas at Austin, 190 p.

SOEGAARD, K., DANIELS, A., YE, H., AND HALIK, N., 1996, Late Cretaceous Early Tertiary Evolution Of Foreland To Sevier Laramide Fold Thrust Belt, Northeast Mexico: In Geological Society of America Abstracts with Programs, v. 28, p. A-115.

VIDETICH, 1985, Electron microprobe study of Mg distribution in recent Mg calcites and recrystallized equivalents from the Pleistocene and Tertiary: Journal of Sedimentary Petrology, v. 55, p. 421–429.

WILMSEN, M., 2003, Taxonomy, autecology and paleobiogeography of the middle Cretaceous genus Parkeria Carpenter, 1870 (spherical hydrozoan): Journal of Systematic Paleontology, v. 1, p. 161-186.

YE, H., 1997, Sequence stratigraphy of the Difunta group in the Paras-La Popa foreland basin, and tectonic evolution of the Sierra Madre Oriental, NE Mexico: Unpublished Ph.D. dissertation, The University of Texas at Dallas, 197 p.

YUREWICZ, D.A., CHUCHLA, R. J., RICHARDSON, M., POTTORF, R.J., GRAY, G.G., KOZAR, M.G., AND FITCHEN, W.M., 1997, Hydrocarbon generation and migration in the Tampico-Misantla Basin and Sierra Madre Oriental, East-Central Mexico: Evidence from an Exhumed Oil Field in the Sierra de El Abra: Dallas Geological Society and Society of Economic Paleontologists and Mineralogists, p. 1-24.

Chapter IV: EVOLUTION OF SIX ORDERS OF MAGNITUDE OF PORE SPACE IN PLATFORM CARBONATES

ABSTRACT

Cyclic deposition of El Abra Formation was punctuated by repeated subaerial exposure resulting in complex paragenetic sequences, investigated by employing four methods of measuring pore space ranging through six orders of magnitude ($<10^{-6}$ um to $>10^{-1}$ m). Paleomorphology of the eastern platform margin produced quantitative variations in spatial distribution of near-surface diagenetic processes. Microporosity (1" perm plugs) averages only 3.3 % and permeability 0.04 md in the inner margin and 3.6% and 0.03 md in the outer margin. Mesoporosity (thin-section counts) is heavily reduced and occluded to an average of less than 1%. Centimeter-scale megaporosity (4" perm plugs) averages 7.6 % and permeability ranges from 0.8 md to 553 md in the outer margin. Decimeter-scale megaporosity (outcrop photopan counts) in vuggy limestone averages to 12 % in the outer margin and 6% in the inner margin. In order of increasing volume in the inner margin: radiaxial fibrous cement-2, early equant cement, crystalline internal sediment, and late equant cement reduced the reservoir quality. In the outer margin, in order of increasing volume: crystalline internal sediment, radiaxial fibrous cement-2, radiaxial fibrous cement-1, and late equant cement reduced reservoir quality. Diagenesis associated with repeated disconformities greatly reduced total porosity in El Abra Formation in the inner margin. Outer-margin rocks preserve more porosity and higher permeability due to less subaerial exposure and more favorable dissolution. The outer margin is thus the optimum zone for reservoir quality in a heavily cemented shallow-water peritidal carbonate system.

INTRODUCTION

Understanding pore networks in vuggy carbonate rocks has long been the buried treasure of hydrocarbon exploitation (Lucia 1998, 2007; Moore 2001). Documenting porosity, and to a lesser extent permeability, on four scales ranging over six orders of magnitude provides a treasure map. Outcrops of El Abra limestone (mid-Cretaceous: Albian-Cenomanian) in the Sierra El Abra, Mexico, a flushed giant reservoir, are the laboratories. Multiple disconformities are an important part of the story. These breaks in sedimentation can lead to enhancement, degradation, or compartmentalization of carbonate reservoirs due to consequential modifications in the pore network upon exposure to subaerial diagenesis. Previous studies have generated abundant data on identifying disconformities in shallow-water carbonate rocks (Bathurst 1974; Esteban and Klappa 1983; James and Choquette 1984; Budd et al. 1995; Goldstein 1998; Chapter II of this study), but quantitative understanding of the effect of disconformities on pore-space evolution is limited. This study examines the effects of closely spaced (mean 2.7 m) disconformities on the evolution of sub-micrometer- to decimeter-scale pore space in the cyclic El Abra Formation on the eastern edge of the Valles-San Luis Potosí platform. The focus of this study is the effects of disconformities on pore space, measured in 1-inch perm plugs (10^{-6} to 10^{-2} m pores), thin sections (10^{-3} to 10^{-2} m pores), 4-inch perm plugs (pores $\leq 10^{-1}$ m), and outcrop photopans (pores $> 10^{-1}$ m). Measurements of various scales of porosity and permeability could lead to breakthroughs in understanding complete pore networks and to enhanced exploitation of hydrocarbons, metallic ores, and water in diagenetically modified carbonate reservoirs. These results will help in constructing reservoir analogs for understanding the vast ranges of porosity and permeability associated with closely spaced disconformities common in shallow-water, platform-margin carbonates, a favorite exploration target.

GEOLOGICAL SETTING

El Abra Formation formed on an isolated mid-Cretaceous (Albian-Cenomanian) platform in northeast Mexico surrounded by intracratonic basins (Carrillo 1971; Enos 1974, 1983). It is spectacularly exposed in the Sierra El Abra, a low-relief; asymmetric anticline, 3-5 km wide and 125 km long (Yurewicz et al. 1997), which breached and drained a giant reservoir (estimated 1 bbl. of oil). Extensive quarries provide nearly continuous, dip-parallel exposures for 3.5 km from the platform slope break (Fig. 4-1). Two generalized facies belts can be recognized in El Abra Formation within the Sierra El Abra: tidally influenced, cyclic deposits in the inner platform margin and Taninul or "reef" facies of the outer margin (Aguayo 1975, 1998; Minero 1983, 1988; Enos 1986). The tidally influenced cyclic rocks comprise peloid-miliolid, bioclastic, skeletal-grainstone, fenestral, and cryptalgal-laminite lithofacies of Minero (1983, 1988). Taninul facies consists primarily of rudist-reef and rudist-debris rudstone and grainstone, deposited below mean sea level. Shoaling-upward cycles, truncated cycles, and rhythms are represented in El Abra Formation in the platform margin. Closely spaced (2.7 m) disconformities punctuated inner-margin deposition. Thick soil horizons, microkarst surfaces, solution-collapse breccias and ubiquitous solution porosity are associated with disconformities in the inner margin. Equivocal subaerial-exposure features, such as extensive solution porosity, marks possible disconformities in the outer margin.

El Abra deposition on the Valles-San Luis Potosí platform continued from Albian into the Cenomanian, as indicated by early Cenomanian ammonites in Taninul quarry (Aguayo 1993, 1997, 1998, p. 4), and corroborated by Foraminifera (Langoria 1975) and rudists (Alencáster 1984; summarized by Scott, 1990). 'Palimpsest' planktonic fossils in the Sierra El Abra were reported by Aguayo (1978, Turonian and Campanian from inner margin quarries and outer

margin quarries, respectively) and by Enos (1986, p. 169; Cenomanian) from TQ (Fig. 4-1). Most of the Valles-San Luis Potosí platform drowned abruptly in the Turonian and accumulated pelagic sediments throughout the Late Cretaceous including the Agua Nueva (Turonian), San Felipe (Coniacian-Santonian) and Méndez (Campanian-Maastrichtian) Formations. The Agua Nueva and San Felipe lapped out against the exhumed platform slope in the study area (Enos 1982; Minero et al. 1983). It is unclear, however, whether the Méndez once covered the Sierra El Abra locally. What appears certain is that the Sierra El Abra was submerged during most or all of the Late Cretaceous, as most deposits in the area are pelagic, with limited presence of the shallow-water Tamasopo Formation (Basáñez et al., 1993). The presence of Cenomanian, Turonian, and Campanian planktonic fossils in El Abra vugs supports this proposition. The absence of Upper Cretaceous cover locally on the Sierra El Abra could reflect non-deposition and/or erosion, presumably submarine, perhaps localized by an elevated platform rim or a local upwarp, as postulated by Smith (1986, p. 120). The Late Cretaceous-Paleocene Laramide Orogeny deformed the Valles-San Luis Potosí platform, creating the gentle, asymmetric, Sierra El Abra anticline (1-3º E, 5-8º W dips; Enos 1982; Minero et al. 1983, p. 16, Enos 1986, p. 162). Post-Oligocene uplift exhumed and breached El Abra reservoir (Minero 1988; Yurewicz et al. 1997; Brennan 1999).

The duration of the disconformity between the mid-Cretaceous shallow-platform carbonates and Late Cretaceous deep-water deposits is both variable and problematic. The hiatus has been estimated at 5 to 24 Ma, depending on which strata overlie El Abra Formation (Smith, 1986). In the Sierra El Abra, Smith (1986, p. 120) estimated the hiatus at 17 million years, based on Méndez Shale pinching out against the El Abra Formation at the base of the escarpment. It is likely, however, that the Sierra El Abra was submerged during most of this interval, based on the


500 m
C
CM-1
CM-2
D
200 m
TQ
A
GOM
N
500 km
B
El Abra
VIII
VII
VI
V
IV
CM-1
CM-2
TQ
Sierra El Abra
PM-2
PM-1
Las Palmas
N
2 km
© 2016 Google
Image © 2016 DigitalGlobe
© 2016 INEGI
Google earth
E
PM-2
PM-1
N
CA
BP
PM-1
F

FIG. 4-1: A) Google Earth image of the location of the study area. GOM refers to Gulf of Mexico. Yellow box represents area in B. B) Location of quarries in the Sierra el Abra. Sections measured for this study were located in CM (abbreviated from Cementos Mexicanos, which owns this quarry) and PM (abbreviated after the town of Las Palmas in which this quarry is located). Roman numerals follow the identification scheme of Aguayo (1975) and Minero (1983). Dashed line traces the slope break of El Abra platform. C) Google Earth image of CM quarry is showing location of stratigraphic sections (traced). CM-1 exposes the tidally influenced cyclic rocks while CM-2 exposes the skeletal grainstone nearer the margin. The quarries west of CM (shown in B) expose rocks deposited in tidal flats and the subtidal lagoon (Minero 1983). D) Image of TQ quarry, which exposes the reef facies of El Abra Formation (Enos 1986). E) PM quarry. PM-1 (traced) exposes reef facies while PM-2 (traced) exposes interbedded skeletal rudstone and grainstone. CA is the abandoned Cementos Anahuac (CA) quarry (Enos 1982; Minero et al. 1983). BP is a borrow-pit exposing San Felipe Formation, which is overstepped by Méndez Formation at the foot of the El Abra escarpment in CA (Enos 1982; Minero et al. 1983, p. 18). F) PM-1 section. The length of section (dashed line) is 42 m.

lack of subaerial exposure features on top of El Abra Formation (Ch. 2, this study, Minero 1983, p. 136), apparently continuous pelagic deposition in the surrounding basins and adjacent platform from Turonian through Maastrichtian time, and 'palimpsest' planktonic fossils within the uppermost El Abra Formation. There is evidence of a late Cenomanian disconformity of varying duration elsewhere on the platform as reported by Smith (1986). Technically the hiatus ("…rocks … were never deposited or were eroded…." *Glossary of Geology*) following El Abra deposition in the SEA probably extended to the late Campanian or, possibly, to the present. How long the El Abra was subaerially exposed before a marine transgression is the question here. Late Cenomanian exposure in the Sierra El Abra probably lasted no more than 3 million years, approximate duration of late Cenomanian and part of middle Cenomanian. This is the apparent time of extensive dissolution, creating megaporosity, perhaps in a regional meteoric aquifer in El Abra Formation or in migrating mixing zones. This secondary porosity was reduced by a second generation of radiaxial fibrous cements (RFC-2), locally overlain by internal sediment containing Cenomanian planktonic Foraminifera (Enos 1986, p. 169). Sediment containing late Turonian planktonic foraminifers (Aguayo 1978) apparently further reduced large secondary porosity, indicating pores tens of meters below, but connected to the seafloor, during the Turonian transgression. Despite all this record, the absence of subaerial-exposure features from the top of El Abra Formation remains a curious conundrum.

METHODS

Four stratigraphic sections were measured across the platform margin in the Sierra El Abra (Fig. 2-1). Two sections, CM-1 and CM-2, measuring 72.5 m and 18 m, respectively, are inner-margin rocks at Cementos Mexicanos (CM) quarry (Fig. 4-1 B). The CM quarry cuts stratigraphically and spatially much deeper into the platform than when studied by Aguayo

(1975) and Minero (1983). The quarry exposes transitions from tidally influenced, distal margin deposits (CM-1) to the skeletal grainstone interpreted as marginal shoals (CM-2) by Minero (1983). Two sections, PM-1 and PM-2, measuring 42 m and 41 m thick, respectively, are in reef or shoal facies near the margin (Fig. 4-1 C). PM-1 is in predominantly reef facies within 100 m of the slope break. PM-2 exposes interbedded rudstone and skeletal grainstone about 400 m behind the slope break. Measured sections provide qualitative and quantitative data on facies distribution and thickness, macroscopic diagenetic features, Dunham (1962) textures, and sedimentary structures in the cyclic, uppermost El Abra Formation. Multiple disconformities were recognized based on various subaerial exposure features. The lateral spacing of the sections (300-400 m within CM quarry) allowed documentation of continuity or changes of depositional units, subaerial-exposure features, etc. Each CM section was sampled with an average spacing of 50 cm in the tidally influenced cyclic rocks. Rocks at the margin (PM) are sampled with average spacing of 1 m. One hundred 2X3-in. thin sections and polished slabs of variable dimensions were prepared from oriented rock samples. Porosity is quantified in thin sections using a stepping-point counting stage, (http://ws2.petrog.com/steppingstage.html) connected to an Olympus petrographic microscope. A total of 45 thin sections from CM-1 and 25 thin sections from PM-1 were point-counted with a minimum of 350 points per count. Forty-one cylindrical plugs, 1 in (~2.54 cm) in diameter and of variable length, were collected from CM-1 samples. Twenty-four plugs were paired with thin sections cut from the same sample (not from the actual plug). Plugs were oriented both horizontally (24) and vertically (17) (from different samples) to examine possible directional heterogeneity within porosity and permeability. Fifteen 1-inch plugs (vertical) were collected from PM-1 samples; eleven paired with thin sections. Eight plugs, 4 inches (10.2 cm) in diameter and 6-8 inches in length, were obtained from large oriented

blocks collected from the PM-1 section. The plugs were extracted at Instituto Potosíno de Investigación Científica y Tecnológica in San Luis Potosí with an MDP-405 drill (http://www.coretest.com/core-drilling-instrument.html). Such core plugs were not obtained from the CM sections due to administrative difficulties at location. All 1- and 4-inch core plugs were cleaned of remnant hydrocarbon residue and analyzed for porosity and permeability at Weatherford Laboratories, New Orleans, Louisiana. Photopans of quarry walls at CM-1 and PM-1 sections imaged open pores larger than 5 cm (lowest resolution), with some pores exceeding 30 cm in size. Pores visible in the photopans were colored yellow in Adobe Photoshop and their areal percentage analyzed with JMicroVision (http://www.jmicrovision.com).

DEPOSITION AND DIAGENESIS OF EL ABRA FORMATION

Sedimentation of El Abra Formation formed three different stacking patterns: shoaling-upward cycles, truncated cycles, and rhythms. Shoaling upward cycles start with subtidal deposits overlain by tidal units and terminated by a subaerial disconformity. Interrupted sedimentation resulted in truncated cycles, abruptly terminated by subaerial exposure, e.g. a paleosol overlying subtidal rocks. Finally, subtidal and tidal units alternated without the intervention of a disconformity (Enos and Samankassou 1998, p. 220; Chapter 2), forming rhythmic intervals. They possess no definitive depth vector i.e. they can be interpreted as deepening up (BC) as readily as shoaling up (CB). Paleosols, karst surfaces, laminated caliche crusts, ubiquitous solution porosity, blackened clasts, rhizoliths, desiccation and wetting cracks, and solution-collapse breccia record repeated subaerial exposure that terminated cycles. Twenty-seven such intervals were recognized in CM quarry. Alternating sedimentation and exposure, with eventual submergence and burial, led to complex diagenesis in El Abra Formation. This is reflected in a paragenetic sequence that records syndepositional, intraformational, extended

surface, shallow- and deep-burial and exhumation environments (Fig. 4-2). Early marine diagenesis resulted in micritization and precipitation of early marine cements (RFC-1) in the outer margin. Contemporaneous early meteoric diagenesis in the inner margin, repeated at successive disconformities, created dissolution (D-1) porosity (molds and enlarged fenestrae), partially reduced by the crystalline internal sediment (CIS) (vadose silt of Dunham (1969), e.g. sx,irS-FE (terminology of Choquete and Pray 1970). Alternating freshwater to evaporated seawater, including seawater and various mixtures precipitated early equant cements (EEC) to further reduce primary and dissolution porosity. More pervasive dissolution (D-2), apparently in a regional aquifer, produced voluminous vugs, molds, and channels. These were subsequently reduced by a second generation of radiaxial fibrous cement (RFC-2) in the inner margin and by RFC-2 and pelagic internal sediment (PIS) in the outer margin. Shallow burial resulted in physical breakage of skeletal grains followed by precipitation of large volumes of late equant cement (LEC) from a low-salinity (0-4 ppt) aquifer (Ch. 3). Further burial into higher temperature and pressure conditions during Laramide deformation to the west resulted in fracturing and stylolitization. The fracture system served as main conduits for hydrocarbons (Brennan 1999). Post-Oligocene uplift and erosion of the Sierra El Abra drained hydrocarbons and introduced extensive karstification (Brennan 1999; Yurewicz et al. 1997).

The paleomorphology at the eastern edge of Valles San Luis platform resulted in varying degrees of modification during early diagenesis. The tidally influenced rocks at CM-1 section preserve repeated (27) and closely spaced (average 2.7 m) exposure surfaces with unequivocal evidence. In comparison, both the outer margin (PM) and more distal interior rocks (quarries IV, V, and VIII of Aguayo 1978 and Minero 1983) have relatively fewer and subtler exposure

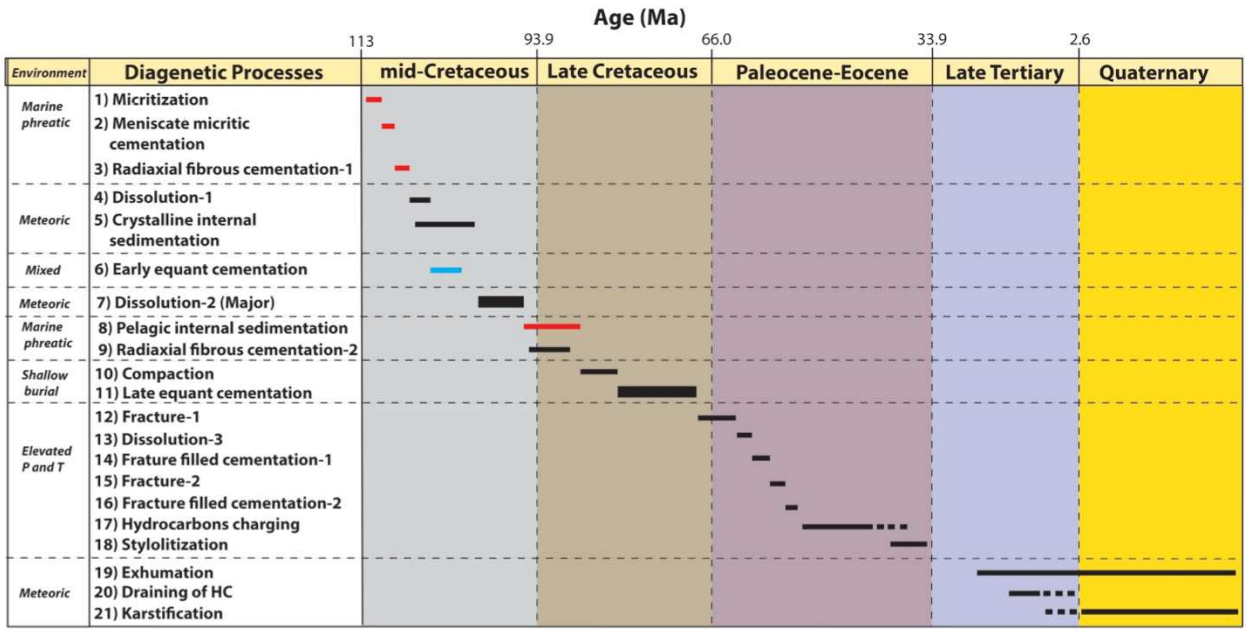

FIG. 4-2: Paragenetic sequences in El Abra Formation. Vertical axis records environments and their diagenetic products. Horizontal axis is time (Gradstein et al. 2004), not to scale. Thicker bars for products 7 and 11 emphasize the intensity of these two events; it is not a quantitative representation. Due to cyclic nature of El Abra deposition and subaerial exposure, meteoric and marine phreatic environments are juxtaposed multiple times with varying expression in inner-margin rocks. However, for simplicity only one common sequence of events is presented. RFC-1 (red bar) occurs only in outer margin and EEC (blue bar) only in inner margin. Thus they are not juxtaposed, although they must have overlapped in time, as each one kept pace with sedimentation. Meniscate micritic cements and pelagic internal sediments are restricted to the outer margin (red bars). Timing of hydrocarbon charging and drainage is based on the study of Brennan (1999) and Yurewicz et al. (1997).

features. At the outer margin (PM) only five possible surfaces of subaerial exposure were identified. This varied expression of early diagenesis profoundly affected pore-space evolution in El Abra Formation.

EXTANT POROSITY

Understanding of pore-space evolution in ancient rocks and locating reservoirs in the subsurface is a challenging task. Integrating paragenesis with quantitative porosity data of various scales will enhance understanding of pore-space evolution in carbonate reservoirs. Extant porosity was measured from 1-in. plugs (10^{-6} to 10^{-2} m pores), thin sections (10^{-3} to 10^{-2} m pores), 4-in. cores (pores < 10^{-1} m), and outcrop photopans (pores >10^{-1} m) (Table 4-1). The

various stages of pore reduction by different cements and internal sediments were quantified by point counting.

Microporosity

Microporosity was defined by Choquette and Pray (1970) as pores <1/16 mm (62 μm), but has assumed a wide variety of definitions ranging to pores of 1 μm or less (Kaczmarek, et al. 2015). Pores < 10 μm are not readily observed through the microscope (Cantrell and Hagerty 1999), but can be measured in standard perm plugs, along with all pores up to cm scale. Microporosity, thus defined, averaged 3.6 % and permeability 0.03 md in outer-margin rocks (PM-1). Inner-margin rocks (CM-1) averaged 3.3% and 0.04 md (Fig. 4-3). Microporous grains, matrix, cements, internal sediment, and cement boundaries could all contribute to microporosity; discrimination among these would require detailed SEM observations. Common oil stains between layers of fibrous cement and within some crystalline internal sediment reveal two loci of microporosity. Differential retention of residual oil in this flushed reservoir (Brennan 1999) is a testimony of the low permeability within the microporosity. Twenty-four horizontal plugs (inner margin) averaged 3.4% porosity and 0.005 md permeability. Sixteen vertical plugs (inner margin) averaged 3.2% and 0.080 md. Thus 1-inch plugs showed insignificant directional variations in porosity (Appendix H and I). Vertical permeability is significantly greater at 95% confidence level (Appendix L and M).

Mesoporosity

Meso-pores visible in thin section (>30 μm) average only 0.30% of bulk volume in the inner margin and 0.13% in the outer margin, including 35 thin sections paired with 1-in. plugs. Visible pore are mostly small molds. Occluded mesopores include intraparticle, fenestrae, shelter, breccia, and solution-enlarged primary pores.

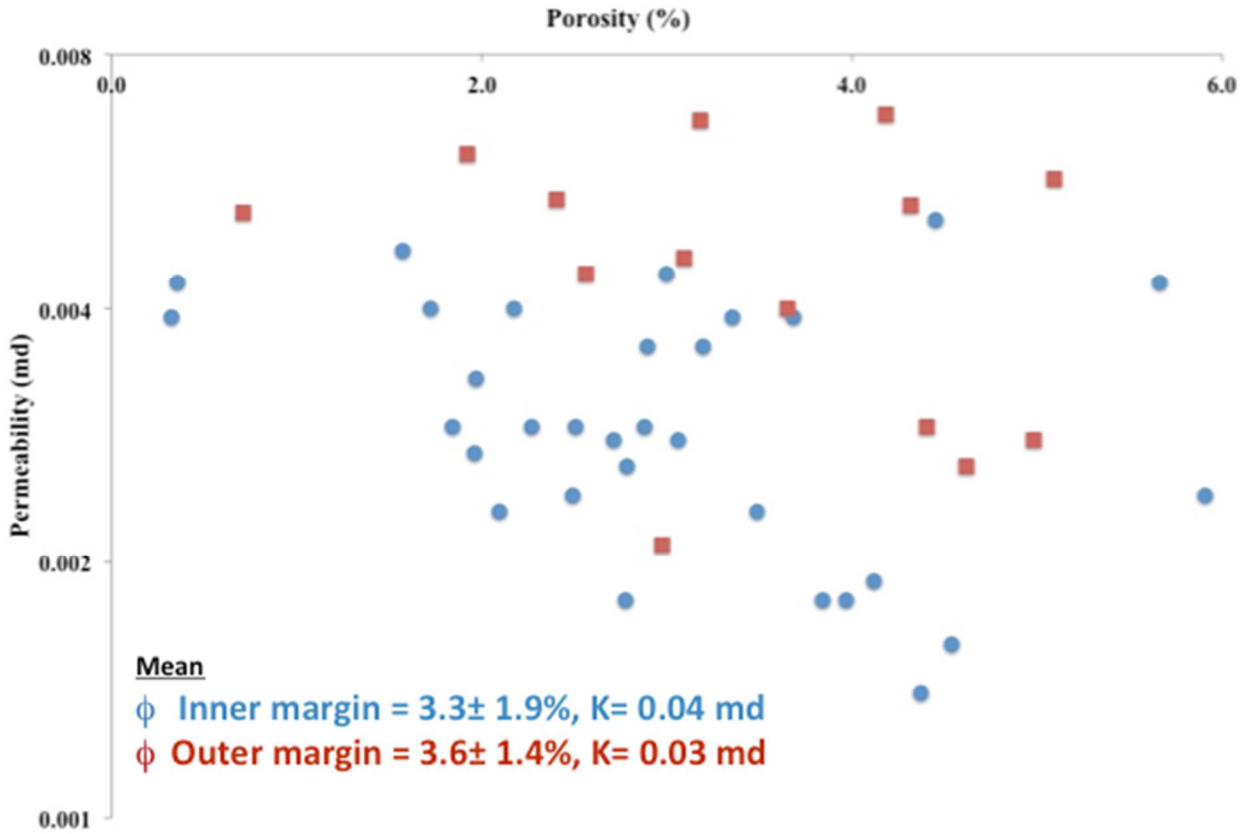

FIG. 4-3: Cross-plot of porosity and $\log_2$ permeability of 56 perm plugs (1-in diameter). Blue circles represent inner platform margin (CM-1) plugs and red squares represent outer margin (PM-1) plugs.

Megaporosity

Megapores in the size range 1-10 cm are abundant in the outer margin, although most have been reduced or occluded by cements and internal sediments. Average porosity from 4-in cores is 7.6 % and permeability ranges from 0.8 md to 552 md (Fig. 4-4; Table 4-1). Megapores are molds, vugs, and channels. Pores larger than 10 cm cannot be measured with conventional full-core analysis. El Abra Formation contains abundant pores larger than 10 cm, especially in the outer margin (Fig. 4-5, 4-6, and 4-7). Distribution of megapores is closely related to the distribution of caprinid rudists, which can reach 35 cm in length and 15 cm in diameter in El Abra Formation. The very thick inner shell layer of caprinids was aragonite, readily dissolved in meteoric water. The thin, calcitic, outer shell layer was invariably broken and removed, so does

not impede MO enlargement to vugs. These were measured by analysis of outcrop photopans. Pore space >10^{-1} m from three photopans averages 6 % in cyclic inner-margin rocks (CM-1) and 12 % in the outer-margin rudstones and grainstones. In CM sections, the secondary pores are predominantly non-fabric selective vugs (Fig. 4-8), but include some molds. In PM molds are dominant among pores up to 20 cm. Some vugs reach nearly 40 cm and channels are exceptionally up to a meter long. Porosity is greatest in rudist rudstones (Fig. 4-5), which are characterized by lenticular distributions.

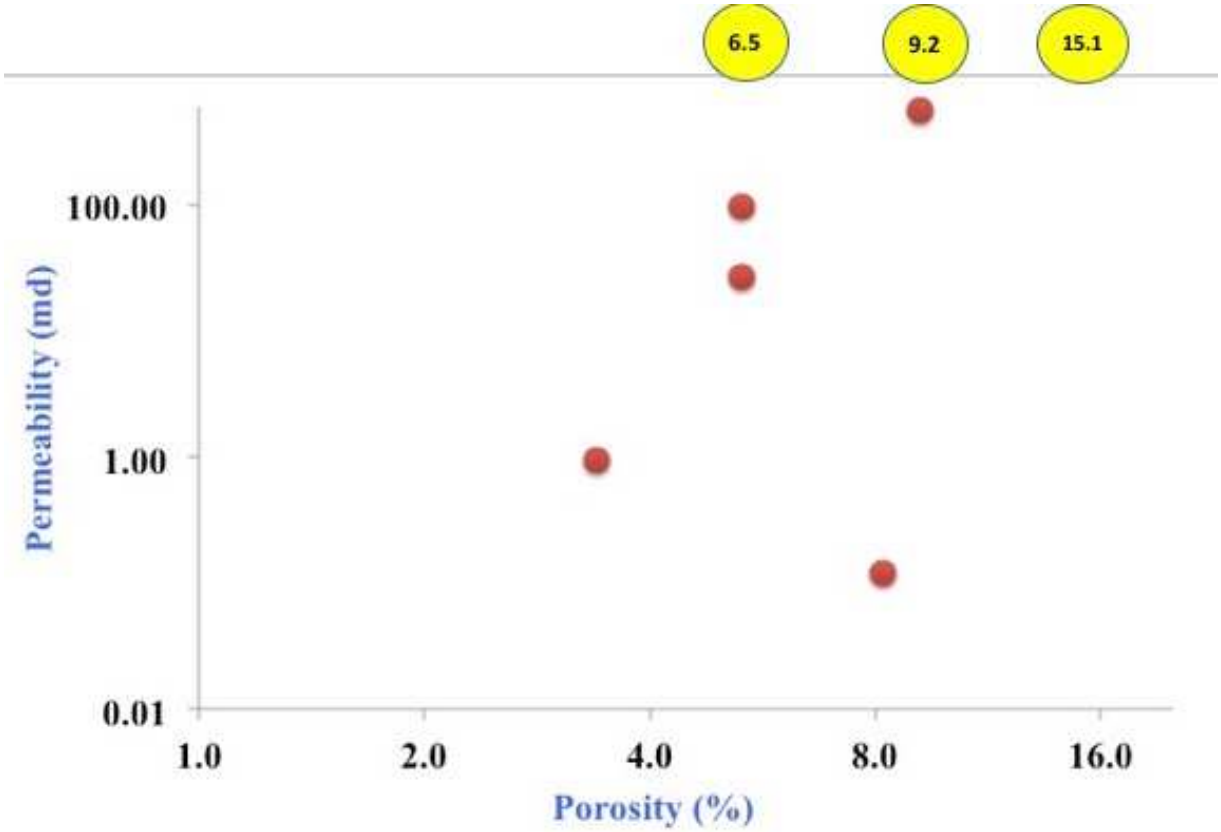

FIG. 4-4: Cross plot of porosity and permeability of eight core plugs (4" diameter) from the PM-1 section. Data points plotted above line (with porosity indicated) were termed "too porous for analysis." The permeability of such rocks would almost certainly be high.

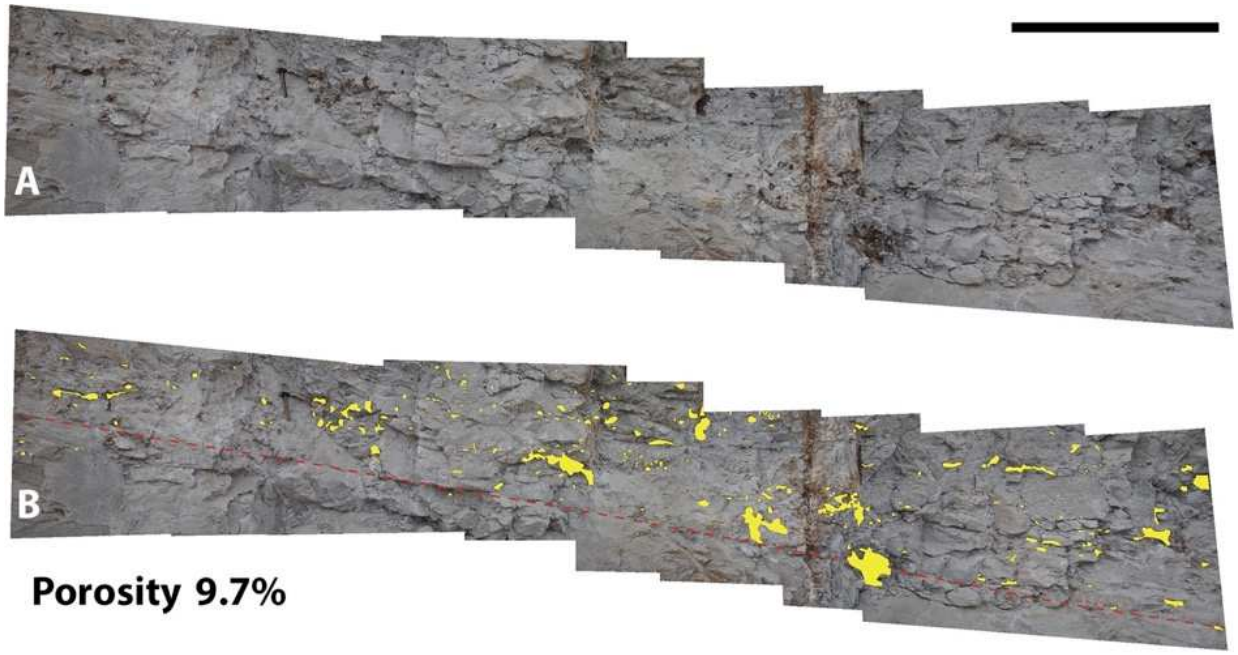

FIG. 4-5: Outcrop photopan used for porosity estimates in the outer margin (PM-1). A) Untouched photopan. B) Porosity is traced and filled (green). Dashed line shows the contact between rudist boundstone (above) and skeletal grainstone, not a disconformity. Visible porosity is entirely molds and vugs. Note greater porosity in the rudist boundstone. Scale bar is 1 m.

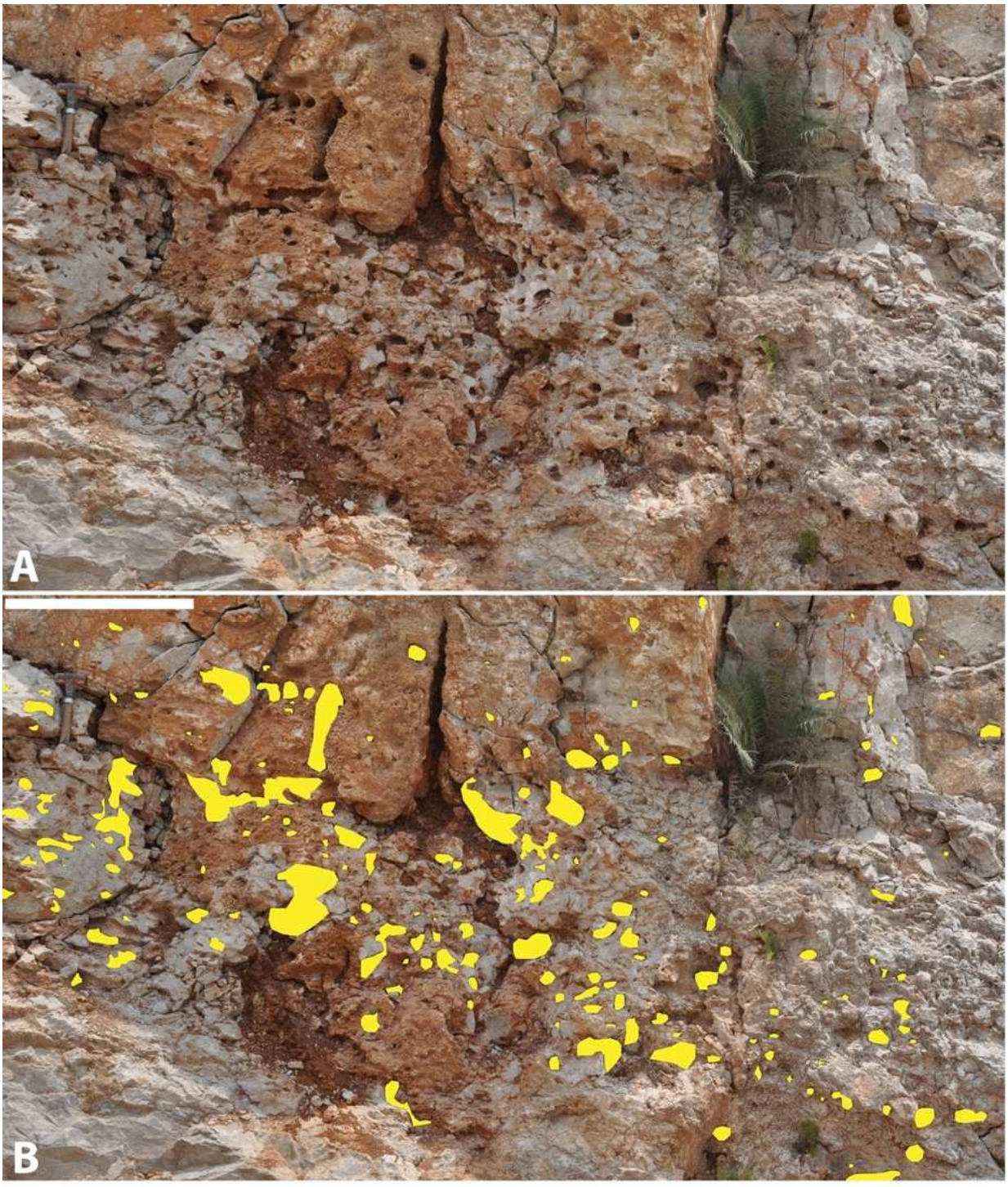

FIG. 4-6: A) Outcrop photopan shows extant porosity, mostly moldic, in outer-margin rudist rudstone. B) Porosity is traced in green. Vertical solution pipes and solution-enlarged fractures, which lack reducing cements, are common near the land surface and result from Quaternary dissolution, so are not included in extant porosity values. Scale bar is 1 m.

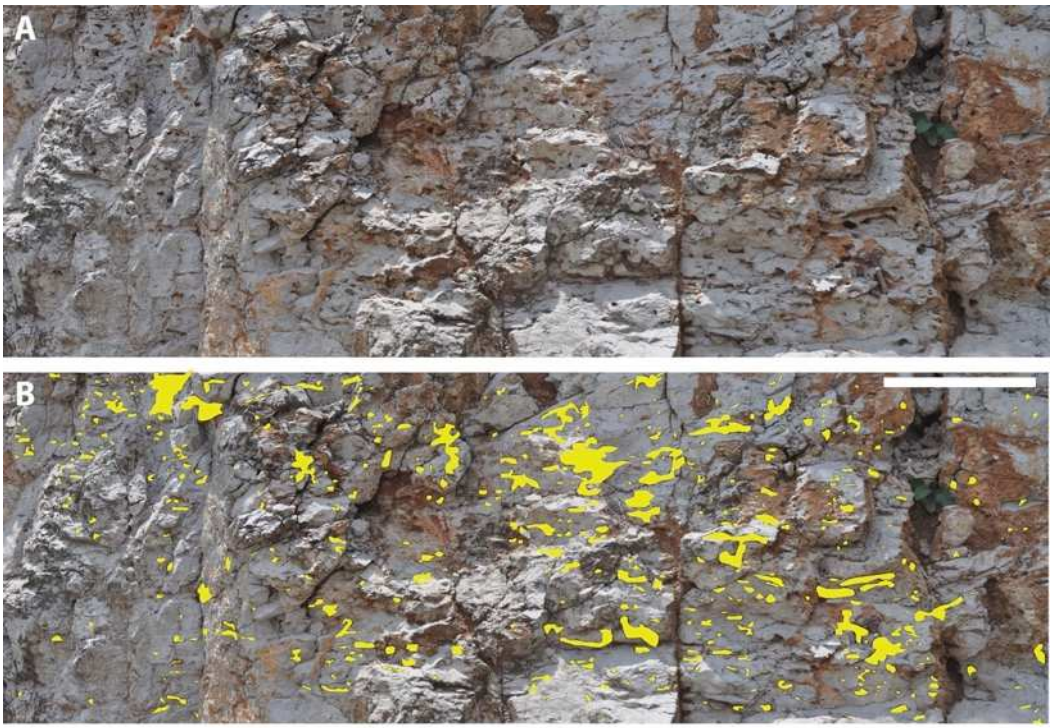

FIG. 4-7: A) Extant megaporosity in a 27-m^2 photopan of the outer margin rudist rudstone, PM-2 section. B) Megaporosity outlined. Solution-enlarged Laramide fractures; Quaternary karst, and gashes produced during quarrying are excluded in porosity estimation. Scale bar is 1 m.

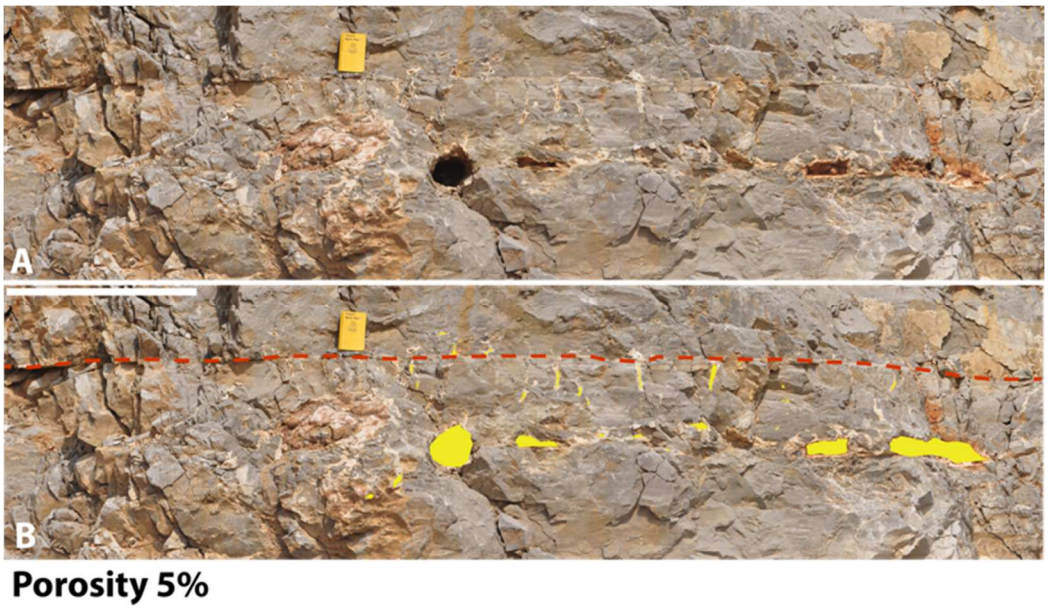

FIG. 4-8: A) Outcrop photopan shows megaporosity in the inner margin (CM-1). B) Dashed line traces a disconformity. Field notebook is 20 cm in length. Note megaporosity concentration within 1 m below the disconformity, including extensive cfVUG and cfMO. The vertical tubes closely below the disconformity (dashed line) are solution enlarged rhizoliths. Scale bar is 1 m.

Extant porosity measured through certain above-mentioned scales can be added together to get a better estimate of the total extant porosity in El Abra Formation. Porosity measured in 1-inch plugs accounts for microporosity but incorporates mesoporosity from the thin sections as well, which is in any case very small. Porosity measured in photopans (Table 4-1) is of completely different scale, >5-10 cm, so these values are additive. As a result, the total extant porosity in the inner margin would be 9.3 % (Table 4-1). Porosity values from the 4-cores (obtained only from the outer margin) incorporate porosity measured in 1-inch plugs and thin sections, but should be added to that measured in photopans. Resultant total extant porosity in PM-1 section is 19.6% (table 4-1). The multiple methods of measurement also give a picture of the distribution of porosity between micropores, mesopores, and two scales of megapores.

			Inner margin		**Outer margin**		
Method	Scale	N	Φ (%)	K (md)	N	Φ (%)	K (md)
1-inch plugs	Micro	41	3.3	0.04	15	3.6	0.03
Thinsections	Meso	45	0.3	X	25	0.13	X
4-Inch cores	Mega (<10 cm)	X	X	X	8	7.6	0.8-552
Photopans	Mega (>10 cm)	3	6	X	3	12	X
	Total extant porosity		9.3			19.6	

Table 4-1: Extant porosity and permeability at four different scales of measurement, covering 6 orders of magnitude of pore size, from inner- and outer-margin rocks of El Abra Formation. X denotes lack of data. Porosity measured in 1-inch plugs and photopans in CM-1 is additive because each scale of observation captures a different scale of pore space. Similarly, porosity measured by 4-inch plugs and photopans in PM-1 is additive.

POROSITY EVOLUTION IN EL ABRA FORMATION

Porosity of the original El Abra sediments is the sum of preserved primary, filled primary porosity, and matrix porosity (Enos 1988). In the inner margin of El Abra Formation the dominant textures are wackestone. Original porosity of 65% is assumed for inner-margin wackestone, based on comparable modern sediments (Enos and Sawatsky 1981). Lithification of the wackestone matrix is assumed, for simplicity, to have been complete before initial dissolution (D-1). Porosity remaining at this stage (WP, FE, SH[?]) is uncertain because thin-section point counts of early cement (EEC) did not distinguish between that filling primary and secondary porosity. It could not exceed the 5.6% volume of EEC in any case. In the outer margin the initial porosity is estimated at 27% by summing volumes of early marine cements and extant porosity. It is important to note that later dissolution (D-2) removed half of the rock volume (Fig. 4-9), therefore, the original volume of early marine cements and extant porosity are projected as double of their preserved volumes during analysis.

Each stage of diagenesis variably contributed to porosity evolution in El Abra Formation. Early marine diagenesis in the outer margin rocks resulted in 8.4 % reduction of porosity (sum of volumetric percentage of radiaxial fibrous cement-1 and meniscate micritic cements) (Fig. 4-9). No early marine cementation was recorded in the inner margin; Rather, the inner margin was dominated by episodic meteoric diagenesis that created ~ 15% of secondary dissolution porosity (D-1) (Fig. 4-9). Deposition of CIS (9 %) and precipitation of EEC (5.6 %) beneath most disconformities in the inner margin occluded all secondary (from D-1) and any remnant primary porosity. Dissolution (D-1) in the outer margin created 1.2 % secondary porosity that was filled by CIS. No EEC is observed in the outer margin.

A second and more extensive episode of dissolution (D-2) in a late Cenomanian meteoric aquifer created secondary megapores, pervasive both in the inner and outer margin of El Abra Formation (Fig. 4-9). During this episode, a total of 21.5 % secondary porosity was created at the inner margin; as the sum of pore-reducing marine cement (RFC-2, 5 %), late meteoric cement (LEC, 7.2 %), and extant porosity (9.3 %). Dissolution in the outer margin generated 46.2% secondary porosity, of which 19.6% remains (Fig. 4-9).

A marine transgression displaced the meteoric aquifer; precipitation of marine cement (RFC-2, 5%) in the inner margin resulted in reduction of porosity to 16.5% (Fig. 4-9). In the outer margin deposition of PIS (3.8 %) and precipitation RFC-2 (4.1%) reduced porosity to 43.3% (Fig. 4-9).

Substantial porosity reduction occurred during shallow burial of El Abra Formation. Cement precipitated during this stage (LEC) reduced the total porosity to 9.3% in the inner margin and 19.6 % in the outer margin (Fig. 4-9). Fractures and stylolites, accompanied by minor dissolution and cement precipitation, produced essentially no change in porosity evolution.

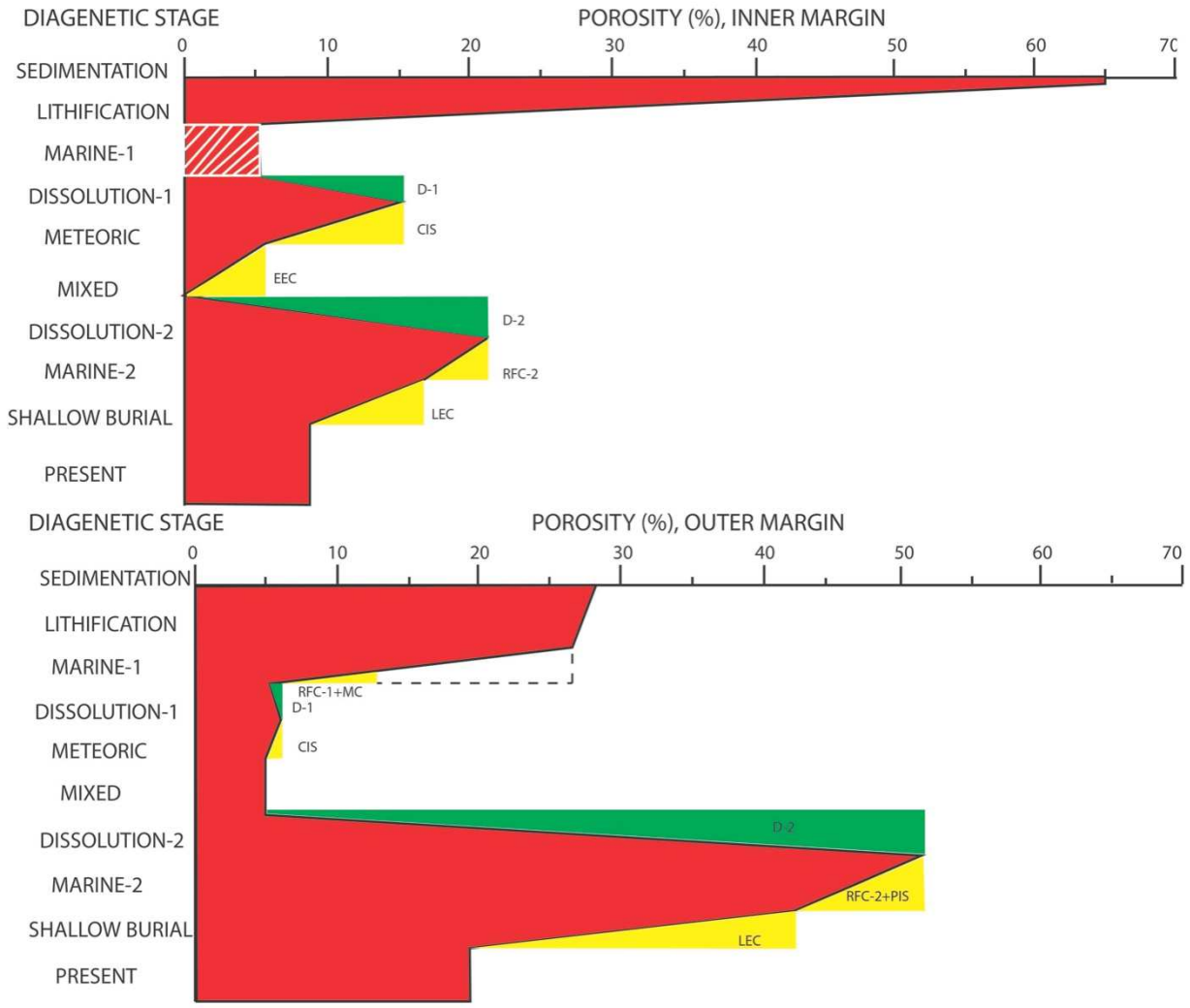

FIG. 4-9: Trend lines illustrating porosity evolution in El Abra Formation, back calculated from thin sections, 1-inch plugs, 4-inch plugs (outer margin only), and photopans. The abscissa indicates percent porosity. Red fill indicates extant total porosity. Yellow indicates porosity filled at each diagenetic stage, back calculated from thin-section counts of volumes of each diagenetic product. Green represents porosity created by dissolution (D-1 and D-2), calculated by summing the volumes of various diagenetic products filling secondary pores attributed to D-1 and by summing extant porosity and later diagenetic filling of D-2 pores. The shaded box in the inner margin plot indicates uncertainty in determining the primary porosity (see text). The dashed triangle in the outer margin plot shows the estimated amount of rock volume removed during D-2. Note that fractures and stylolites are not included because of their insignificant contribution to porosity evolution in El Abra Formation.

DIAGENETIC TRENDS BENEATH DISCONFORMITIES

Trends in pore-space modifications beneath surfaces of subaerial exposure illuminate the role of disconformities in reservoir heterogeneity in shallow-water carbonates. Diagenetic products demonstrably formed beneath most disconformities include secondary porosity from early dissolution, crystalline internal sediment, and early equant cement. Multiple disconformities (27) in the inner margin make CM-1 section most useful in detecting trends. CIS formed contemporaneously with solution porosity (D-1), before and after precipitation of EEC beneath most disconformities (Fig. 4-2). CIS abundance, plotted as a function of depth beneath disconformities decreased to about half its near-surface abundance within 1 m (Fig. 4-10). At depths greater than 1 m, this trend is reversed. EEC shows an approximately complementary trend (Fig. 4-11) as these components compete in filling the early dissolution (D-1) porosity and any primary pores (Fig. 4-12). Following a reduction of nearly half from surface values in the first 50 cm, porosity increased dramatically to depths of 2 m, where the close spacing of disconformities intervenes in data collection. The outer platform margin displays only equivocal evidence of intraformational subaerial exposure, with much less intense (briefer?) meteoric diagenesis. No significant porosity trends related to disconformities are apparent.

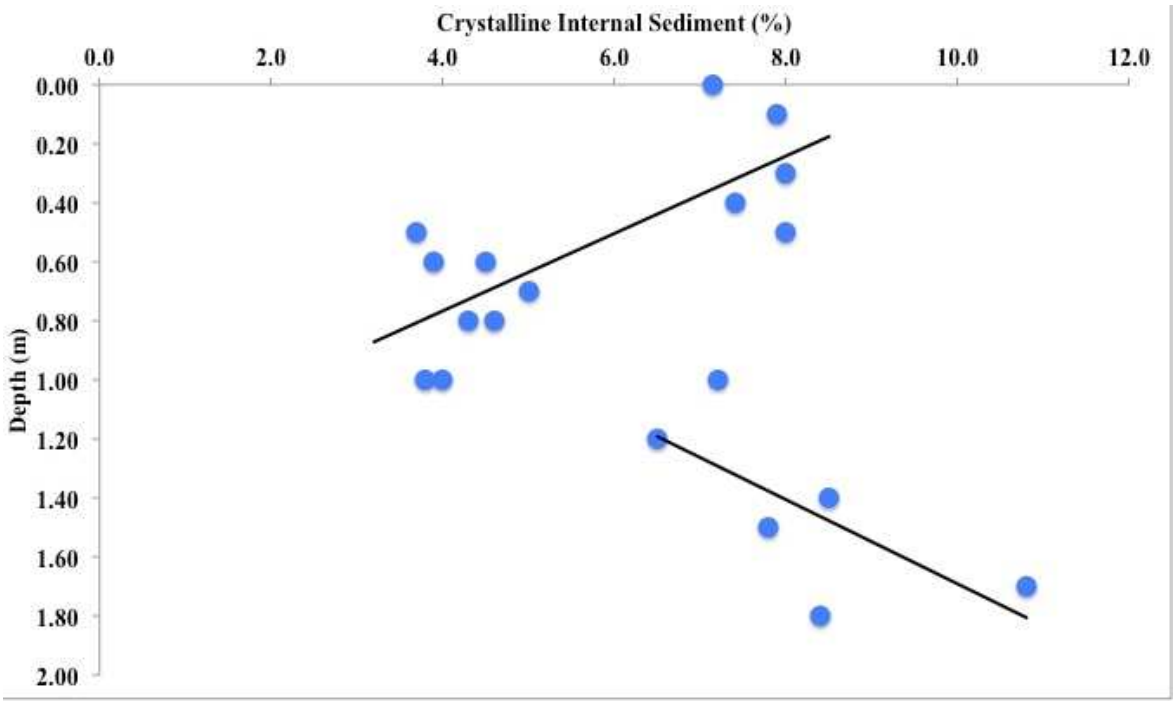

FIG. 4-10: Cross plot illustrates trends in crystalline internal sediment beneath disconformities in the inner margin (CM-1). Data points are 5-point moving averages. Solid lines are linear regression. Linear regressions appear to define two distinct trends.

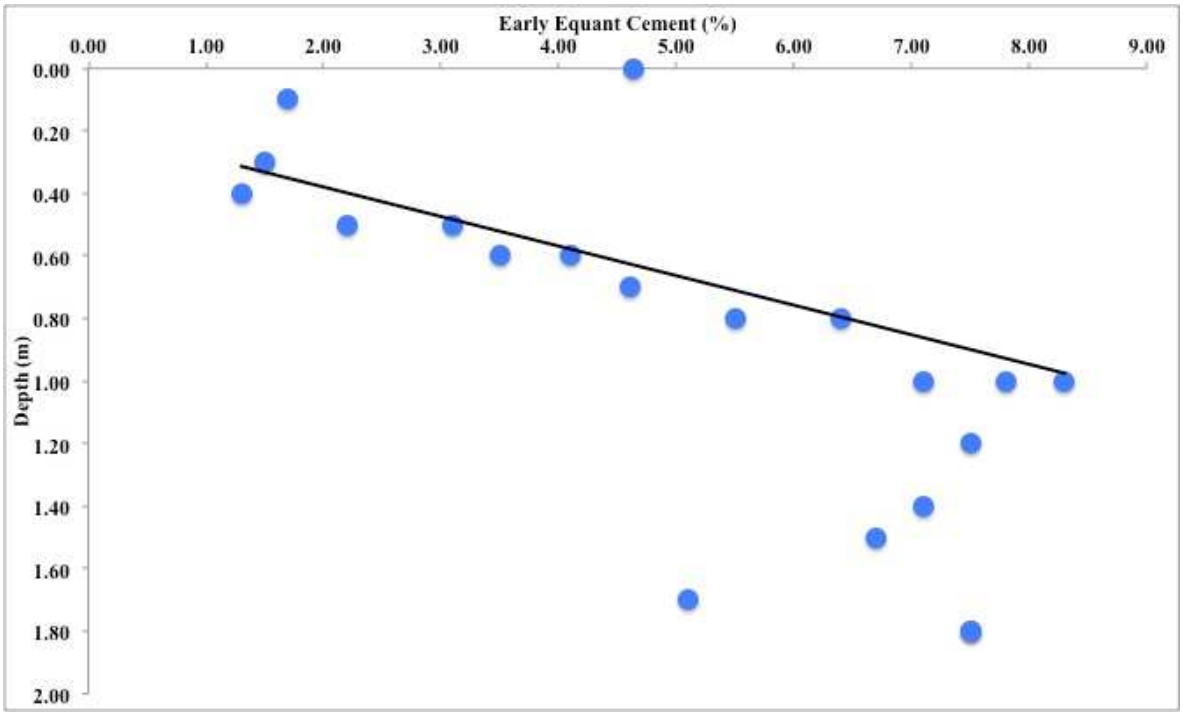

FIG. 4-11: Cross plot illustrates trends in early equant cement (5-point moving average) beneath disconformities in the inner margin (CM-1). Following a sharp reduction in cement abundance immediately beneath unconformities, a linear increase is evident to a depth of 1 m.

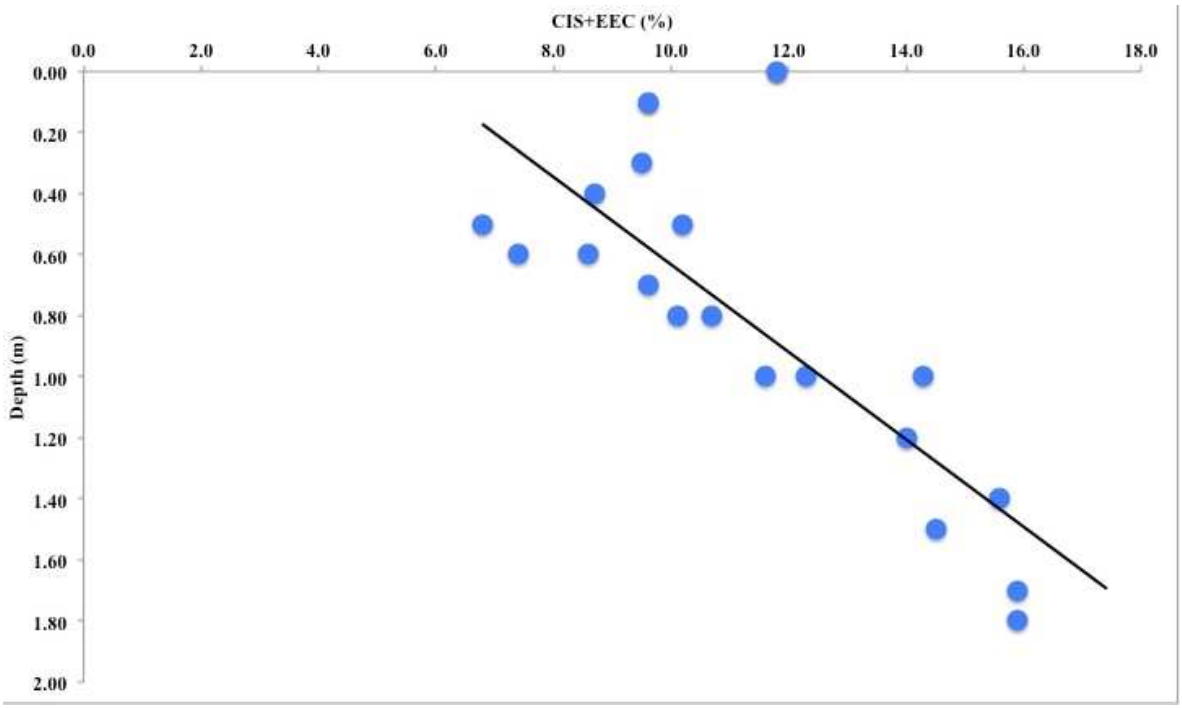

FIG. 4-12: Cross plot illustrates trends (5-point moving average) in filled porosity (some primary, mostly secondary) beneath disconformities in the inner margin (CM-1). Trend line is a linear regression. of values beneath 20 cm.

DISCUSSION

Micrometer to Decimeter Scales of Porosity

Carbonate reservoirs inherit various scales of porosity through depositional and diagenetic processes. Porosity and permeability can vary considerably among scales as demonstrated by this study. Porosity in El Abra Formation measured 1-inch plugs was low, about 3%. Porosity visible in thin sections, some made from many of the same samples as the plugs, averaged only 0.30% in the inner margin and 0.13% in the outer margin. This implies that almost the entire porosity measured in plugs is microporosity, below the limit of detection in thin section (about 30 μm). Pervasive oil staining of some crystalline internal sediment and of boundaries between layers of radiaxial fibrous cement indicates two loci of microporosity. Microporosity might serve as pathways for fluid migration during later diagenesis, but the retention of oil in this flushed reservoir signals low permeability. At larger scales, 4-inch cores

from the outer margin had an average porosity of 7.6% and permeabilities ranging from 0.8 to 552 md. Unfortunately, no cores were obtained from the inner margin. At the largest scale, porosity measured on photopans was 12% for outer-margin rocks and 6% for inner margin. The magnitude of porosity increases with the scale of observation. Extrapolation of this effect is not warranted in the Sierra El Abra, but cavernous porosity is the hallmark of reservoirs in the Golden Lane, age and facies equivalent of El Abra platform-margin limestones (Viniegra and Castillo-Tejero 1970; Minero et al. 1983, p.13)

Traditionally, reservoir studies rely on 1-in. plugs for analysis of porosity and permeability. In vuggy carbonate reservoirs, this can be quite misleading. Consider that a plug from vuggy limestone in outer margin yielded 2.6% porosity and permeability of 0.04 md. A 4-inch plug from the same stratigraphic interval measured 5.3% and 97 md. A photopan of the same interval yielded a porosity estimate of 12%. The relatively high permeabilities of 4-inch plugs (Fig. 4-4) compared with the low matrix permeability measured in 1-inch plugs demonstrate that some intervals of the outer margin have 'touching vugs,' as defined by Lucia (2007), that establish an interconnected network. These comparisons of various scales of porosity and their additive capacity demonstrate the importance of analyzing porosity (and permeability) over a wide range of scales for accurate petrophysical assessment of carbonate reservoirs with major secondary porosity.

Diagenetic Environments

Intraformational disconformities repeatedly exposed the high-Mg calcite and aragonite sediments of the inner margin and, rarely, the outer margin to subaerial exposure with aggressive meteoric waters and ensuing dissolution (D-1). Fine crystals liberated by the dissolution (CIS) were being flushed into both primary and secondary pores by water percolating through the

vadose zone (Dunham, 1969). Calcitic EEC, which reduced both primary and secondary pores in the inner margin, was probably being simultaneously precipitated as the more soluble phases supercharged the pore water. Thus the volume of porosity was in constant flux, not a sequential series of volumes as represented, for simplicity, in Fig. 4-9. Intraformational subaerial diagenesis was much less frequent and intense in the outer margin, as evidenced by limited early (D-1) secondary porosity, minor CIS, and absence of EEC. This contrast indicates that rocks of the inner margin were deposited on the highest elevations on the platform, on tidal flats and as rubble islands (Minero, 1983, 1988; Wahab et al. 2016

Early marine cementation (MC & RFC-1; 8.4% of bulk rock volume) greatly reduced depositional porosity in outer-margin grainstones and rudstones. The late episode of dissolution (D-2) removed nearly half of the rock volume (Fig. 4-9). Therefore, the original volume of early marine cement (and pores that it filled) could theoretically have been double of what is preserved for analysis. However, much of the late dissolution (D-2) was partially or entirely fabric selective: vugs (sxS-VUG) and skeletal molds (sxS-MO), respectively. Early marine cements, in contrast, were neomorphically altered without creation of visible pore space, so were probably preferentially preserved.

Duration of exposure, among other variables, is presumably key to the volumes of dissolution porosity produced. The second episode of dissolution (D-2), created pervasive secondary megapores, in both the inner and outer margins of El Abra Formation (Fig. 4-9). This pervasiveness suggests dissolution in a regional meteoric aquifer, at least as wide, and perhaps as long, as the exposed Sierra El Abra. This aquifer probably lasted no more than 3 million years during the end-Cenomanian hiatus, discussed in *Geologic Setting*. Large vugs, channels, solution pipes, and caverns are attributed to this episode. The distribution of this mega-porosity was not

uniform across the platform margin, tallying 21.5% (filled and extant) in the inner margin and 46.2% in the outer margin. This marked disparity, despite apparent homogeneity of the aquifer (Ch. III; cement stratigraphy) and probable nearly equal durations of exposure, is likely a consequence of differences in the earlier diagenetic history of the inner and outer platform margins. Initial porosity was higher in the inner margin (Fig. 4-9), but permeability in these muddy sediments would have been much lower (cf. Enos and Sawatsky, 1981). Moreover, repeated early subaerial diagenesis (CIS and EEC) apparently sealed primary and secondary porosity alike, despite significant intermittent dissolution (Fig. 4-9). Finally, lower porosity development immediately beneath the closely spaced unconformities (Fig. 4-12) probably created permeability barriers that further compartmentalized fluid circulation. In contrast, the coarse, grain-supported sediments of the outer margin had lower initial porosity, but orders of magnitude higher permeability, judging from modern analogs (Enos and Sawatsky, 1981). Early marine cementation (MC and RFC-1) reduced porosity significantly, but likely preserved considerably more permeability than in the inner margin rocks, paving the way for better fluid circulation and enhanced dissolution during D-2. Secondary factors possibly contributing to the contrast in extant porosity were the much higher mud content of inner-margin sediments and perhaps mineralogy. Aragonite may have been more prevalent in the rudist-dominated outer-margin deposits and would have been particularly prone to dissolution in the 'calcite seas' of the Cretaceous greenhouse earth.

The Turonian marine transgression displaced the regional meteoric aquifer, which had created large-scale porosity in both inner and outer platform-margin rocks. Extensive marine cementation (RFC-2), accompanied by pelagic marine internal sediment (PIS) in the outer margin, reduced porosity by 5% in the inner margin and by 7.9% in the outer margin. The

preferential infiltration of internal sediment into outer margin rocks presumably reflects better connectivity of pore networks, i.e. permeability, as well as more exposure to the pumping action of deep-water waves on the windward platform edge. Such infiltration was not an exclusive feature of the inner margin, however. Aguayo (1975, 1978) reported Turonian planktonic microfossils from deposits that we interpret as internal sediment in elongate vugs (Ch. II) from inner-margin quarries (VI, VII, VIII; Fig. 4-1B). These deposits, ~30 m below the present land surface, indicate very open connections to the erstwhile Turonian sea floor.

Remnant porosity was reduced to essentially present levels by fresh-water cementation during shallow burial of El Abra Formation in the Late Cretaceous. The requisite large volumes of freshwater may have entered through synorogenic clastic wedges of the Difunta Formation that were building into the foreland basin of the Sierra Madre Oriental, northwest of the Valles-San Luis Potosí platform, as early as Campanian time (Murray et al. 1962; McBride et al. 1975, Ye 1997). These fluids could have migrated through limestone and shale of San Felipe Formation, possibly fractured near the orogenic front, and, confined by impermeable deep-water shale of the overlying Méndez Formation, exited through the El Abra Formation locally exposed on the Campanian seafloor (Chapter III).

Fracturing and stylolitization during Laramide orogeny resulted in negligible porosity enhancement, but possibly significant permeability enhancement for charging a billion-barrel oil reservoir (Brennan 1999; Yurewicz 1997; Bitter 1986).

Role of Disconformities in Reservoir Heterogeneity

Trends in development of early porosity with depth beneath intraformational unconformities (Fig. 4-12) suggest a minimum in porosity, and presumably permeability, within

50 cm beneath the unconformities. This indicates that closely spaced intraformational unconformities, exemplified by the El Abra Formation, could lead to significant compartmentalization of reservoirs. The relative lack of exposure to subaerial diagenesis in the outer margin resulted in less pore-space modification and influenced the ultimate preservation of significant porosity without compartmentalization. The spatial distribution and varied expression of disconformity-controlled diagenesis thus influenced quantitative variations in porosity in El Abra Formation. As a result, 19.6% porosity and significant permeability are preserved in the outer margin, whereas the inner margin has 9.3% porosity and 0.04 md matrix permeability. The outer margin is a much better potential reservoir along the eastern margin of Valles-San Luis Potosí platform.

CONCLUSIONS

Diagenesis giveth and diagenesis taketh away. An **e**xtensive diagenetic history, most of it near-surface, resulted in 19.6% extant porosity and permeability as much as 553 md in the outer-platform-margin rocks of El Abra Formation. Inner-margin rocks were not so blessed, but retain 9.3% porosity. Microporosity of inner-margin rocks averages 3.3% with permeability of 0.04 md. Outer-margin rocks likewise retain 3.6% microporosity and permeability of 0.03 md. Mesoporosity, visible in thin section, is negligible for both settings. This range of values underscores the need to measure porosity and permeability in vuggy carbonate rocks over the widest range of scales feasible, more than six orders of magnitude in this study. It also clarifies that, although matrix porosity is very low, large vugs are interconnected, at least locally. Various diagenetic stages affected porosity evolution on different scales and different magnitudes. In order of increasing volume in the inner margin: radiaxial fibrous cement-2, early equant cement, crystalline internal sediment, and late equant cement reduced the reservoir quality. Late, near-

surface dissolution produced considerably more pore space than intraformational dissolution episodes beneath successive disconformities. Intraformational diagenesis beneath disconformities compartmentalized the inner margin by reducing porosity to half of its surface values in the first 50 cm, followed by a dramatic increase to a depth of 2 m. In the outer margin, in order of increasing volume: crystalline internal sediment, radiaxial fibrous cement-2, radiaxial fibrous cement-1, and late equant cement reduced reservoir quality. The late dissolution event, which pervaded the entire platform margin, produced virtually all of the extant porosity in the outer margin, much of it large scale and locally interconnected. The outer margin in El Abra Formation preserved significant vuggy megaporosity and permeability due to less overall exposure and, consequently, more favorable diagenetic modification. The outer margin is thus the optimum zone for reservoir quality in a heavily cemented shallow-water peritidal carbonate system.

REFRCES CITED

ADOBE SYSTEM INCORPORATED, 1982, Adobe Photoshop CC 2015 [Computer Software]: San Jose, California, USA.

AGUAYO-CAMARGO, J.E., 1975, Sedimentary environments and diagenetic implications of the El Abra Limestone at its type locality, east Mexico: Unpublished M.S. Thesis, University of Texas at Dallas, 159 p.

AGUAYO-CAMARGO, J.E., 1978, Sedimentary environments and diagenesis of a Cretaceous reef complex, eastern Mexico: Anales Centro Ciencias del Mar Limnologia., Universidad Nacional Autonoma, Mexico, v. 5, p. 83-140.

AGUAYO-CAMARGO, J.E., 1993, The middle Cretaceous EI Abra Limestone at its type locality and Laguna Colorada, east-central Mexico, *in* Alencaster, Gloria, and Buitron, B. E., eds., Universidad Nacional Autonoma de Mexico, Instituto de Geologia: Third International Conference on Rudists, Mexico, D.F., Nov. 20-28, Guidebook for field trip "A", 43 p.

AGUAYO-CAMARGO, J.E., 1998, The middle Cretaceous El Abra Limestone at its type locality (facies, diagenesis and oil emplacement), east-central Mexico: Revisita Mexicana de Ciencias Geológicas, v. 15, p. 1-8.

ALENCÁSTER, G., 1984, Late Jurassic-Cretaceous molluscan paleogeography of the southern half of Mexico, *in* Westermann, G.E.G., eds., Biochronology and paleogeography of North America: Geological Association of Canada Special Paper 27, p. 77–88.

BATHURST, R.G.C., 1974, Marine diagenesis of shallow water calcium carbonate sediments: Annual Review of Earth and Planetary Sciences, v. 2, p. 257.

BITTER, M.R., 1986, Sedimentology and petrology of the Chicontepec formation, Tampico-Misantla Basin, eastern Mexico: Unpublished M.S. Thesis, University of Kansas, Lawrence, 174 p.

BRENNAN, S.T., 1999, Impact of fluid and thermal history on reservoir properties of El Abra Limestone, Sierra el Abra, Mexico: Unpublished Master Thesis, University of Kansas, Lawrence, 183 p.

BUDD, D.A., SALLER, A.H., AND HARRIS, P.M., 1995, Unconformities and porosity in carbonate strata: American Association of Petroleum Geologists, Memoir, 63, 301 p.

CANTRELL, D.L., AND HAGERTY, R.M., 1999, Microporosity in Arab Formation carbonates, Saudi Arabia: Geo Arabia, v. 4, p. 129-154.

CARRILLO-BRAVO, J., 1971, La Plataforma Valles-San Luis Potosí: Boletín de la Asociación Mexicana de Geólogos Petroleros, v. 23, p. 1-113.

CHOQUETTE, P.W., AND PRAY, L.C., 1970, Geologic nomenclature and classification of porosity in sedimentary carbonates: American Association of Petroleum Geologists, Bulletin, v. 54, p 207-250.

DUNHAM, R.J., 1962, Classification of carbonate rocks according to depositional texture, *in* Ham, W.E., eds., Classification of carbonate rocks: American Association of Petroleum Geologists, Memoir 1, p. 108-121.

DUNHAM, R.J., 1969, Early vadose silt in Townsend Mound (Reef), New Mexico, *in* Friedman, G.M., eds., Depositional Environments in Carbonate Rocks: Society of Economic Paleontologists and Mineralogists, Special Publications, v. 14, p. 139-181.

ENOS, Paul, 1974, Reefs, platforms, and basins of middle Cretaceous in northeast Mexico: American Association of Petroleum Geologists, Bulletin, v. 58, p. 800-809.

ENOS, Paul, 1982, Basin-to-platform transition, mid-Cretaceous, Mexico (abstract): American Association of Petroleum Geologists, Bulletin, v. 66, p. 567.

ENOS, Paul, 1983, Late Mesozoic paleogeography of Mexico: In Reynolds M.W., Dolly E.D., eds., Mesozoic paleogeography of west-central United States: Society of Economic Paleontology and Mineralogy, Rocky Mountain Sect, Symposium 2, p. 133-157.

ENOS, Paul, 1986, Diagenesis of mid-Cretaceous rudist reefs, Valles platform, Mexico, *in* Schroeder, J.H. and Purser, B.H., eds., Reef diagenesis: Springer-Verlag, Berlin, p. 160-185.

ENOS, Paul, 1988, Evolution of pore space in the Poza Rica trend (Mid□Cretaceous), Mexico: Sedimentology, v. 35(2), p. 287-325.

ENOS, Paul, AND SAMANKASSOU, Elias, 1998, Lofer cyclothems revisited (Late Triassic, northern Alps, Austria): Facies, v. 38, p.207-228.

ENOS, Paul, AND SAWATSKY, L.H., 1981, Pore networks in Holocene carbonate sediments: Journal of Sedimentary Research, v. 51(3), p. 961-985

ESTEBAN, Mateo, AND KLAPPA, C.F., 1983, Subaerial exposure, *in* Scholle, P.A., Bebout, D.G., and Moore, C.H., eds., Carbonate depositional environments: American Association of Petroleum Geologists, Memoir, 33, p. 1-63.

GOLDSTEIN, R.H., 1988, Paleosols of Late Pennsylvanian cyclic strata, New Mexico: Sedimentology, v. 35, p. 777-803.

GRADSTEIN, F.M., OGG, J. G., & SMITH, A. G., 2004, A geologic time scale Cambridge University Press, London, 488 p.

JAMES, N.P. AND CHOQUETTE, P.W., 1984, Limestones - The meteoric diagenetic environment: Geoscience Canada, v. 11, no. 4, p. 785-799.

KACZMAREK, S.E., FULLMER, S., AND HASIUK, F.J., 2015, A universal classification scheme for the microcrystals that host limestone microporosity: Journal of Sedimentary Research, v. 85, p. 1197-1212, DOI: 10.2110/jsr.2015.79.

LANGORIA, J.F., 1975, Estatigrafia de le Sierra Comancheana del Noreste de Mexico: Boletin Sociedad Geologia Mexicana, v. 36, p. 31-59.

LUCIA, F.J., 1998, Carbonate reservoir classification: Springer, New York, 216 p.

LUCIA, F.J., 2007, Carbonate reservoir characterization: an integrated approach: Springer Science & Business Media, 333 p.

MCBRIDE, E.F., WEIDIE, A.E AND WOLLEBEN, J. A., 1975, Deltaic and associated deposits of Difunta Group (Late Cretaceous to Paleocene), Parras and La Popa basins northeastern Mexico, *in* M. L. S. Broussard, ed.s, Deltas: Houston Geological Society, p. 485-522.

MDP-405: A manual drill press, Cpm-400 Core Preparation Mill. (N.D.), http://www.coretest.com/core-drilling-instrument.html., Checked May 2016.

MINERO, C.J., 1983, Sedimentary environments and diagenesis of the El Abra Formation (Cretaceous), Mexico: Unpublished Ph.D. dissertation, State University of New York at Binghamton, 367 p.

MINERO, C.J., 1988, Sedimentation and diagenesis along an island-sheltered platform margin, El Abra Formation, Cretaceous of Mexico, *in* James, N.P. and Choquette, P.W. eds., Paleokarst: Springer-Verlag, Berlin, p. 385-405.

MINERO, C.J., ENOS, P., AGUAYO-CARMAGO, J.E., 1983, Sedimentation and diagenesis of mid-Cretaceous platform-margin east-central Mexico, with accompanying field guide: Dallas Geological Society, Dallas, 168 p.

MOORE, C.H., 2001, Carbonate reservoirs – Porosity evolution and diagenesis in a sequence stratigraphic framework: Amsterdam, Elsevier: Developments in Sedimentology 55, 460 p.

MURRAY, G.E., WEIDIE JR, A.E., BOYD, D.R., FORDE, R.H., AND LEWIS JR, P.D., 1962, Formational divisions of Difunta Group, Parras Basin, Coahuila and Nuevo León, Mexico: American Association of Petroleum Geologists, Bulletin, v. 46, p. 374-383.

RODUIT, N., 2008, JMicroVision: Image analysis toolbox for measuring and quantifying components of high-definition images, Version 1.2. 7 [Computer Software], available for free download at http://jimcrovision.com.

SCOTT, R.W., 1990, Models and stratigraphy of mid-Cretaceous reef communities, Gulf of Mexico: Society of Economic Paleontologists and Mineralogists, Special Publications, Tulsa, p. 102.

SMITH, B.A., 1986, Upper Cretaceous stratigraphy and the mid-Cenomanian unconformity of the east central Mexico: Unpublished Ph.D. dissertation, University of Texas at Austin, 190 p.

STEPPINGSTAGE: A digital Stepping stage used for point counting thin sections, http://ws2.petrog.com/steppingstage.html. Checked May 2016.

VINIEGRA-O., F., AND CASTILLO-TEJERO, C., 1970, Golden Lane fields, Veracruz, Mexico, *in* M. T. Halbouty, ed., Geology of giant petroleum fields: American Association of Petroleum Geologists, Memoir. 14, p. 309-325.

WAHAB, A., ENOS, Paul, AND GOLDSTEIN, R.J., 2016, Disconformity-controlled diagenesis in El Abra carbonate platform (mid-Cretaceous), Mexico (abs.): Geological Society of America, Abstract with Programs, v. 48, no. 7, doi: 10.1130/abs/2016AM-280172.

YE, H., 1997, Sequence stratigraphy of the Difunta group in the Paras-La Popa foreland basin, and tectonic evolution of the Sierra Madre Oriental, NE Mexico: Unpublished Ph.D. dissertation, The University of Texas at Dallas, 197 p.

YUREWICZ, D.A., CHUCHLA, R.J., RICHARDSON, M., POTTORF, R.J., GRAY, G.G., KOZAR, M.G., AND FITCHEN, W.M. 1997, Hydrocarbon generation and migration in the Tampico-Misantla Basin and Sierra Madre Oriental, East-Central Mexico: Evidence from an Exhumed Oil Field in the Sierra de El Abra: Dallas Geological Society and Society of Economic Paleontologists and Mineralogists, 24 p.

CHAPTER V: CONCLUSIONS

The purpose of this study was to investigate diagenetic trends and porosity evolution associated with closely spaced disconformities in the mid-Cretaceous El Abra Formation exposed on the eastern margin of the Valles-San Luis Potosí platform in the Sierra El Abra, Mexico.

El Abra Formation is composed of shallowing-upward cycles, truncated cycles and rhythms. Cyclothems average 1.7 m thick and record time spans approximately similar to sub-Milankovitch cycles (<12 ka). High-frequency and low-amplitude (10's m) sea-level oscillations introduced alternating subaerial and subtidal conditions. The El Abra platform apparently missed some sea level oscillations above platform top, resulting in subtidal units two or more times average thickness. Although evidence for mid-Cretaceous glaciation is equivocal and controversial, this seems the most probable mechanism driving cyclicity. Paleosols, microkarst horizons, rhizoliths, blackened clasts, and pervasive solution porosity indicate repeated emergence of El Abra Formation. Marine-phreatic diagenesis dominated the outer margin, as shown by extensive micritization and meniscate-micritic and radiaxial-fibrous cement, contemporaneous with meteoric diagenesis in the inner margin. The products of intraformational meteoric diagenesis, e.g. early secondary porosity, crystalline internal sediment, and early equant cement are vastly more abundant in the inner-margin than the outer-margin rocks. A regional meteoric aquifer developed in the late Cenomanian, resulting in large-scale secondary porosity throughout the Sierra El Abra, later reduced by radiaxial-fibrous cement and pelagic internal sediment. Late equant calcite cement, the last major episode of porosity reduction, precipitated during shallow burial. Deeper burial and the Laramide orogeny produced only fractures, minor fracture-filling cement, and stylolites. Fractures and stylolites served as main conduits of

hydrocarbon migration. Early diagenetic features help elucidate the paleo-morphology of the platform margin. The tidally influenced rocks in the inner margin experienced more subaerial exposure than the rest of El Abra platform, suggesting relatively higher elevation on the platform.

Petrography, cement stratigraphy, and fluid-inclusion analyses of the calcite cements in El Abra Formation provided insights into cement distribution, timing, and a feasible hydrological scenario for cement precipitation. Crosscutting relationships document the intraformational origin of EEC, with cyclic cementation beneath successive disconformities. Salinities of the precipitating fluids ranged from freshwater to evaporated seawater, including normal seawater and various mixtures. Contemporaneous marine-phreatic diagenesis resulted in precipitation of the first generations of marine cements in the outer margin. A pervasive dissolution (D-2) event created voluminous megaporosity, reduced by a second generation of marine cements. Following the Turonian transgression, late equant cements, the most voluminous cements in the Sierra El Abra, were deposited in approximate synchronicity throughout the platform margin, as indicated by continuity of four distinctive cathodoluminescence zones. Precipitation was from freshwater at temperatures less than about 50°C. This freshwater may have infiltrated clastic wedges developed at the front of the rising Sierra Madre Oriental, passed through fractured (?) basinal rocks and porous platform limestones, to exit through the elevated rim of the Vallea-San Luis Potosí platform onto the Campanian seafloor.

Extensive near-surface diagenesis resulted in 19.6 % extant porosity and permeability as much 552 md in the outer-platform-margin rocks of El Abra Formation. Inner-margin rocks were not so blessed, but retained 9.3 % porosity. Microporosity of inner margin rocks averages 3.3% with 0.04 md permeability. Outer-margin rocks retained about 3.6% microporosity and

permeability of 0.03 md. Mesoporosity was negligible for both settings. This range of values underscores the need to measure porosity and permeability in vuggy carbonate rocks over the widest range of scales feasible, more than six orders of magnitude in this study. It also clarifies that, although matrix porosity is vary low, large vugs are interconnected, at least locally. Various diagenetic stages affected porosity evolution on different scales and different magnitudes. In order of increasing volume in the inner margin: radiaxial fibrous cement-2, early equant cement, crystalline internal sediment, and late equant cement reduced the reservoir quality. Late, near-surface dissolution produced considerably more pore space than intraformational dissolution episodes beneath successive disconformities. Intraformational diagenesis beneath disconformities compartmentalized the inner margin by reducing porosity to half of its surface values in the first 50 cm, followed by a dramatic increase to a depth of 2 m. In the outer margin, in order of increasing volume: crystalline internal sediment, radiaxial fibrous cement-2, radiaxial fibrous cement-1, and late equant cement reduced reservoir quality. The late dissolution event, which pervaded the entire platform margin, produced virtually all of the extant porosity in the outer margin, much of it large scale and locally interconnected. The outer margin in El Abra Formation preserved significant vuggy megaporosity and permeability due to less overall exposure and, consequently, more favorable diagenetic modification. The outer margin is thus the optimum zone for reservoir quality in a heavily cemented shallow-water peritidal carbonate system.

APPENDIX A

*[1]*Key To Measured Sections*

1: Key for Measuring Carbonate Stratigraphic Section. Modified Handout, Carbonate Petrology 932 (Instructor: Enos, Paul), University of Kansas.

APPENDIX B

Measured Section CM-1

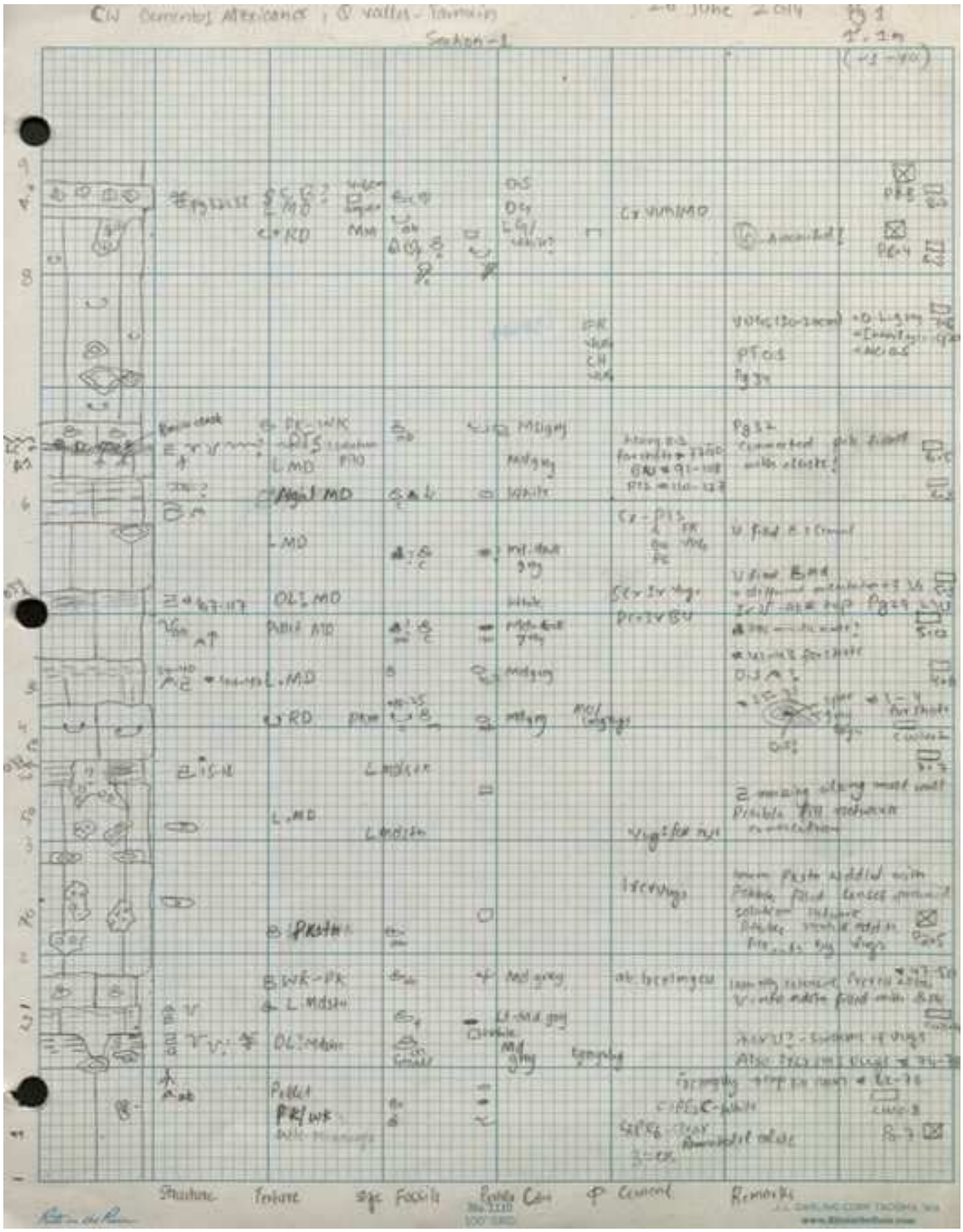

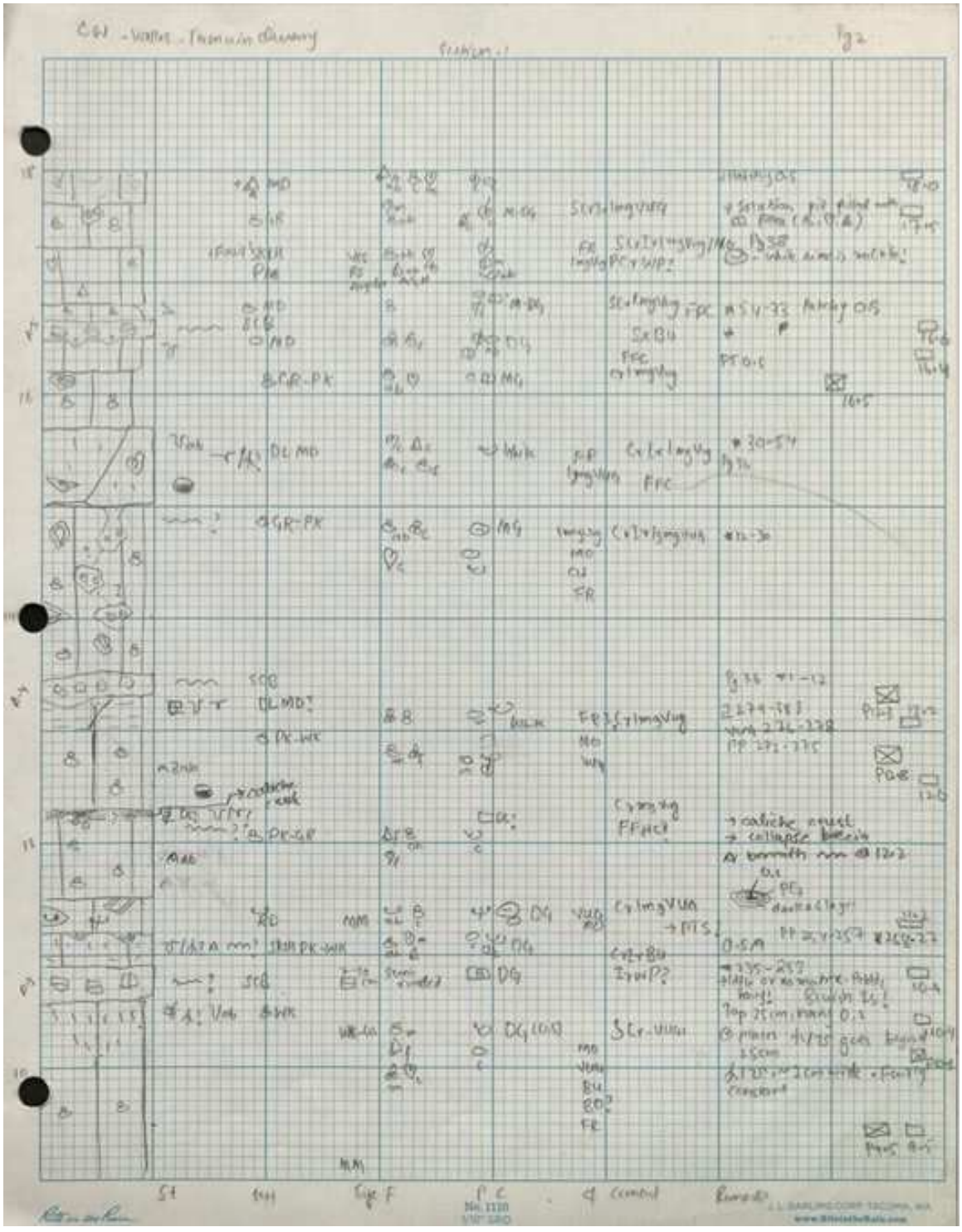

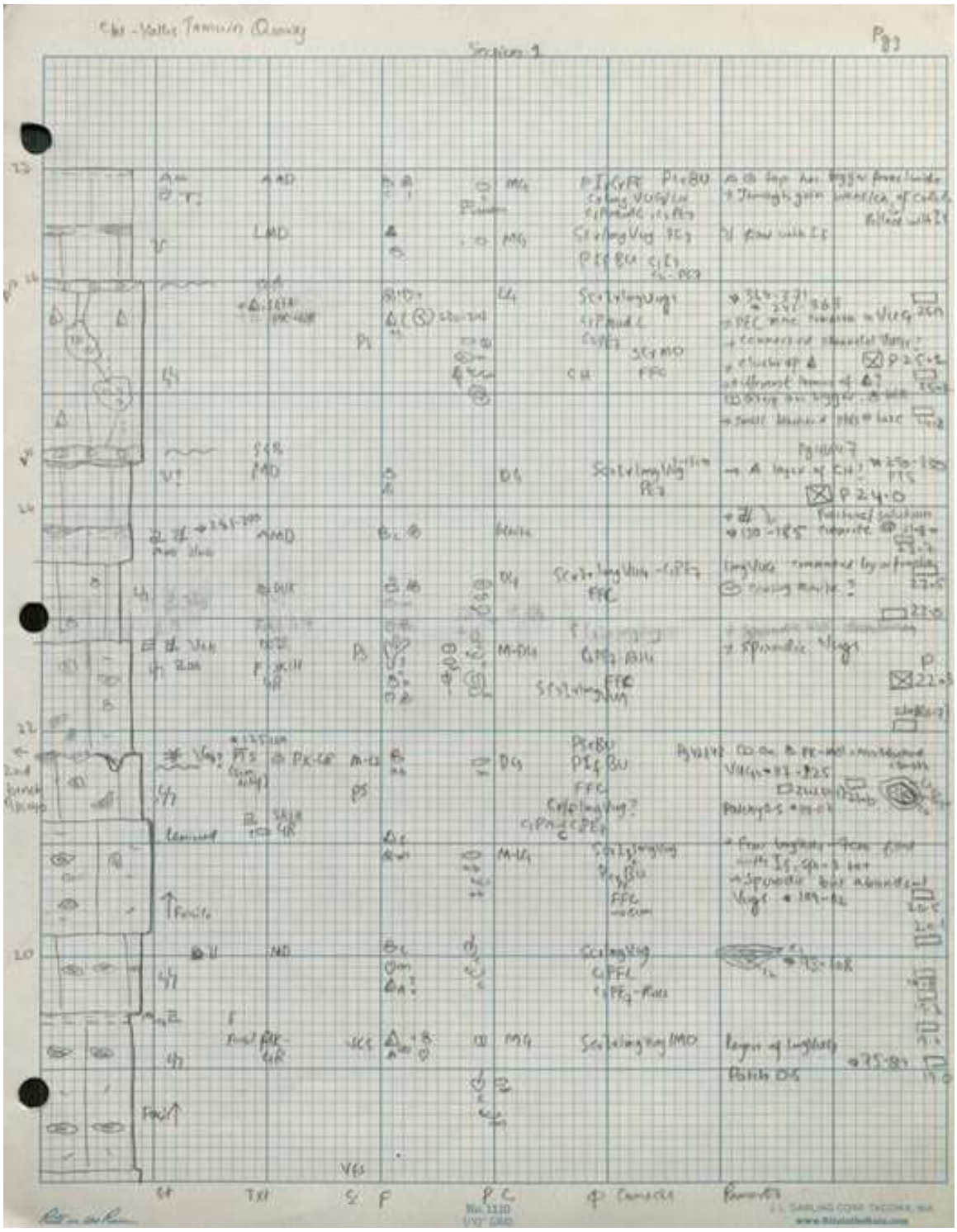

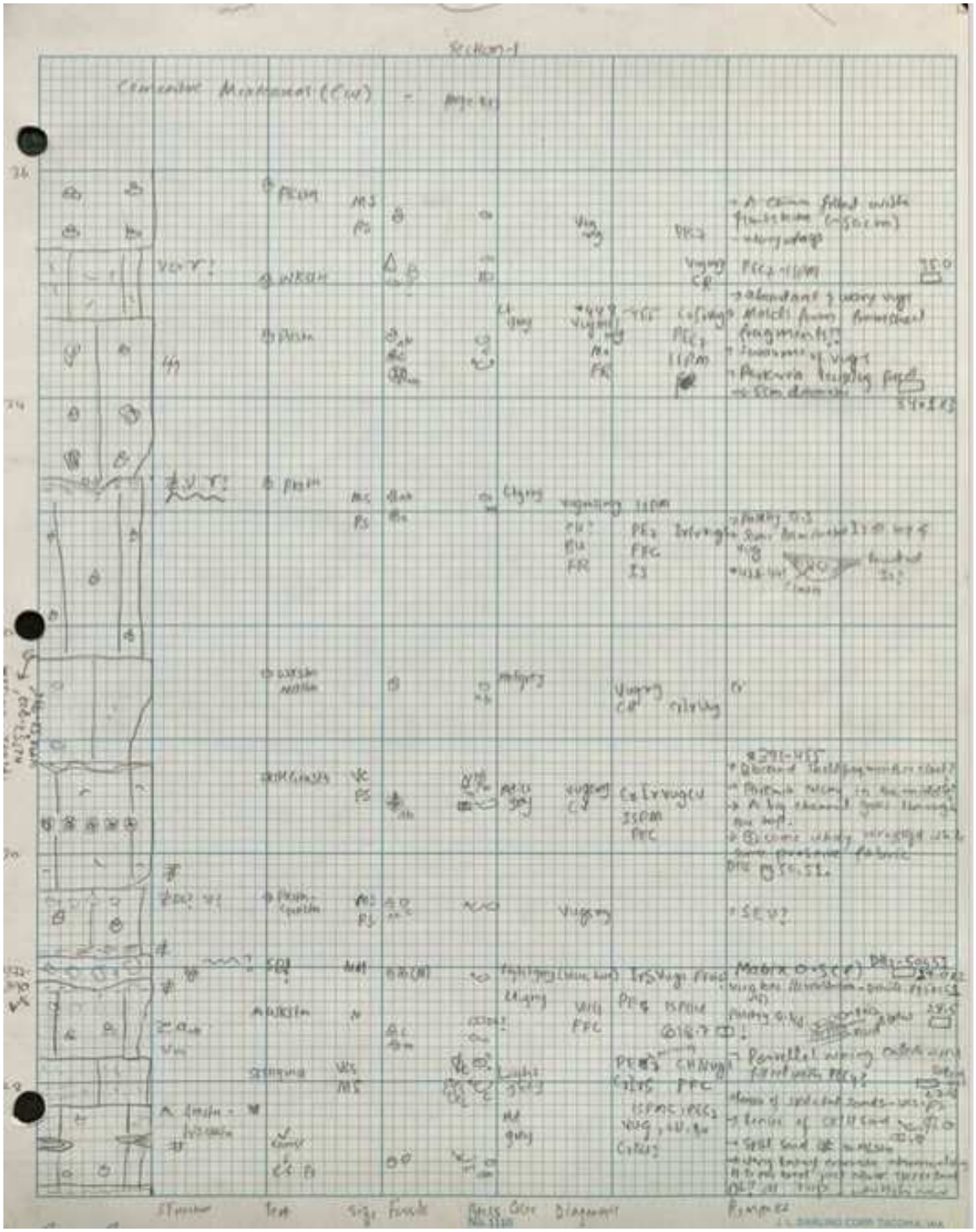

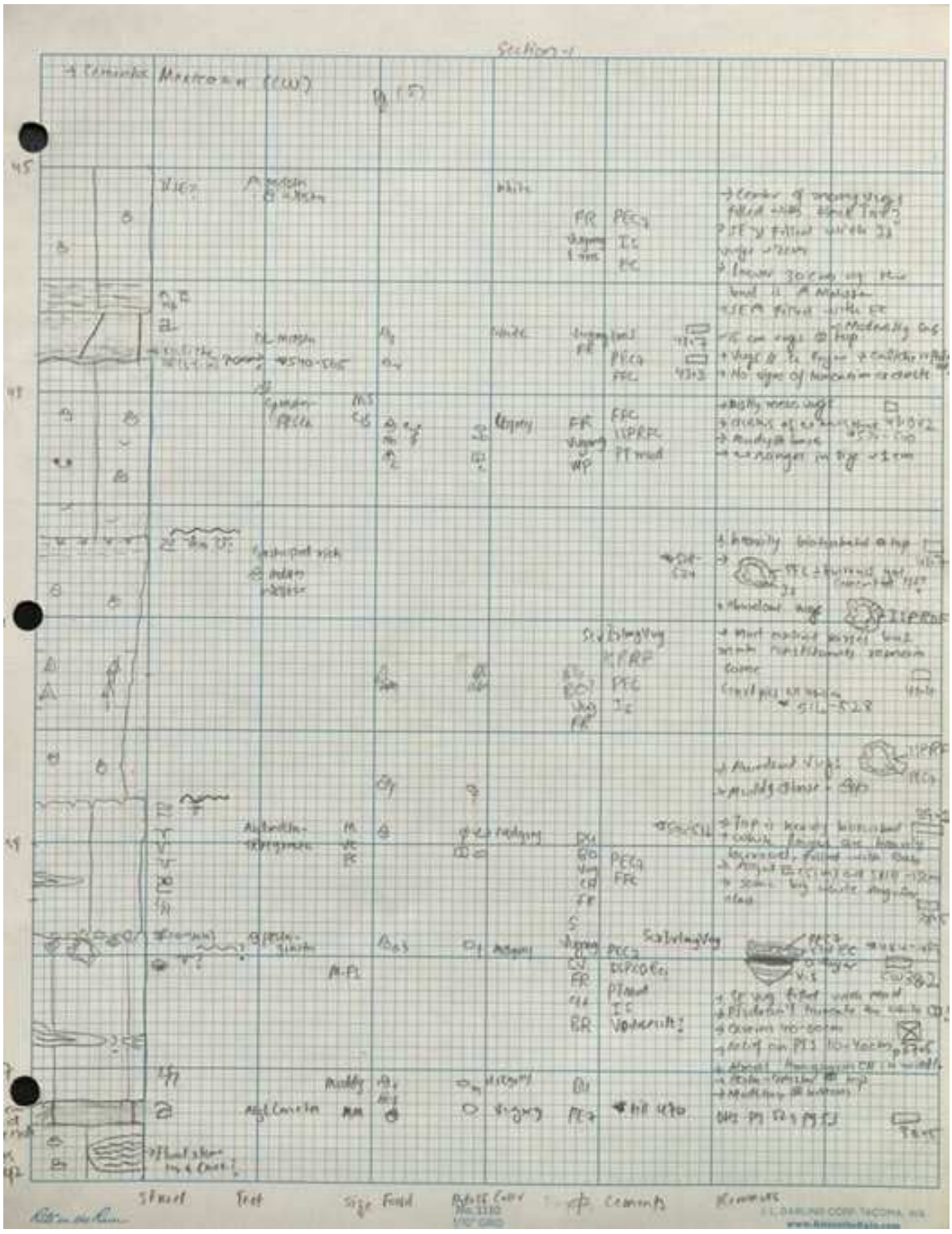

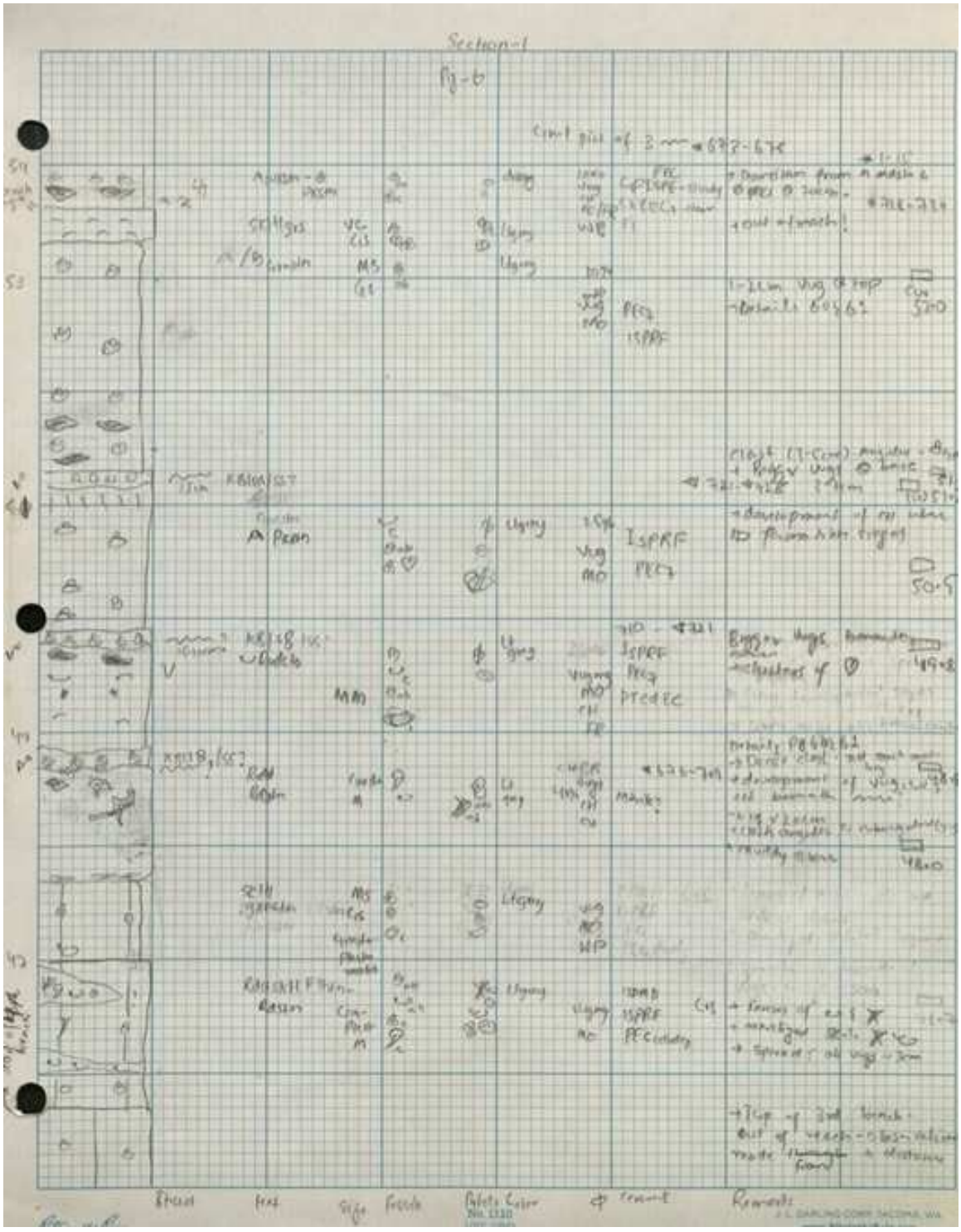
Section-1
Remarks

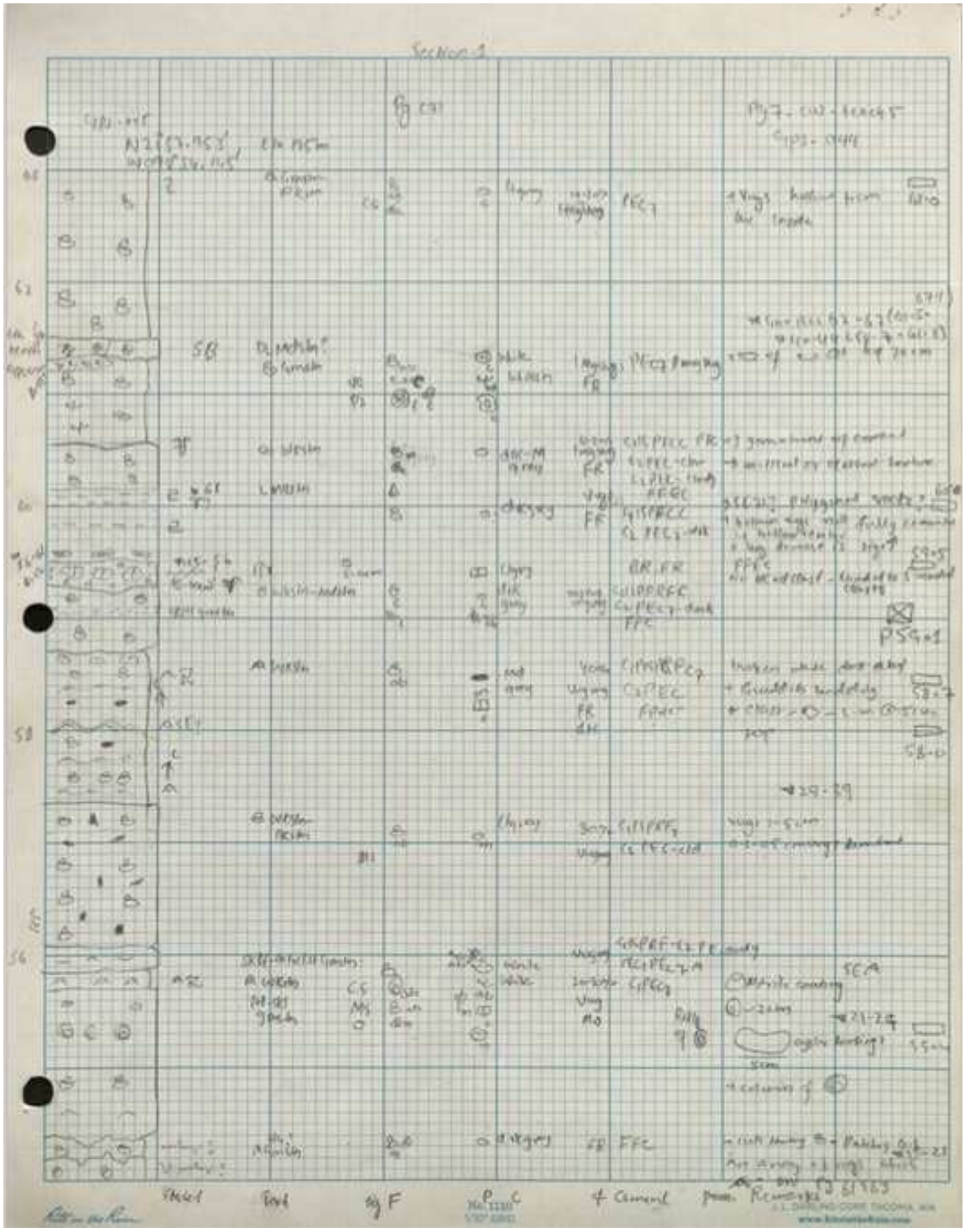

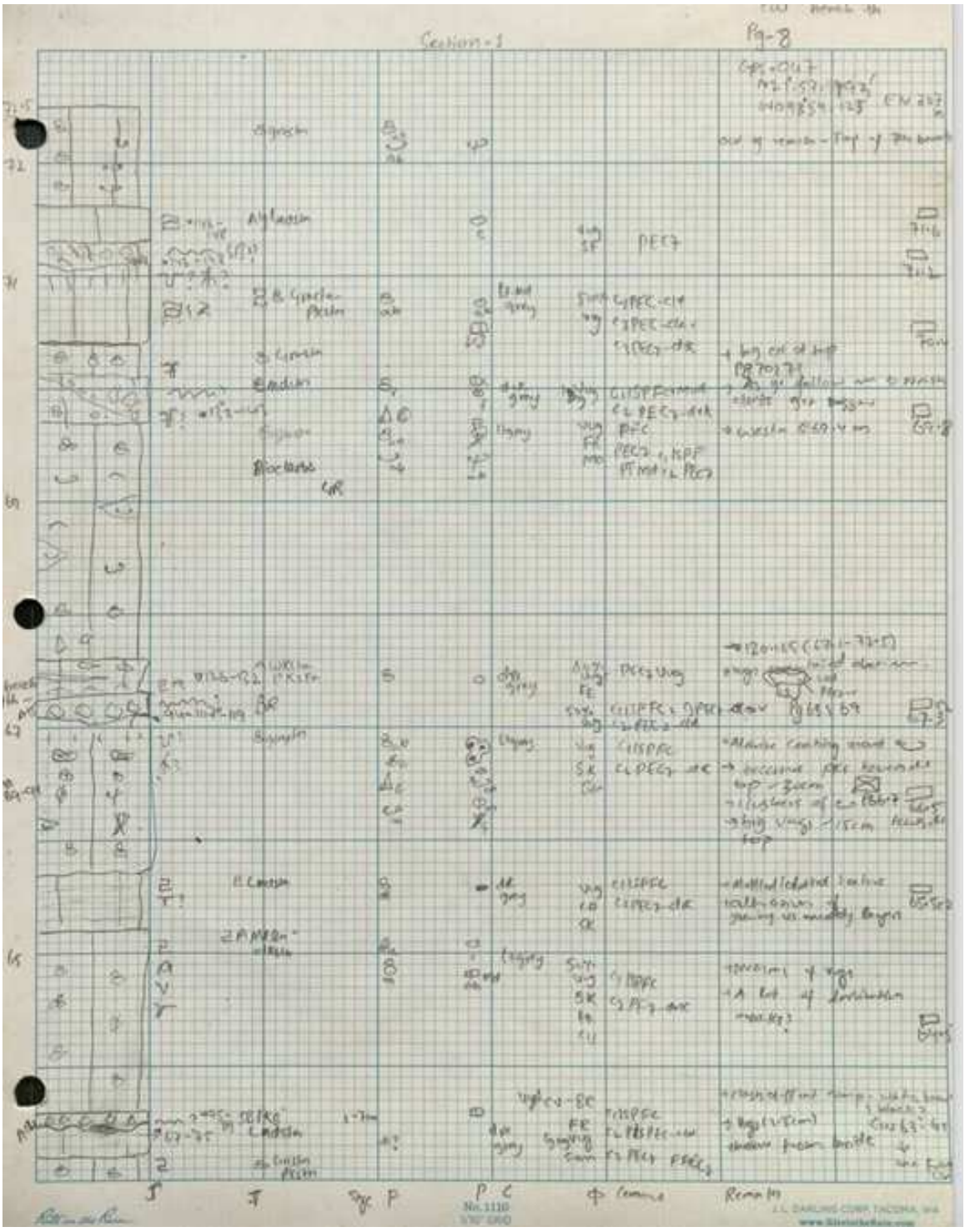
Section 3
Pg-8

APPENDIX C

Measured Section CM-2

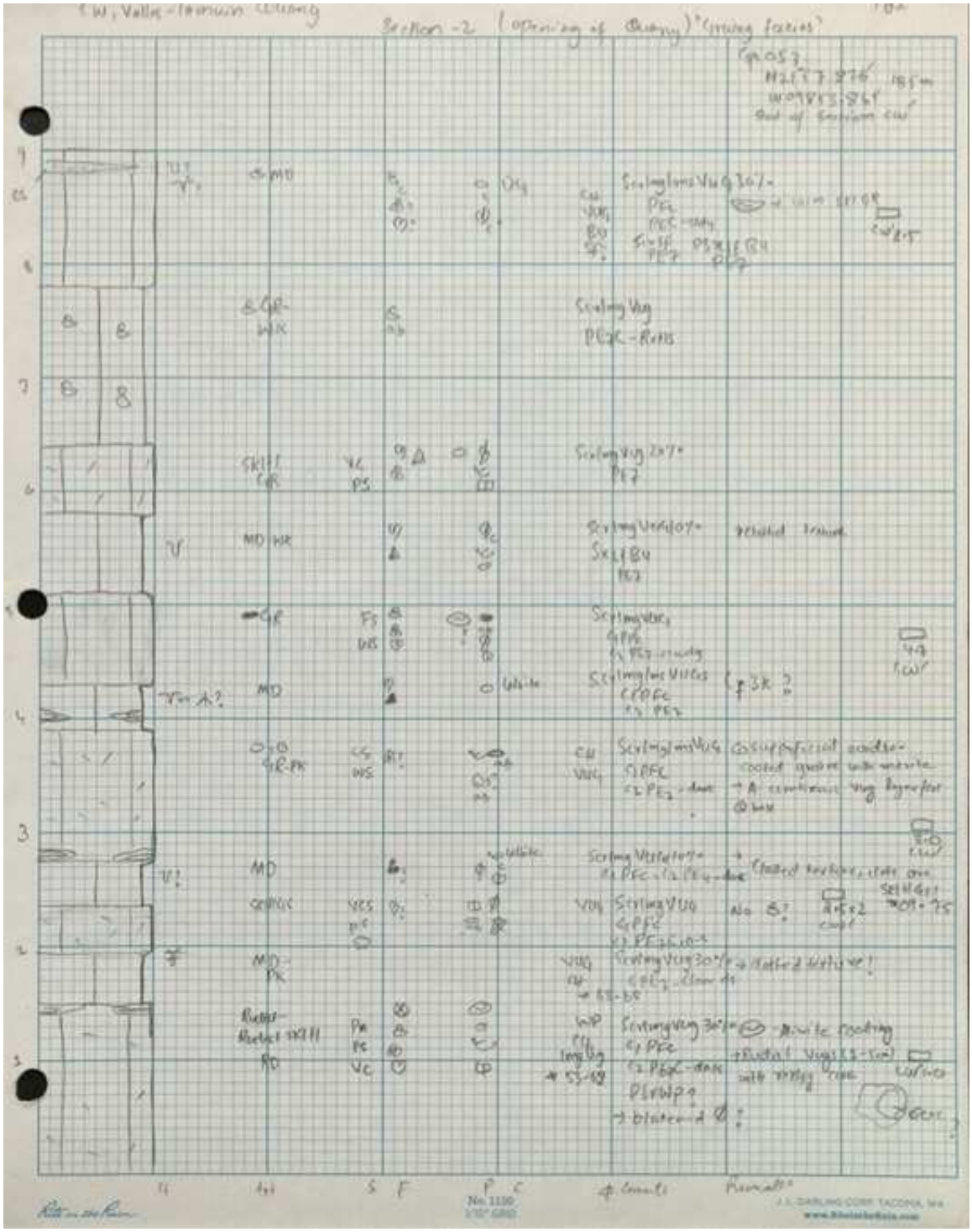

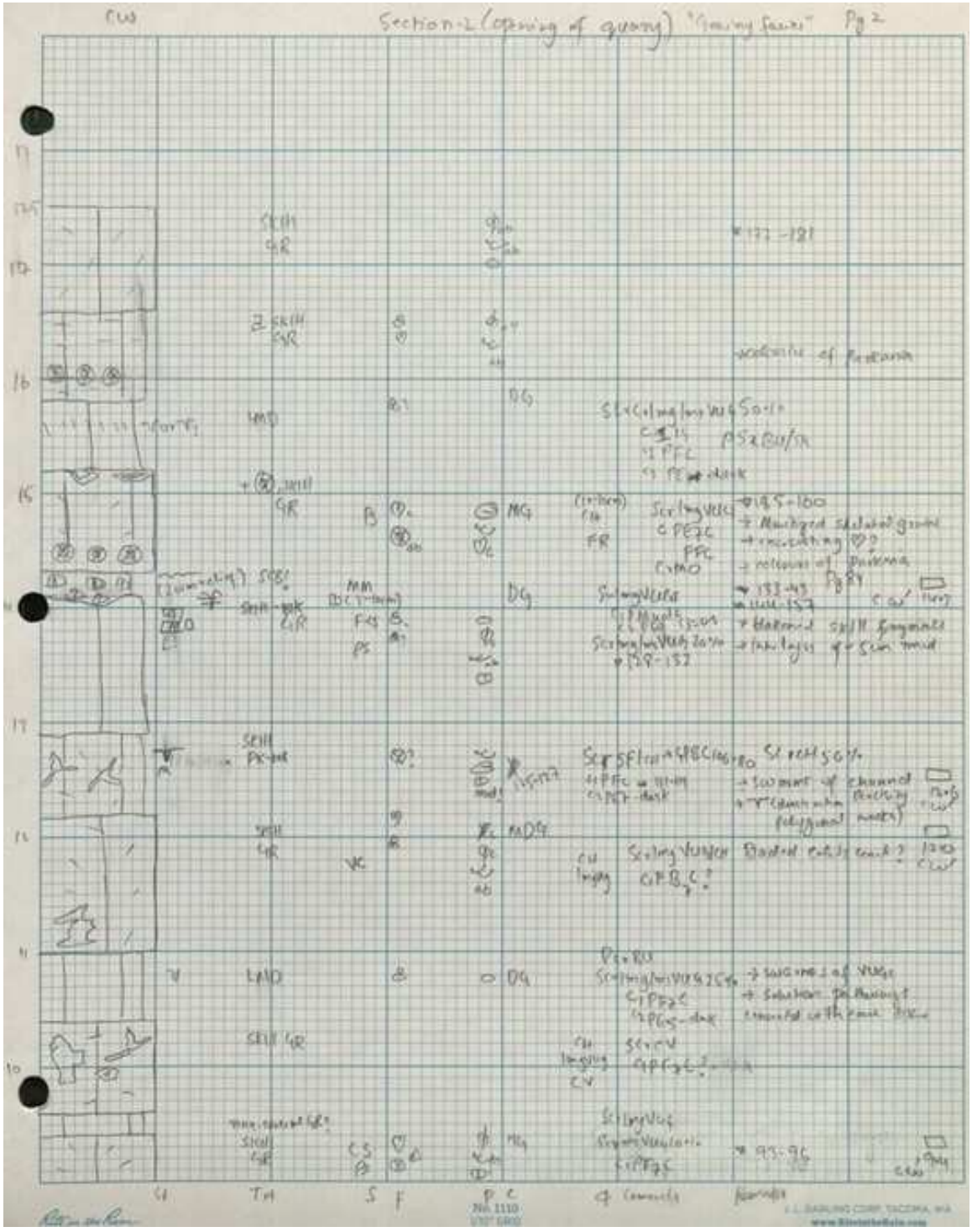
Section 2 (opening of quarry) "Grassy Seam" Pg 2

APPENDIX D

Measured Section PM-1

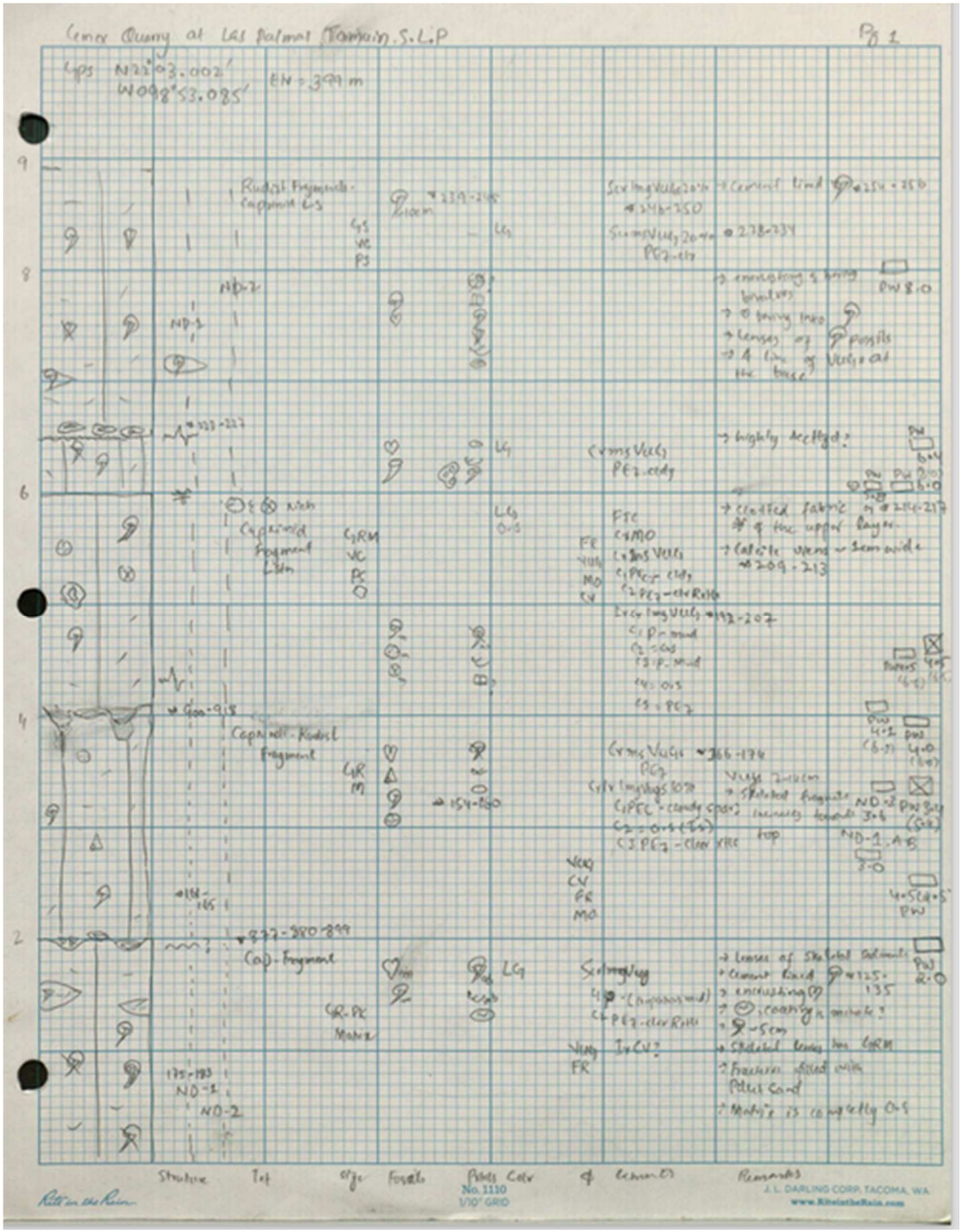

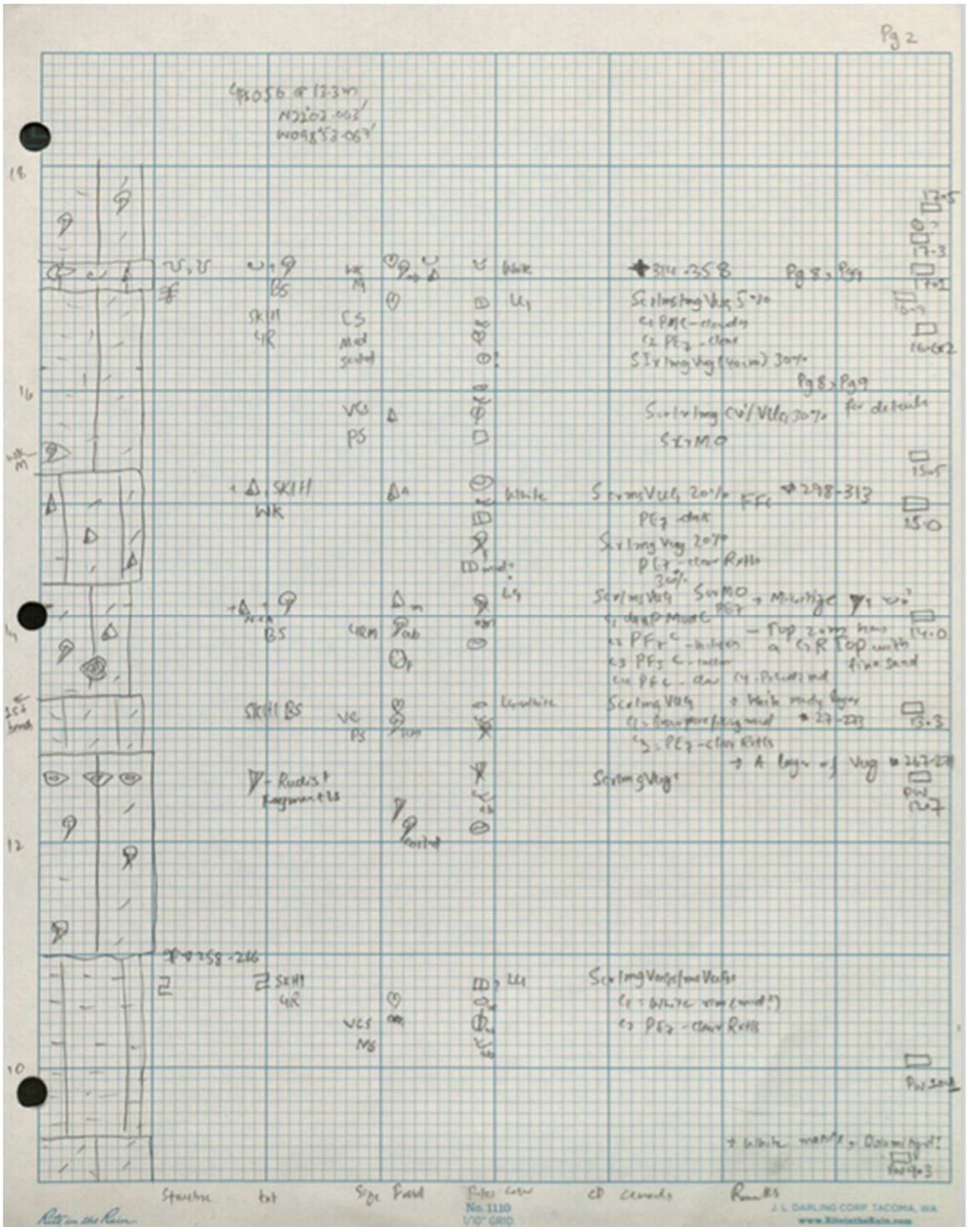
Pg 2
Structure
txt
Size
Rock
Notes color
No. 1110
1/10" GRID
J. L. DARLING CORP. TACOMA, WA
www.RiteInTheRain.com

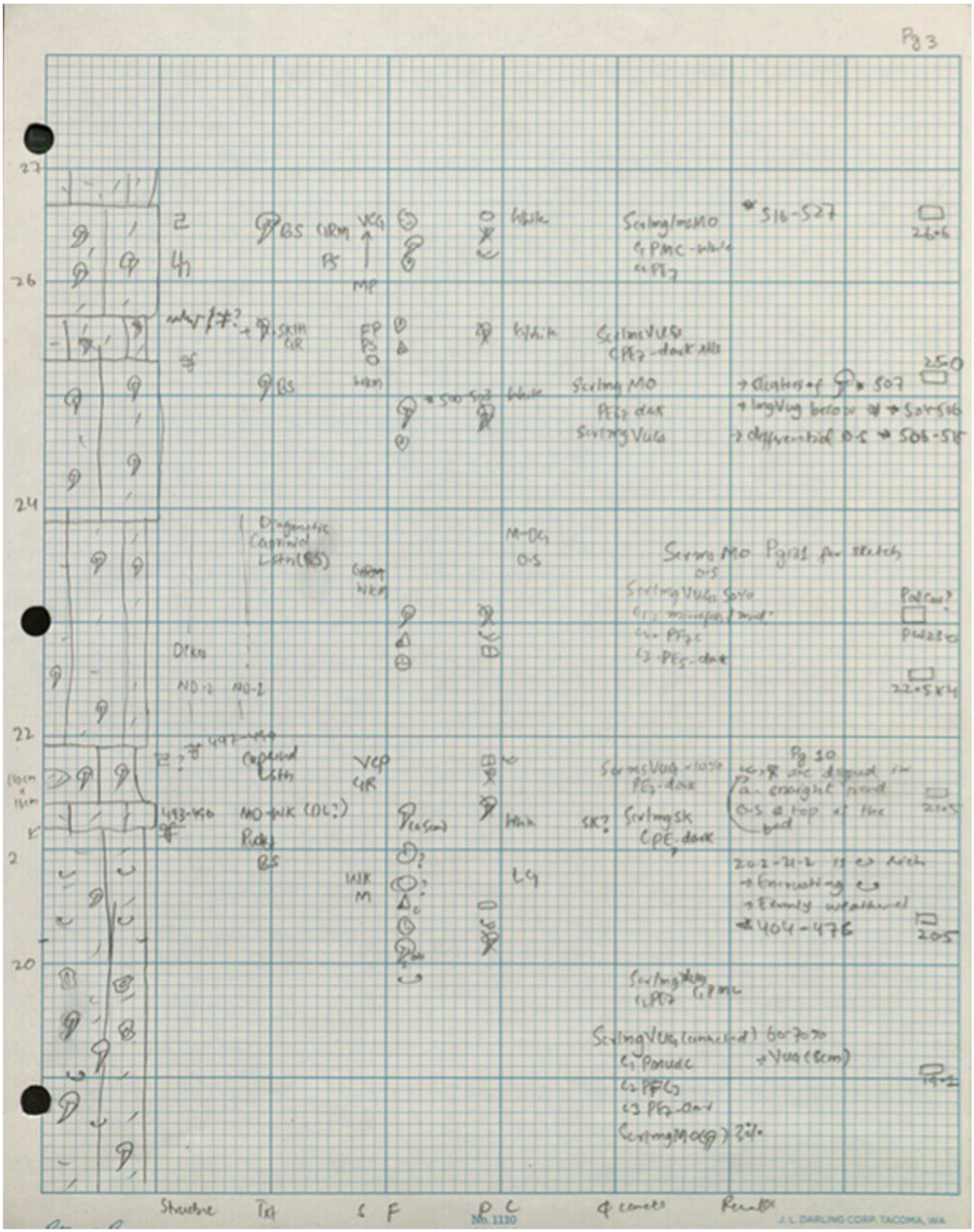

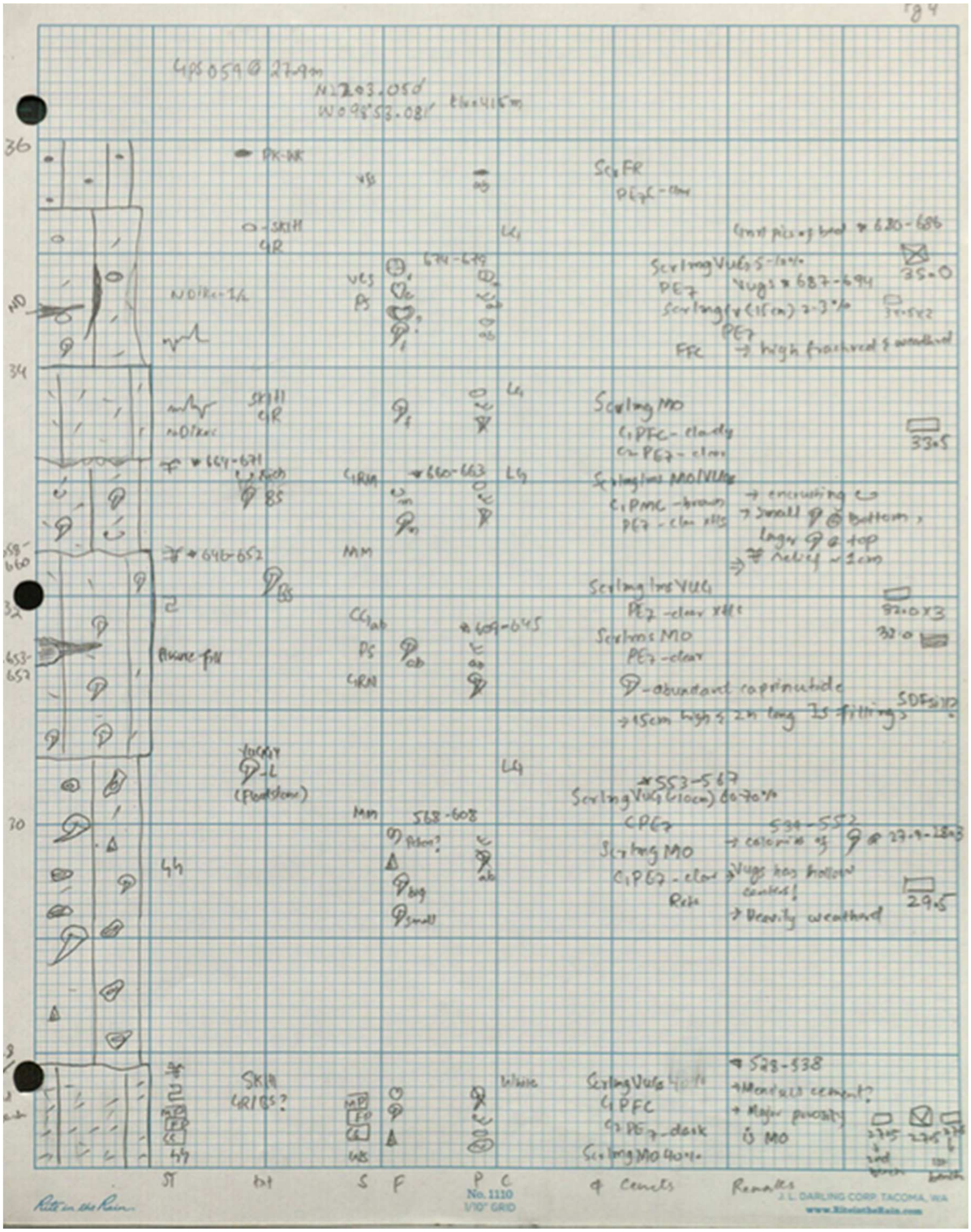
ST
bt
S
F
P
C
Ф Cements
Remarks
No. 1110
1/10" GRID
J.L. DARLING CORP. TACOMA, WA
www.RiteintheRain.com
Rite in the Rain
PE7
→ high fractured & weathered
→ encrusting
Scrlmg MO
→ heavily weathered
→ Major porosity

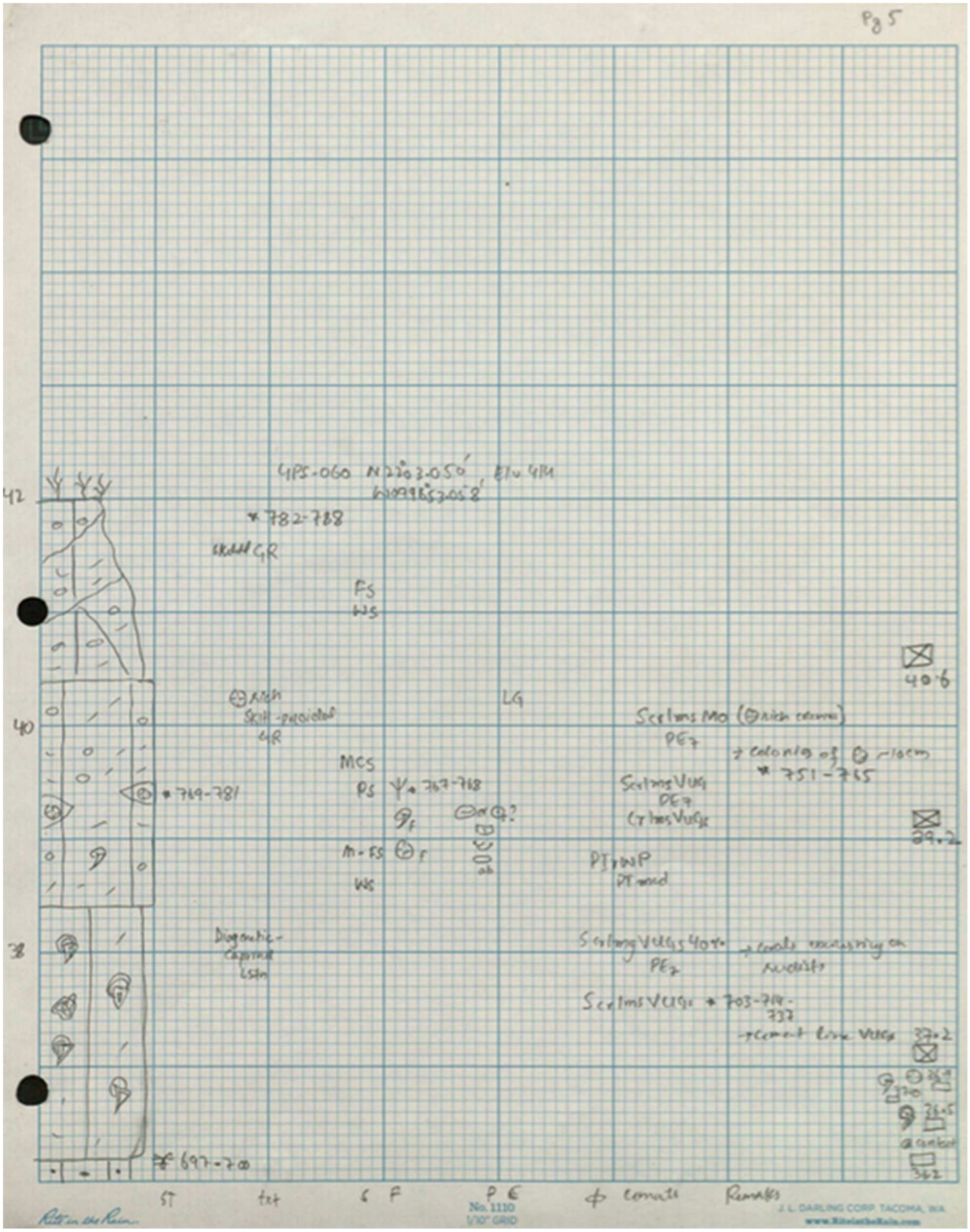
Pg 5
42
40
38
*782-788
FS
WS
LG
MCS
PS
M-FS
WS
ST
txt
P E
Remarks
No. 1110
1/10" GRID
J. L. DARLING CORP. TACOMA, WA

APPENDIX E

Fluid-Inclusion Data In Early Equant Cements (EEC)

Disconformity elevation (m)	Sample elevation (m)	Tm ice (°C)	Salinity (ppt)
3.8	1.8	0.0 -0.5 -0.5 0.0	0.0 9.0 9.0 0.0
		-1.6 -1.6	30.0 30.0
		-1.6 -2.7	30.0 49.0
6.5	5.3	-1.8	33.0
		-1.9	35.0
		-2.6	47.0
15	14	-0.3 -0.3	6.0 6.0
		-0.3 -0.3	6.0 6.0
		-0.3	6.0
		-0.5	9.0
67.3	65.5	0.0	0.0
		0.0	0.0

Fluid inclusion data of early equant cements from CM-1. Column 1 shows elevation of disconformity. Column 2 shows elevation of sample. Column 3 shows melting temperature of ice (Tm ice) in fluid inclusions. Note that values in red represent an FIA and values in black represent single isolated fluid inclusions. Column 4 shows salinity values using seawater-salt model (Goldstein and Reynolds, 1994) to convert Tm ice into salinities.

APPENDIX F

Fluid Inclusion Data In Late Equant Cements (LEC)

Sample elevation (m)	Tm ice (°C)	Salinity (ppt)
PM-1 16.6	0.0	0.0
PM-1 16.6	0.0	0.0
PM-1 16.6	0.0	0.0
PM-1 16.6	0.0	0.0
CM-1 38.2	0.0	0.0
CM-1 38.2	0.0	0.0
CM-1 38.2	0.0	0.0
CM-1 38.2	0.0	0.0
CM-1 63.0	-0.1	2.0
CM-1 63.0	-0.2	4.0

Sample elevation is actual elevation on the measured section. Sample 16.6 is from the outer margin and sample 38.2 and 63 are from the inner margin.

APPENDIX G

Porosity And Permeability Data From CM-1 (1-Inch Plugs)

Sample Number	Elevation in CM-1 section (m)	Permeability Horizontal (Kair) md	Porosity (Helium) %	Grain Density gm/cc
1	CM-1 0.7 H	0.009	1.6	2.69
2	CM-1 1.4 V	0.004	3.7	2.70
3	CM-1 2.5 V	0.004	2.2	2.70
4	CM-1 3.7 V	0.004	2.9	2.70
5	CM-1 5 V	0.010	5.1	2.71
6	CM-1 5.3 V	0.001	6.5	2.78
7	CM-1 6.5 H	0.002	3.8	2.70
8	CM-1 8.4 H	0.004	3.0	2.68
9	CM-1 8.8 H	0.003	2.5	2.70
10	CM-1 9.5 H	0.003	2.3	2.70
11	CM-1 10.4 H	0.004	0.3	2.67
12	CM-1 12.5 H	0.003	9.9	2.70
13	CM-1 12.6 H	0.004	3.2	2.76
14	CM-1 12.8 V	0.004	0.4	2.68
15	CM-1 13.2 H	0.002	5.9	2.70
16	CM-1 13.3 V	0.003	2.0	2.69
17	CM-1 14 H	0.003	2.7	2.68
18	CM-1 16.5 V	1.230	1.6	2.69
19	CM-1 19.8 H	0.003	3.1	2.70
20	CM-1 24 H	0.002	2.1	2.70
21	CM-1 28.5 H	0.005	1.6	2.70
22	CM-1 37.5 V	0.001	4.4	2.70
23	CM-1 38.2 H	0.005	4.5	2.70
24	CM-1 38.2 V	0.010	5.3	2.70
25	CM-1 38.5 V	0.003	2.0	2.70
26	CM-1 40.4 H	0.011	7.3	2.69
28	CM-1 41.7 H	0.003	2.8	2.70

29	CM-1 48 H	0.004	3.4	2.70
30	CM-1 49.8 H	0.023	2.9	2.70
31	CM-1 49.8 V	0.004	1.7	2.69
32	CM-1 51.5 H	0.002	2.5	2.70
33	CM-1 51.5 V	0.002	2.8	2.70
34	CM-1 53 V	0.002	3.5	2.70
35	CM-1 59.1 H	0.003	2.9	2.70
36	CM-1 63.6 H	0.004	5.7	2.70
37	CM-1 66.6 H	0.002	4.1	2.70
38	CM-1 66.6 V	0.002	4.0	2.70
39	CM-1 67.3 H	0.002	4.5	2.70
40	CM-1 12.8 H	0.010	0.9	2.70
41	CM-1 24 V	0.003	1.8	2.70
	Mean	**0.04**	**3.3**	**2.69**
	S.D	**±0.01**	**±1.9**	**±0.02**

Numerical values in column 2 represent actual elevation of sample from CM-1 section. H and V denote plugs that were extracted horizontally and vertically from the bulk samples, respectively. Weatherford Laboratories cleaned the plugs using the Dean Stark (1920) method to extract any residue hydrocarbon.

References cited

DEAN, E. W., & STARK, D. D., 1920, A Convenient Method for the Determination of Water in Petroleum and Other Organic Emulsions: Industrial & Engineering Chemistr*y*, v. 12(5), p. 486-490.

APPENDIX H

TTEST for 1-inch plugs (horizontal and vertical permeability) from CM-1

	Sample size	**Mean**	**Standard Deviation**	**Variance**
Permeability-H	24	0.005	0.005	2.119E-05
Permeability-V	16	0.080	0.307	0.094
t-test assuming unequal variances (heteroscedastic)				
Hypothesized Mean Difference		0		
Pooled Variance		0.037		
Test Statistics		0.986		
Two-tailed distribution				
p-level	0.34	*Critical Value (5%)*	2.131	
One-tailed distribution				
p-level	0.17	*Critical Value (5%)*	1.753	

APPENDIX I

FTEST for 1-inch plugs (horizontal and vertical permeability) from CM-1

	Permeability-H	**Permeability-V**	
Sample size (N)	24	16	
Mean	0.005	0.080	
Variance	2.119E-5	0.094	
Standard Deviation	0.005	0.307	
Mean Standard Error	9.396E-4	0.077	
Summary			
F	4,435.438	F Critical value (5%)	2.128
p-level 1-tailed	0	p-level 2-tailed	0
H0 (5%)?	***Rejected***		

APPENDIX J

TTEST for 1-inch plugs (horizontal and vertical porosity) from CM-1

	Sample size	Mean	Standard Deviation	Variance
Porosity-H	24	3.48	2.09	4.37
Porosity-V	16	3.12	1.63	2.66
t-test assuming unequal variances (heteroscedastic)				
Degrees of Freedom	37			
Hypothesized Mean Difference	0			
Pooled Variance	3.694			
Test Statistics	0.611			
Two-tailed distribution				
p-level	0.545	*Critical Value (5%)*	2.026	
One-tailed distribution				
p-level	0.273	*Critical Value (5%)*	1.687	

APPENDIX K

FTEST for 1-inch plugs (horizontal and vertical porosity) from CM-1

	Porosity-H	**Porosity-V**	
Sample size (N)	16	24	
Mean	3.119	3.479	
Variance	2.664	4.366	
Standard Deviation	1.632	2.09	
Mean Standard Error	0.408	0.427	
Summary			
F	1.639	F Critical value (5%)	2.297
p-level 1-tailed	0.163	p-level 2-tailed	0.326
H0 (5%)?	***Accepted***		

APPENDIX L

Porosity And Permeability Data From PM-1 (1-Inch Plugs)

Sample Number	Elevation in PM-1 (m)	Permeability Horizontal Kair (md)	Porosity Helium %	Grain Density gm/cc
1	PM-1 2	0.005	4.3	2.69
2	PM-1 2.5	0.003	5.0	2.68
3	PM-1 3.4	0.003	4.4	2.68
4	PM-1 6.5	0.002	3.0	2.68
5	PM-1 8	0.003	4.6	2.70
6	PM-1 9.3	0.400	6.5	2.69
7	PM-1 13.3	0.007	3.2	2.69
8	PM-1 15	0.006	1.9	2.70
9	PM-1 16.9	0.007	4.2	2.70
10	PM-1 22.5	0.004	2.6	2.69
11	PM-1 25	0.006	5.1	2.69
12	PM-1 26.6	0.005	2.4	2.68
13	PM-1 27.5	0.005	3.1	2.69
14	PM-1 39.2	0.004	3.7	2.70
15	PM-1 40.6	0.005	0.7	2.70
	Mean	**0.03**	**3.6**	**2.69**
	S.D	**±0.10**	**±1.4**	**±0.01**

Numerical values in column 2 represent actual elevation of sample from PM-1 section. All plugs extracted from bulk samples from PM-1 are vertical. Weatherford Laboratories cleaned the plugs using the Dean Stark (1920) method to extract any residue hydrocarbon.

References cited

DEAN, E. W., & STARK, D. D., 1920, A Convenient Method for the Determination of Water in Petroleum and Other Organic Emulsions: Industrial & Engineering Chemistry, v. 12(5), p. 486-490.

APPENDIX M

Porosity And Permeability Data From PM-1 (4-Inch cores)

Sample #	Permeability	Porosity	Grain
	Kair	Helium	Density
	md	%	gm/cc
PM-1 10	553	9.2	2.71
PM-1 11	0.08	8.2	2.70
PM-1 21	0.03	3.4	2.69
PM-1 29	X	6.5	2.69
PM-1 30	97	5.3	2.69
PM-1 30	X	15.1	2.70
PM-1 33	27	5.3	2.70
PM-1 38	X	9.2	2.70
MEAN	**135.422**	**7.8**	**2.70**
S.D	**±192**	**±3.6**	**±0.01**

Numerical values in column 1 represent actual elevation of sample from PM-1 section. X in column 2 means that the cores had a large vug at a crucial spot that could cause leakage and were therefore not analyzed for permeability values. Weatherford Laboratories cleaned the plugs using the Dean Stark (1920) method to extract any residue hydrocarbon.

References cited

DEAN, E. W., & STARK, D. D., 1920, A Convenient Method for the Determination of Water in Petroleum and Other Organic Emulsions: Industrial & Engineering Chemistry, v. 12(5), p. 486-490.

APPENDIX N

Point Count Data From CM-1 Section

Elevation	[1]IS	[2]EEC	[3]RFC-2	[4]LEC	[5]TOP	[6]EX-Φ	[7]T-Φ	[8]Matrix	[9]MX+T-Φ
0.8	5.6	8.8	6.2	15.5	36.1	0.0	36.1	63.9	100.0
1.4	1.2	3.8	0.4	1.0	6.4	0.4	6.8	93.2	100.0
1.8	13.3	6.7	8.6	7.8	36.4	0.0	36.4	63.6	100.0
2.5	4.7	16.5	8.9	13.6	43.6	0.0	43.6	56.4	100.0
4.6	20.1	0.0	0.0	6.8	26.9	0.0	26.9	73.1	100.0
5.0	0.0	11.3	0.0	2.7	14.0	0.0	14.0	86.0	100.0
5.3	5.3	8.3	1.0	9.0	23.6	0.0	23.6	76.4	100.0
6.5	18.9	4.0	1.7	6.7	31.2	0.0	31.2	68.8	100.0
8.4	26.8	0.0	0.0	13.6	40.4	1.4	41.8	58.2	100.0
8.7	2.2	0.0	0.0	5.5	7.7	0.4	8.1	91.9	100.0
8.8	7.4	0.0	0.0	2.5	9.9	0.7	10.6	89.4	100.0
9.5	20.5	0.0	0.0	5.1	25.6	0.0	25.6	74.4	100.0
11.5	6.0	5.2	9.0	8.9	29.2	0.0	29.2	70.8	100.0
12.0	5.8	2.3	9.8	3.1	21.0	0.0	21.0	79.0	100.0
12.6	0.0	0.0	4.0	22.4	26.4	0.0	26.4	73.6	100.0
12.8	5.0	0.0	7.0	10.7	22.7	0.0	22.7	77.3	100.0
13.2	3.3	0.0	15.7	3.7	22.7	0.0	22.7	77.3	100.0
13.3	8.7	5.7	6.1	1.7	22.2	0.0	22.2	77.8	100.0
14.0	4.0	7.6	0.0	10.9	22.5	0.0	22.5	77.5	100.0
14.5	51.4	4.0	0.0	7.9	63.4	0.4	63.7	36.3	100.0
16.6	4.6	1.5	12.4	4.6	23.2	0.0	23.2	76.9	100.0
21.6	6.2	12.8	0.4	1.0	20.4	0.0	20.4	79.6	100.0
23.0	1.3	10.0	11.5	3.1	25.9	0.0	25.9	74.1	100.0
23.5	5.0	5.5	6.4	0.9	17.8	0.0	17.8	82.2	100.0
24.0	0.3	2.7	2.3	8.0	13.3	0.0	13.3	86.7	100.0
25.2	59.2	0.0	3.8	4.8	67.8	1.7	69.6	30.5	100.0
27.0	8.5	12.2	5.4	2.0	28.2	0.0	28.2	71.8	100.0
28.5	2.7	3.5	0.3	7.0	13.5	0.0	13.5	86.5	100.0
29.0	0.0	29.2	2.7	4.0	35.9	0.0	35.9	64.1	100.0
38.2	13.9	3.1	11.6	2.0	30.6	1.4	32.0	68.0	100.0
38.5	13.6	1.7	17.1	0.0	32.4	0.0	32.4	67.6	100.0
48.0	2.3	0.0	3.3	15.1	20.7	0.0	20.7	79.3	100.0
48.8	3.0	0.0	1.7	6.7	11.3	0.7	12.0	88.0	100.0
49.8	3.0	3.1	3.0	2.0	11.1	0.0	11.1	88.9	100.0
50.5	1.7	0.0	0.0	25.8	27.5	0.0	27.5	72.5	100.0
51.5	4.5	0.0	13.0	27.5	44.9	3.6	48.6	51.4	100.0
58.7	0.0	0.0	15.1	6.3	21.4	0.0	21.4	78.6	100.0
59.5	0.7	0.0	8.8	14.6	24.1	3.4	27.5	72.5	100.0
63.0	0.0	47.2	0.0	1.6	48.8	0.0	48.8	51.2	100.0
65.5	0.0	7.3	4.0	5.3	16.7	0.0	16.7	83.3	100.0

66.7	1.8	12.3	2.8	2.3	19.3	0	19.3	80.7	100.0
67.3	18.7	4.1	1.8	4.1	28.7	0.0	28.7	71.3	100.0
71.2	15.3	0.0	11.6	2.1	28.9	0.0	28.9	71.1	100.0
Mean	9	5.6	5	7.2	26.6	0.3	26.9	73.1	100

1: Crystalline internal sediments, 2: Early equant cement, 3: Late marine cements, 4: Late equant cements, 5:Total occluded porosity, 6: Extant porosity, 7: Total porosity, 8: Matrix includes all the original sediments, grains, and mud. 9: Sum of matrix and total porosity. Each category from 1-4, 6, and 8 were point counted for 350 times. Values in column 1 represent actual height of samples in CM-1 section.

APPENDIX O

Point Count Data From PM-1 Section

Elevation	[1]MC	[2]CIS	[3]RFC-1	[4]RFC-2	[5]PIS	[6]LEC	[7]TOP	[8]EX-Φ	[9]T-Φ	[10]Matrix	[11]MX+T-Φ
2.0	8.1	0.0	1.7	0.0	0.0	29.0	38.7	0.0	38.7	61.3	100.0
2.5	5.4	0.0	0.0	0.0	0.0	0.0	5.4	0.0	5.4	94.6	100.0
4.5	9.5	0.0	2.0	1.9	0.0	40.1	53.4	0.0	53.4	46.6	100.0
6.5	4.0	0.0	8.8	3.9	4.4	28.9	50.0	0.0	50.0	50.0	100.0
10.1	0.0	0.7	14.1	1.2	0.0	52.0	68.0	1.1	69.0	31.0	100.0
12.7	0.0	0.0	0.0	0.0	0.0	22.0	22.0	0.0	22.0	78.0	100.0
13.3	0.0	22.2	2.0	0.0	0.0	24.6	48.8	0.0	48.8	51.2	100.0
15.0	2.4	0.0	4.5	0.0	0.0	9.8	16.6	0.0	16.6	83.4	100.0
15.8	0.0	0.0	0.0	0.0	0.0	31.2	31.2	0.0	31.2	68.8	100.0
16.6	0.0	0.0	1.0	2.1	23.3	9.0	35.4	0.3	35.8	64.2	100.0
16.9	0.0	0.0	0.0	0.0	0.0	15.3	15.3	0.0	15.3	84.7	100.0
22.5	0.0	1.3	18.2	20.1	3.7	3.3	46.7	0.0	46.7	53.3	100.0
23.0	0.0	0.0	0.0	13.9	48.8	21.4	84.0	0.0	84.0	16.0	100.0
25.0	0.0	0.0	0.0	0.0	0.0	19.8	19.8	1.4	21.2	78.8	100.0
26.6	0.7	0.0	0.0	0.0	0.0	14.3	15.0	0.0	15.0	85.0	100.0
27.5	0.0	0.0	26.8	0.0	0.0	22.4	49.2	0.0	49.2	50.8	100.0
32.0	0.0	0.0	20.1	14.3	0.0	33.6	68.1	0.0	68.1	31.9	100.0
33.5	5.6	0.0	5.1	2.4	0.0	48.5	61.5	0.0	61.5	38.5	100.0
34.5	2.1	0.0	17.2	8.3	0.0	40.6	68.1	0.0	68.1	31.9	100.0
39.5	0.5	0.0	6.5	0.0	0.0	19.5	26.5	0.0	26.5	73.5	100.0
40.6	2.1	0.0	8.9	17.0	0.0	12.1	40.1	0.0	40.1	59.9	100.0
Mean	1.9	1.2	6.5	4.1	3.8	23.7	41.1	0.13	41.3	58.7	100.0

1: Micrite cements, 2: Crystalline internal sediments, 3: early marine cement, 4: Later marine cement, 5: Pelagic internal sediments, 6: Late equant cements, 7: Total occluded porosity, 8: Extant porosity 9: Total porosity, 10: Matrix, it includes all the original sediments, grains, and mud, 11: Sum of matrix and total porosity. Each category from 1-6, 8, and 10 were point counted for 350 times. Values in column 1 represent actual height of samples from PM-1.